PHONOCARDIOGRAM FREQUENCY ANALYSIS TECHNIQUES AND NON-INVASIVE DETERMINATION OF HEART VALVE CALCIFICATION

by

D. Nandagopal B.E., M.S.,
University of Adelaide

Thesis submitted for the degree of

Doctor of Philosophy

in the Department of Electrical and Electronic Engineering,

University of Adelaide, Australia

May 1984

CONTENTS

SUMMARY

Phonocardiogram data acquisition and analysis procedures are outlined. Application of Fourier transform techniques in the frequency analysis of heart sounds is briefly reviewed. Fast Fourier transform (FFT) analysis of phonocardiograms using moving windows is illustrated. Application of the linear prediction (LP) technique in the frequency analysis of heart sounds is explored. Spectral distributions of second heart sounds, in normal children, are determined using both FFT and selective linear prediction methods. FFT and LP spectra are compared. Spectral energies in various frequency bands of the second heart sounds are correlated with the aortic valve size parameter derived from 2-dimensional echocardiograms.

An approach to quantitative inferences of valvular calcification by mathematical modelling of the vibrations of heart valves and relating the frequencies to the spectral characteristics of appropriate heart sounds is outlined. A non-invasive procedure for determining the pressure drop across the aortic valve by using the data of the left ventricular outflow tract from two-dimensional echocardiography is presented.

SIGNED STATEMENT

The contents of this thesis have not been submitted to any university for the purpose of obtaining any other degree or diploma, and to the best of my knowledge, it contains no material previously published by any other person, except where due reference is made in the text.

D. Nandagopal

PREFACE

I would like to express my deep sense of gratitude to Dr. J. Mazumdar for his continued guidance, interest and support during the course of this research work. I also would like to convey my warmest appreciation to Professor R.E. Bogner and Mr. G. Karolyi for providing the encouragement and technical expertise which has made this work possible.

I am very much indebted to Dr. D.N. Ghista, Professor of Medicine, McMaster University Medical Center, Hamilton, Canada, for his endless willingness in sharing his expertise and research facilities, and for his valuable advice and generous help in countless ways, including the editing of this manuscript. My special thanks are due to Dr. T.C. Hearn, University of Guelph, for his most valuable suggestions and discussions on heart valve modelling throughout the preparation of this thesis and the final checking of it for grammar.

The research work reported in this thesis was carried out in part in the Departments of Cardiology at the Royal Adelaide and Adelaide Childrens Hospitals and in the Department of Biomedical Engineering at McMaster University Medical Center. In this regard, I would like to gratefully acknowledge everyone who has made available their assistance and advice. In particular, my sincere thanks are due to Dr. E. Goldblatt, Adelaide Childrens Hospital, Dr. L. Mahar, Royal Adelaide Hospital, and their technical staff.

In addition, I am thankful to many final year Electrical and Electronic Engineering students who have contributed to building and testing of some of the electronic circuits developed for use in this research work. Any expression of thanks to the technical and office staff of the Department of Electrical and Electronic Engineering cannot adequately reflect their cooperation and assistance during my stay in Adelaide and I am grateful to them.

Finally, I am forever indebted to my wife Malar for sharing her knowledge of medicine with me and providing me with everlasting moral support.

CHAPTER I

INTRODUCTION

Heart disease still continues to pose etiological problems, in spite of major advancements made in cardiovascular diagnostic procedures as a result of revolution in the "chip" industry. Since the beginning of the eighteenth century, auscultation has been one of the important differential diagnostic tools. The cardiac structural vibrations, induced by a sudden accelerating or decelerating blood flow, are transmitted to the chest wall, and result in complex acoustic phenomena. This dissertation aims to investigate methodologies to extract the frequency contents of auscultatory sounds, so as to make it eventually possible to discern pathologies of valvular and myocardial tissues, by correlating the heart sounds' frequencies with the vibration analysis of the corresponding cardiac structures.

1.1 Brief introduction of the heart and heart sounds

The heart is a neuroelectrically actuated mechanical pump. The electrical activity of the heart causes the heart muscles to undergo contraction and relaxation processes alternately. Electrical impulses are generated at regular intervals at a site called the sino atrial (S.A.) node. (Refer to figure 1.1.) The generated impulses are then

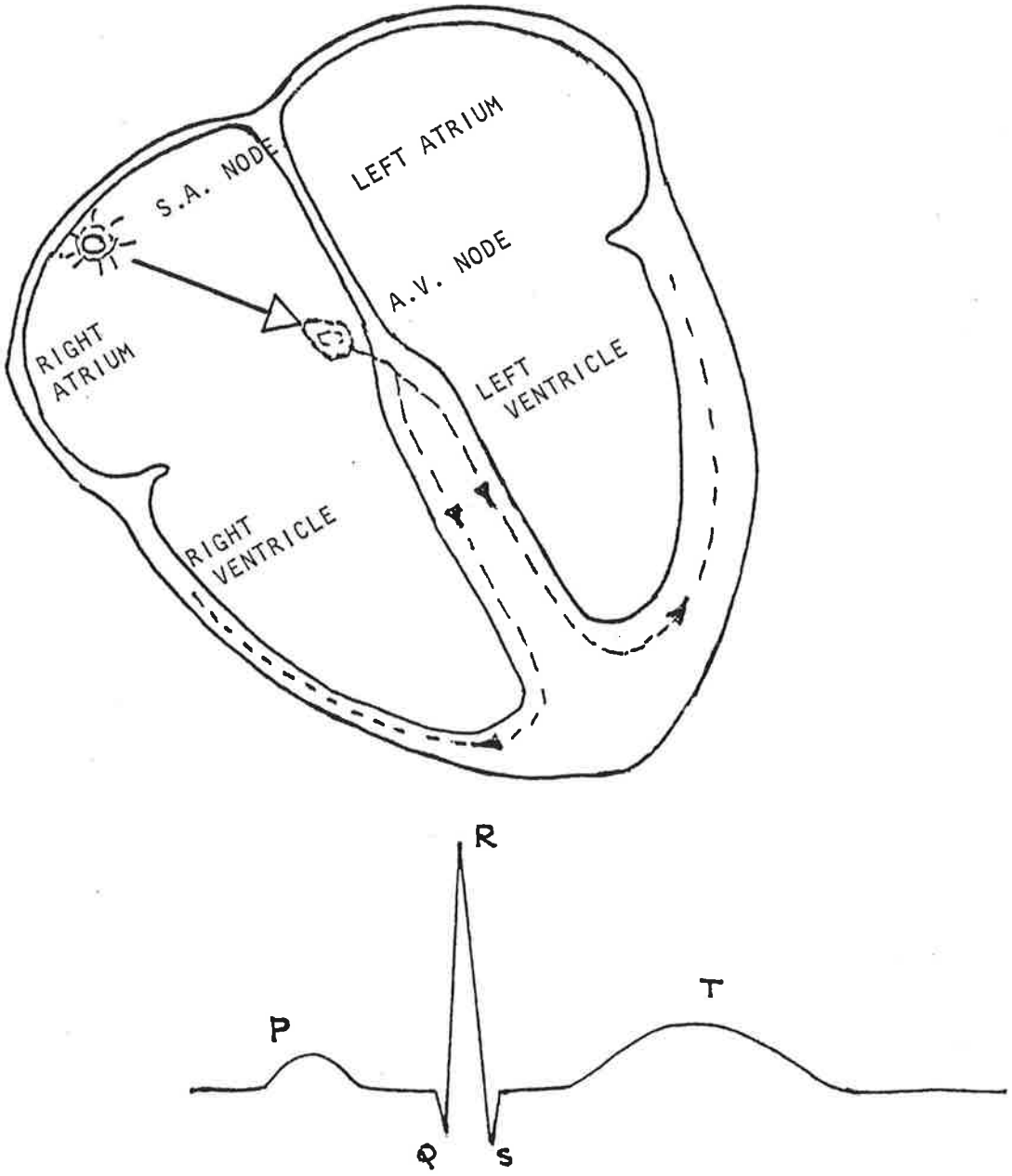

FIG. 1.1: ELECTRICAL CONDUCTION PATH IN HEART AND ELECTROCARDIOGRAM

propagated to the atrium, atrio-ventricular junction and then down to the ventricular musculature. As the electrical pulse travels down the myocardium, it depolarises the myocardium and thereby causes myocardial contraction. Once the electrical pulse has travelled past a site the contracted muscles are repolarised producing myocardial relaxation. Thus the heart muscles continually undergo a contraction and relaxation process alternately and this makes the heart pump blood periodically.

Atrial and ventricular contractions are produced sequentially. When the atrial myocardium contracts, blood is squeezed into the ventricles and as the ventricles contract, the blood is ejected into the aorta and pulmonary artery. A functional diagram of the heart is represented in figure 1.2. As the blood moves from one chamber into another, it goes through heart valves, which act as "diodes" allowing flow in one direction only.

The atrioventricular valves, as the name implies, are located between the atria and ventricle. Interposed between the left atrium and left ventricles is a valve with two cusps known as the mitral valve, while a tricuspid valve is located between right atrium and right ventricle. The aortic valve is situated between the left ventricle and the aorta, while the pulmonary valve facilitates unidirectional flow of blood from the right ventricle to the lungs via the pulmonary artery. The right ventricle receives venous blood via the right atrium and pumps it into the pulmonary artery. After

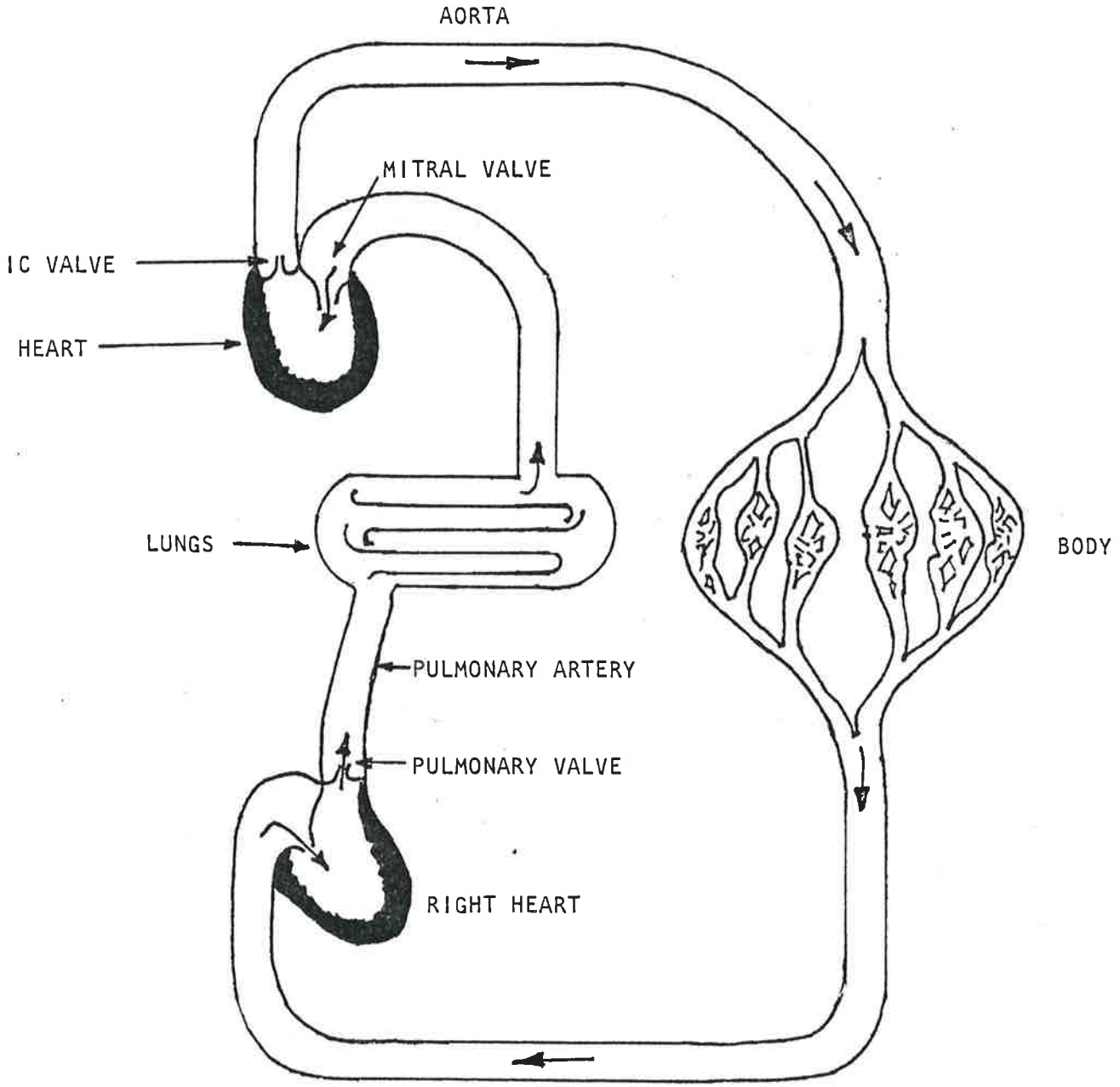

FIG. 1.2: FUNCTIONAL DIAGRAM OF THE HEART

oxygenation in the lungs, the blood returns via the pulmonary vein and left atrium to the left ventricle, which in turn pumps it into the aorta.

The cardiac cycle consists of a period of ventricular contraction (called systole) and a period of ventricular relaxation (called diastole). Accordingly, during systole the heart chambers empty blood and during diastole fill with blood. The spread and regression of the ventricular impulse wave can be represented by a time varying voltage vector, with a magnitude which is proportional to the voltage generated by the accession wave and whose direction is given by the gradient of the wavefront surface. The projections of this voltage vector on the reference lines of the leads, constitute the recorded electrocardiogram signals. (Refer figure 1.1). The "P" wave in the electrocardiogram represents atrial depolarisation or atrial contraction. The "QRS" complex corresponds to ventricular contraction. The "T" wave corresponds to ventricular relaxation.

Intra cardiac blood flow, accelerations and decelerations and concomitant vibrations of the cardiac structures result in sounds and murmurs. These sounds radiate to the torso surface, where they can be detected by a stethoscope and categorised to aid in the diagnosis of cardiac abnormalities. These recordings at the human thorax constitute the phonocardiogram (PCG).

The acoustic events of the heart can be divided into two categories; the heart sounds and murmurs. Heart sounds are

short-lived bursts of vibrational energy and are transient in character. Heart murmurs are stochastic in nature, are longer in duration and are associated with turbulent flow of blood in the heart and large vessels. Heart sounds are classified into four basic groups on the basis of their occurrence in the cardiac cycle. The two main sounds are known as the first heart sound (SI) and second heart sound (SII) while the other two sounds are referred to as the third heart sound (SIII) and fourth heart sound (SIV). The genesis of these sounds has been the subject of very many research investigations for nearly a century. Rushmer (1970) has proposed a cardiohemic system relating oscillations of the blood, valves and myocardium, to explain the origins of heart sounds (refer figure 1.3).

1.2 Relationship of heart sounds to cardiodynamic events

There have been several controversial theories put forward to explain the origin of these sounds (Smith, et al., 1950; Sabbah and Stein, 1976; Stein and Sabbah, 1978; Ionescu and Stonescu, 1980). As the first heart sound occurs during early ventricular systole, many theories were proposed concerning the role of atrioventricular valves (mitral and tricuspid valves) in the production of SI. The controversies have existed mainly due to inadequate hitherto employed instrumentation, which introduced delays in monitoring the intracardiac pressures. But now with the advent of

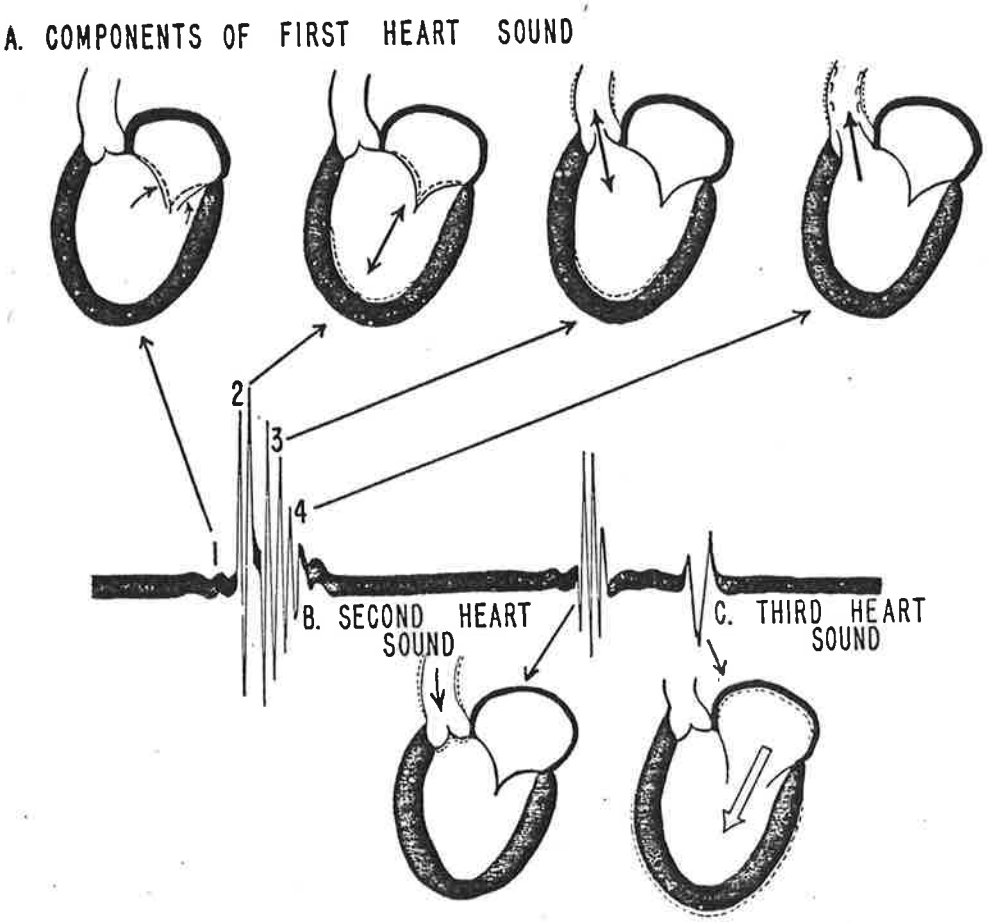

FIGURE 1.3

"Schematic drawings of the causes of various components of the heart sounds based on the concept that the vibrations are induced by acceleration or deceleration of the blood within elastic chambers.

A, The first sound can be divided into four components. The initial vibrations occur when the first myocardial contractions in the ventricle shift blood toward the atrium to approximate and seal the atrioventricular valves. The second component begins with abrupt tension of closed atrioventricular valves decelerating the moving blood. It may represent oscillation of blood initiated by overdistention of the atrioventricular valves, countered by recoil of the contracting ventricular myocardium. The reaction would be similar to tapping a balloon filled with water. The third component may involve oscillations of blood between the distending root of the aorta and the ventricular walls. The fourth component probably represents vibrations due to turbulence in blood flowing rapidly through the ascending aorta and pulmonary artery.

B, The second heart sound is introduced by a few low-frequency vibrations which may accompany the deceleration and reversal of flow through the aorta and pulmonary artery prior to the closure of the semilunar valves. The audible portion of the second sound begins with closure and tensing of the semilunar valves. Although the primary vibrations occur in the arteries, they are also transmitted to the ventricles and atria by movements of the blood, valves and valve rings.

D, The third heart sound occurs at the end of the rapid filling phase. Sudden termination of the rapid-filling phase may throw the entire atrioventricular system into vibrations which have very low frequency because the walls are relaxed." (Rushmer, 1970)

echocardiography, one can monitor the movements of intracardiac structures with minimal time delay.

According to Laniado (1973) the atrioventricular valves close after the crossover point when the ventricular pressure exceeds the atrial pressure. The closure of the mitral and tricuspid valves coincides with the two major components of the first heart sound. But the present concept, according to Luisada (1983), favours that the mitral valve plus chordae contribute small fractions of the energy of the first heart sound and a good correlation between ventricular wall tension and the first heart sound has been demonstrated.

The second heart sound (SII) seems to be associated with the vibrations of the just-closed aortic and pulmonary valves as well as of the ascending aorta. The recent works of Stein and Sabbah (1978) on the second heart sound production mechanism have pointed out that even though coaptation of the leaflet is silent, the rapid vibrations of the closed leaflets that begin immediately after coaptation create the sound. This theory has been supported by combined phono echocardiographic studies made by others (Anastassiades et al, 1976; Kotler et al, 1978).

The third heart sound (SIII) is a low frequency sound in early diastole, during the early rapid filling phase of the ventricle. It occurs from 0.13 to 0.20 seconds after SII. Because of its low intensity and low pitch it is not commonly heard. The pathogensis of SIII is still controversial. However recent studies support the theory that SIII is due to

a sudden intrinsic limitation of longitudinal expansion of the left ventricular wall during early diastolic filling (Ozawa, et al, 1983).

The fourth heart sound (SIV) is a low frequency sound in late diastole. This faint sound is also called an atrial presystolic sound or atrial gallop. It occurs at the time of atrial contraction immediately before ventricular systole. This sound is more difficult to hear than SIII. Figure 1.4 illustrates the heart sounds, their duration and their relationship with other cardiac parameters.

1.3 Diagnostic implications of first and second heart sounds

There has always been a need for non-invasive cardiac assessment techniques. Phonocardiography is one such technique. Phonocardiography (heart sound recording) evolved from auscultation and provides a record of the vibrations of the chest wall originating from the heart. Phonocardiography removes subjective influence from conventional auscultation, while continuing to be a non-invasive method.

As the first and second heart sounds are most likely related to the vibrations of just closed atrioventricular and semilunar valves and to some extent to the ventricular wall tension, their spectral content could be related to the vibratory characteristics of the valves and thereby made to reflect the material properties of these vibrating structures. With the availability of advanced mathematical and digital processing techniques to carry out vibrational

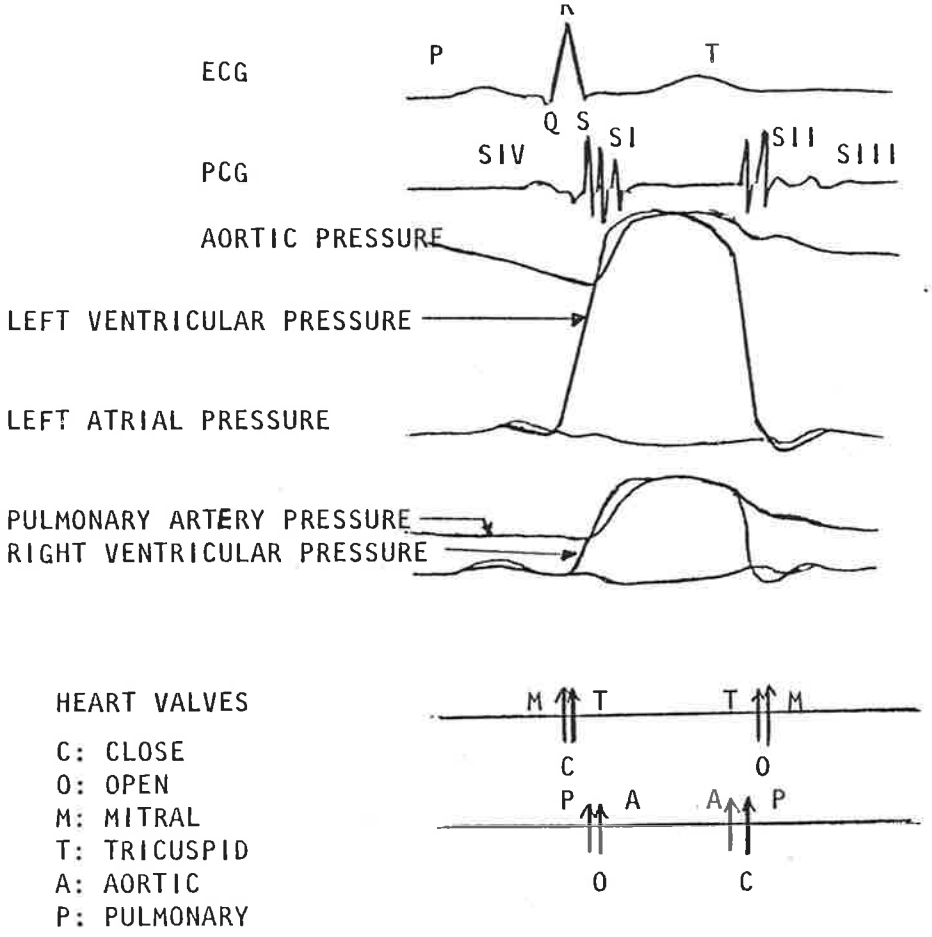

HEART SOUNDS	DURATION SECS.	FREQUENCY RANGE (HZ)
FIRST HEART SOUND (SI)	0.1 - 0.12	20 - 150
SECOND HEART SOUND (SII)	.08 - .14	50 - 600
THIRD HEART SOUND (SIII)	.04 - .05	20 - 25
FOURTH HEART SOUND (SIV)	.04 - .05	LESS THAN 25

FIG. 1.4: HEART SOUNDS AND ITS RELATIONSHIP WITH OTHER CARDIODYNAMIC EVENTS

and sound analysis, there has been added interest in the diagnostic potential of the heart sounds.

Since the first heart sound has two major components believed to be associated with the mitral and tricuspid valves, by doing frequency analysis using time varying windows, and by correlating spectral frequencies with the valve size and valve leaflet constitutive property (through simultaneous echocardiographic and phonocardiographic studies), one can extract valuable pathological information on the valves (Hearn, 1980). A similar study can be made for the second heart sound to identify the aortic and pulmonary valves.

1.4 State of the art on clinical applications of heart sounds

Heart sound studies in general have been carried out by numerous investigators. Luisada (1958, 71) and Rushmer (1970) have done much of the pioneering work. A number of studies have been carried out in the recent past on the analysis of phonocardiograms and their clinical significance (Van vollenhoven, et al, 1969; Adolph, et al, 1970; Yoganathan, et al, 1976; Hearn, et al, 1979; Van Vollenhoven, et al, 1979; Stein, et al, 1980).

As the heart muscle and the valvular system provide a considerable contribution to the production of heart sounds, it has occured to investigators to (i) relate the leaflet pathology to the vibrational frequencies and (ii) associate

these vibrational frequencies with the spectral peaks of phonocardiograms. Thereby the constitutive properties of the cardiac structures can be obtained from the heart sound analysis.

The fast Fourier transform (FFT) technique has been used extensively in the frequency analysis of heart sounds (Yoganathan, et al, 1976a; 1976b; Sarkady, et al, 1976). Studies on the first heart sound using frequency analysis techniques in normal and pathological cases have clearly indicated the relationship between the quality of resonant peaks (frequency and sharpness of the peak) and valvular pathology (Adolph, et al, 1970; Renner and Renner, 1979; Stein, et al, 1980).

Frequency analysis studies of the second heart sound have recently shown that the amplitude and dominant frequency peak in the aortic component of the second heart sound are affected by calcific aortic stenosis (Sabbah, et al, 1978; Stein, et al, 1980). The works of Renner, et al, (1979), Stein et al, (1980) and Adolph (1978) have clearly established the correlation of spectral parameters of heart sounds with specific pathological conditions like myocardial infarction, valvular stenosis etc.

This significantly enhances the clinical application of heart sound signals. The correlative studies of phonocardiograms with echocardiograms provide additional information on the timing of valvular events (Prakash, et al, 1976; Kotler, et al, 1978; Lewis, et al, 1979; Isner, et al,

1979; and Ronan, 1981), thus enhancing the potential clinical usefulness of heart sounds.

1.5 Scope of the research

The need, importance and diagnostic potential of heart sound signal analysis has been discussed in the previous section. The mathematical modelling of atrioventricular and semilunar valve vibrations are employed to express the primary vibrational frequencies of the valve leaflets in terms of their pathologies (Ghista and Rao, 1970; Mazumdar, et al, 1978; Blick, et al, 1979). Then by relating the heart sound and model vibrational frequencies, the leaflet constitutive parameters can be determined from the heart sound spectral frequencies. FFT techniques have been used extensively to perform the frequency analysis of first and second heart sounds. This has improved considerably the basic understanding of the phonocardiograms and their relationship to the cardiodynamic events. However, the FFT has a basic limitation on the frequency resolution dictated by the window size.

Since the diagnostic potential of heart sounds is dependent on accurate determination of the spectral content of heart sounds, it is important to have an accurate method for discerning the spectral frequency content of heart sounds. The purpose of this thesis is therefore, to develop more accurate techniques for analyses of phonocardiograms, so as to enhance their clinical applicability.

The thesis contains nine chapters. Chapter two of the thesis deals with the instrumentation system for phonocardiogram acquisition and an analysis procedure, based on the use of interactive graphics. In chapter three, a general overview of the application of Fourier transform technique is provided. Also, use of moving windows for heart sound analysis is considered, along with 3-dimensional spectral representation for heart sound signals. In chapter four, the application of linear prediction coding (LPC) method to heart sound analysis is outlined. Frequency and band width evaluation techniques are also discussed.

Chapter five deals with the selective linear prediction method in the analysis of heart sounds; a discussion on the difference between conventional filtering and the selective filtering procedure is given. Chapter six describes the frequency analysis of the second heart sound in normal children using the selective linear predictive coding (SLPC) technique. A brief introduction to echocardiography is given in chapter 7 along with the results of spectral energy correlations of the second heart sound with echocardiographically derived valvular dimensions.

An approach to quantitative inferences of valvular calcification by mathematical modelling of the vibrations of heart valves and relating the frequencies to the spectral characteristics of appropriate heart sounds is outlined in chapter eight. A noninvasive method, based on two-dimensional echocardiography, for the determination of

the pressure drop across the aortic valve is also described in chapter eight. A comprehensive conclusion and recommendation for further research work is provided in chapter nine.

CHAPTER II

INSTRUMENTATION SYSTEM

2.1. Phonocardiogram versus auscultation

The heart sound signal record, resulting from vibrations of cardiac structures, monitored on the human thorax is known as the phonocardiogram (PCG). Compared with conventional auscultation as conceived by the stethoscope, phonocardiography has advantages, since it provides quantification of the auscultatory record and makes auscultation interpretation independent of auditory acuity, training, technique of listening and capacity to perceive certain low frequency sounds (third heart sound). Further, spectral phonocardiography can yield diagnostic information associated with the pathology of the vibratory cardiac structures. Figure 2.1 and 2.2 indicate the differences between auscultation and the phonocardiogram acquisition system.

In the phonocardiogram acquisition system, the heart sounds are detected by a microphone which is normally a piezo electric crystal transducer with a flat frequency response from d.c. to 2 KHZ. The microphone can be held in position on the chest by means of a suction type rim attached to the transducer or by a rubber strap. The transduced sounds are amplified by a preamplifier with a frequency response similar to that of the microphone. The heart sounds are then selectively filtered to extract either low frequency or high

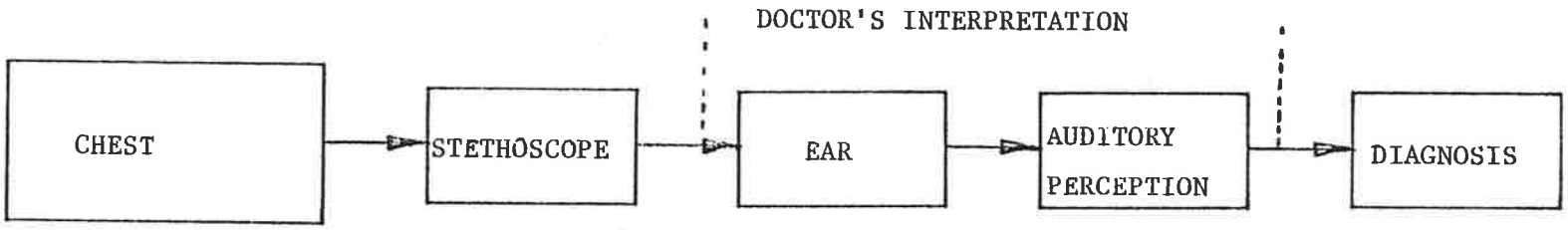

FIGURE 2.1 CONVENTIONAL AUSCULTATORY ROUTE.

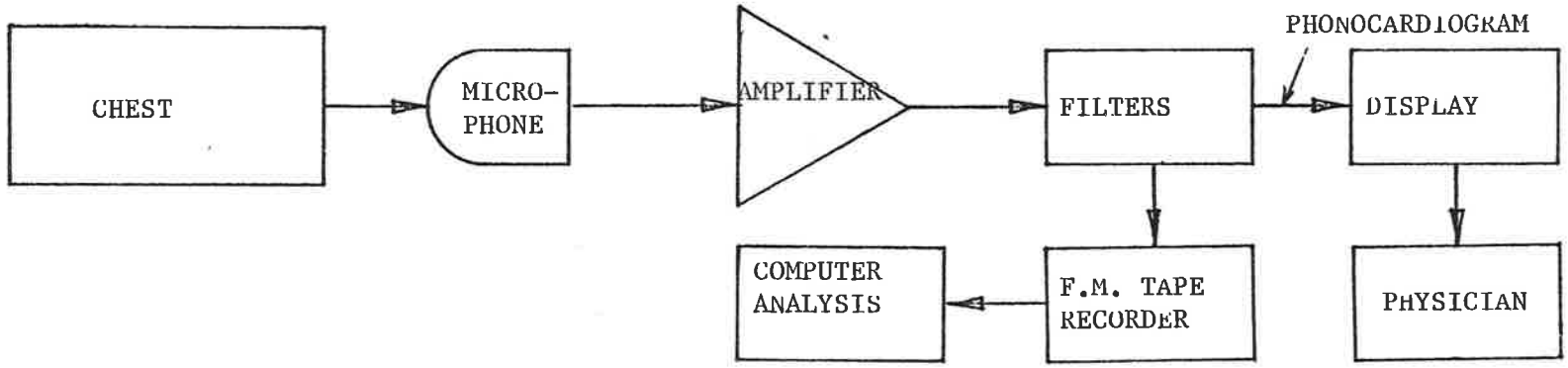

FIGURE 2.2 PHONOCARDIOGRAM AQUISITION ROUTE

frequency components by appropriate selection of the desired band on the filter amplifier. The filtered heart sounds are displayed on an oscilloscope or recorded on a chart recorder for the physician to look at and interpret. Sometimes, the heart sound signals are also recorded on an FM tape recorder for computer analysis. An instrumentation system developed by the author, for phonocardiogram acquisition is described in the following section.

2.2 Phonocardiogram acquisition system

Detailed guidelines for standardization of phonocardiography have recently been outlined by Van vollenhoven et al (1979). Normally, the heart sounds have a frequency spectrum ranging from approximately 20 HZ to about 500 HZ. Therefore phonocardiogram signals need to be recorded on a frequency modulated (FM) tape recorder for subsequent analysis. For phonocardiographic studies, one needs to monitor the electrocardiogram (ECG) signal as well, for referencing the phonocardiographic activity in the cardiac cycle.

As commercial FM tape recorders are too expensive, an inexpensive FM recording system is developed using a stereo cassette tape deck for recording PCG and ECG. The preamplifiers are designed to have low noise with gains of 80dB, and flat frequency response from 10 HZ to 1.5 KHZ. No additional filters are used in the system assuming that any required filtering can be done digitally on the computer. A

block diagram of the instrumentation system for phonocardiogram acquisition is shown in figure 2.3. In the frequency modulation (FM) system, modulation and demodulation are carried out by four phase locked loop (PLL) integrated circuit chips.

The preamplified signals are buffered appropriately with the required offset so that the voltage controlled oscillator (VCO) in the PLL oscillates with a centre frequency of 4 KHZ. Thus an FM wave is generated by the VCO with an instantaneous frequency 'f_t' given by

$$f_t = f_c + \frac{K_c}{2} S(t) \qquad .....(2.1)$$

where f_c denotes the centre frequency

$S(t)$ represents the PCG or ECG signal

K_c is the VCO gain constant which is the ratio of angular frequency range to control voltage range.

In figure 2.3, the PLL(1) and PLL(2) act as modulators which allow the modulated output to be recorded on the cassette. In order to recover the analogue signals from the recorder, the tape is played back via two signal conditioners which are simply Schmitt triggers limiting the waveforms at appropriate levels, so that PLL(3) and PLL(4) can be driven.

A typical demodulator circuit is shown in figure 2.4. The capacitor C and the resistors R1 and R2 are selected to suit the centre frequency and lock range of the demodulator. The exclusive OR gate in the PLL is a phase comparator which provides a phase error signal. Whenever an FM input signal

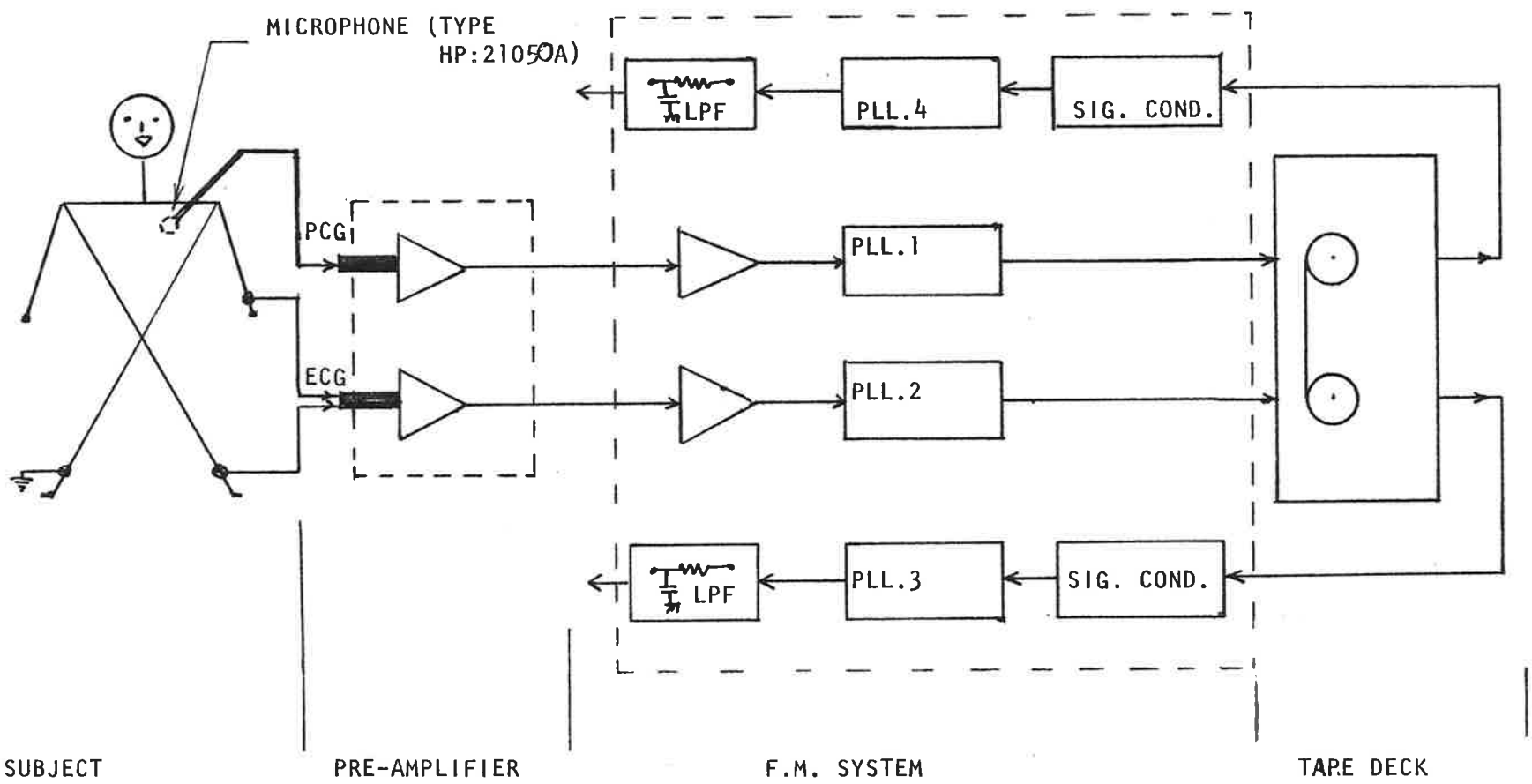

FIG. 2.3: INSTRUMENTATION SYSTEM FOR PHONOCARDIOGRAM ACQUISITION

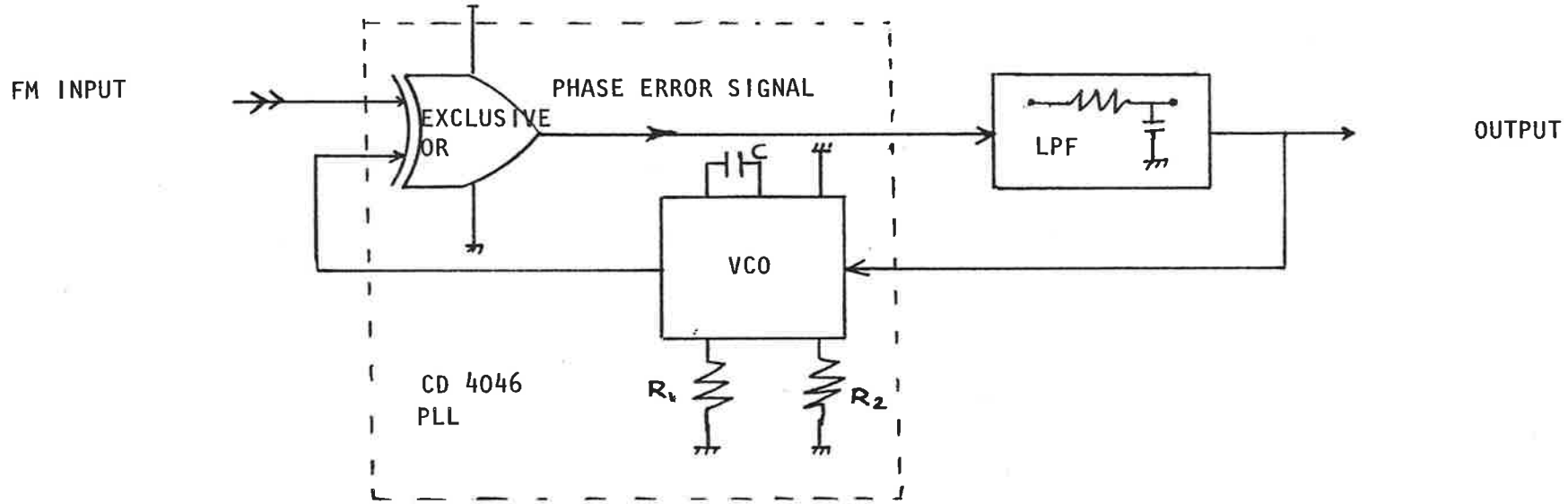

FIG. 2.4: DEMODULATOR

is applied to the PLL, while in lock as in figure 2.4, the changing phase error voltage caused by the variation of the input frequency will tend to adjust the VCO frequency so as to track the input, provided the VCO range is not exceeded. The phase error voltage will then vary as the frequency varies in the input FM signal.

A low pass filter (LPF) is necessary to remove the double frequency from the phase error signal. The filter output is then proportional to the input frequency, thus the PLL acts as a frequency demodulator to recover the PCG and ECG signals from the tape. The stereo tape deck used was an ultradynamic low noise deck made by 'MARANTZ' (USA). The detailed circuit diagram of the PLL modulation and demodulation system is provided in appendix A.

The design of the preamplifier circuits for the PCG and ECG will not be discussed here, as their design is very standard. Simultaneous recordings of the PCG and ECG were done on this system as well as on a commercially available FM tape recorder. The recovered signals (upon playing back) were compared both in the time and frequency domains, and found to be identical.

2.3 Microprocessor interface for data acquisition

For computer processing of the heart sounds, the PCG and ECG signals are to be digitized. This means a signal digitizer (analog to digital converter) must be interfaced between the tape recorder and the main computer. Accordingly

a microprocessor based data acquisition system has been designed and constructed to enable digitization of laboratory signals and subsequent transfer of digitized data to the main computer disk for storage and further analysis. A brief summary of the interface system is given here.

Intels' SDK85 microprocessor system has been used to control various peripherals in the interface. This selection is made on the basis of the availability of SDK85 kits for teaching purposes in the Electrical Engineering department and also because of large numbers of I/O ports, teletype interface and bus drivers all being on one board. The processor controlling the entire interface is the Intels' 8 bit 8085 microprocessor chip. The interface has been built to have the following capabilities:

1. Two analog to digital convertors to digitize the PCG and ECG signals simultaneously.
2. buffer memory of 8 kilowords.
3. Two digital to analog converters for the display of stored data.
4. Transfer of data from memory to the Adelaide University's CYBER173 computer.
5. Software controlled sampling rate.

The basic system configuration is shown in figure 2.5. The 8 bit analogue to digital converters (A/D), digital to analogue converters (D/A), buffer memory and the serial interface for the Cyber 173 are all built around the SDK85 kit. The detailed circuit diagrams for some of the

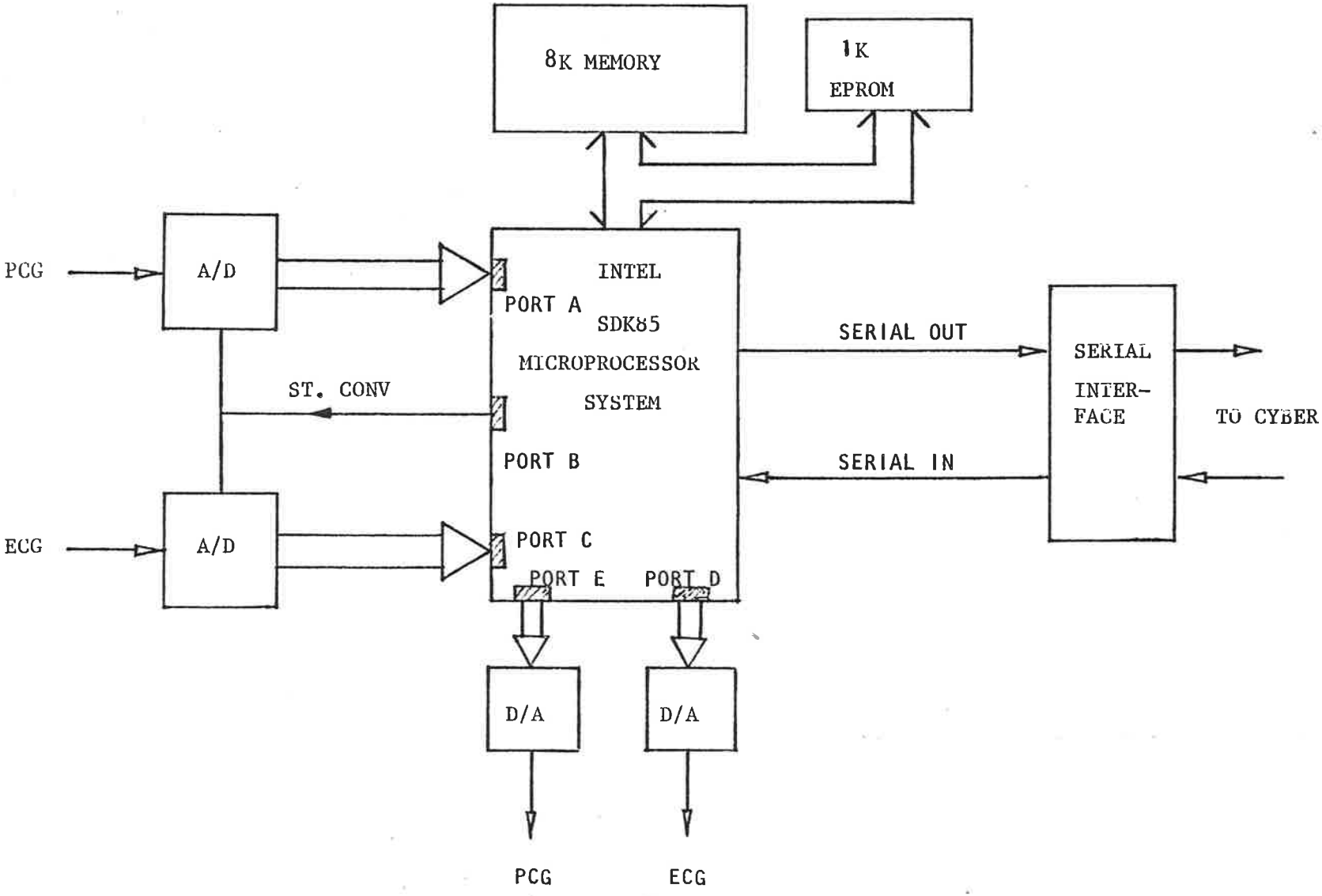

FIG.2.5: BASIC CONFIGURATION OF THE MICROPROCESSOR INTERFACE

peripherals are given in appendix B. The input and output signals were limited to ±5V peak to peak. The result of the conversion is an 8 bit unsigned number. The sampling rate is software controllable up to a maximum of 4000 samples per second. The signals are sampled such that 4K of data can be stored for each signal (PCG and ECG) in the buffer memory. If the sampling is done at 2000 samples/second, then 2 secs of data can be stored in the buffer memory. The program (in machine code) is stored in an E2708 1K X 8 bit EPROM. The random access memory (RAM) required is 8K; hence Intel 2114/3 1K X 4 bit static RAM chips are used.

2.4 Online data collection:

The final system developed for phonocardiogram and electrocardiogram data collection is indicated in figure 2.6. The PCG and ECG signals can be recorded on the tape deck through the FM system described earlier, and then digitized by playing back the signals through the FM system and micrprocessor interface. The FM system and tape deck can be bypassed to have an online data acquisition system. The digitized PCG and ECG signals can be looked at through an oscilloscope connected to the microprocessor interface via D/A convertors.

Digitization can be started at any instant of time by control from the key board of the SDK-85 kit or can be triggered by the 'R' wave of the ECG. Once the analogue to digital conversion is initiated, the system continues to

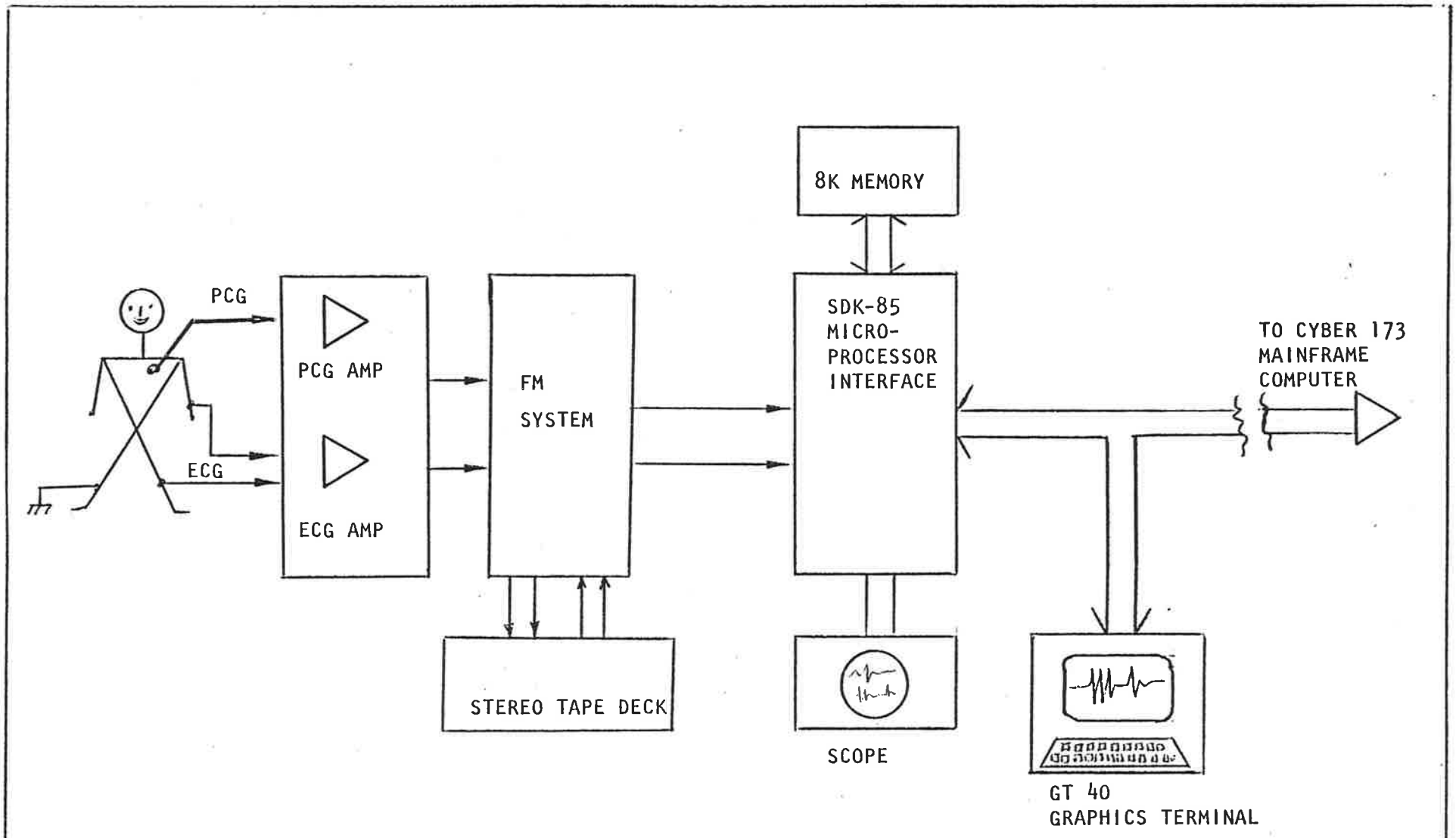

FIG. 2.6: FINAL DATA AQUISITION SYSTEM

digitize and store the data in the buffer memory, until 4K data samples are collected from each channel. The digitized data from the memory can be viewed on an oscilloscope through D/A S for any artifacts. The digitisation rate is specified before the A/D S are initiated. The sample rate is normally calculated from the number of states the CPU (central processing unit) takes to execute the machine code program that carries out analogue to digital conversion. The sample rate can be decreased by incorporating delay loops in the above program. A sample rate of 2042 HZ is normally used for PCG and ECG digitization. The data from the buffer memory is then transferred to the CYBER 173 computer through serial interface at 300 baud for storage and further analysis.

2.5 Data storage:

The PCG and ECG data transferred from the microprocessor memory to the CYBER 173 computer is normally in hexadecimal format. Therefore, the first processing step is to convert the data from hexadecimal to real. The data record is then processed to remove any dc offset produced during digitization. This is achieved by executing a computer program that determines the mean value of the data file and subtracts the mean value from each sample. The offset removed files are then stored as indirect permanent files of length 2048 samples each on the CYBER 173 disk. An indirect permanent file library of raw data (PCG and ECG) is thus

created on the CYBER disk. The data is easier to retrieve if the data files are stored using an indirect permanent file library utility on the CYBER computer.

CHAPTER III

HEART SOUND ANALYSIS BY FOURIER TRANSFORM METHOD

3.1 Fourier transform method

Interest in Fourier transform technique in Biomedical signal analysis has increased significantly after the publication of the 'fast Fourier transform' (FFT) by Cooley and Tukey [1965]. The Fourier transform is a frequency domain representation of a signal function, in continuous systems, and is described mathematically by the relationship

$$S(f) = \int s(t) e^{-j\,2\pi ft}\, dt \qquad .....(3.1)$$

where s(t) is the signal in time domain

S(f) is the Fourier transform of s(t),

i.e., the signal in frequency domain.

$$j = \sqrt{-1}$$

The inverse transform is given by:

$$s(t) = \int S(f)\, e^{j2\pi ft}\, df \qquad .....(3.2)$$

Equation (3.2) allows the recovery of the function in the time domain from its Fourier transform. For computer implementation of the Fourier transform, the signal must be represented in discrete form. Accordingly, the discrete Fourier transform of a time series S(n) having 'N' samples is given by:

$$S(k) = \frac{1}{N} \sum_{n=0}^{N-1} S(n)\, e^{(-j\,2\pi n\, k/N)} \qquad ....(3.3)$$

for n = 0,1,2,...,N-1 and K = 0,1,2,...m-1

where $S(k)$ is the k^{th} coefficient of the discrete Fourier transform

In order to compute the finite discrete Fourier transform of a series of N complex data points, N^2 operations are required. But, with the introduction of the fast Fourier transform (FFT), the number of operations has reduced to approximately $N \log_2 N$. Therefore the FFT is simply an algorithm that can compute the discrete Fourier transform much more rapidly than other available algorithms.

3.2 Fourier transform in heart sound analysis

The application of FFT in the analysis of biomedical data has been well reviewed by Yoganathan et al., [1976]. For a long time, frequency analysis of heart sounds has been carried out using band pass filters. Heart sound signals were scanned through several narrow band pass filters with different centre frequencies, the associated outputs recorded and used to plot the heart sound spectrum [Adolph, et al., Renner and Renner, 1979]. Single filters with tunable centre frequencies were used by some investigators. Sound spectrograph machines were also used to determine the spectral phonocardiograph, displaying frequency as a function of time with the darkness representing relative amplitude [Hearn et al., 1979].

Only recently, the Fast Fourier transform has found extensive application in the frequency analysis of heart sounds [Yoganathan, et al., 1976; Rukavina, 1979; Sarkady,

1980; Hearn et al., 1979]. In the conventional heart sound analysis procedure, using FFT, the phonocardiogram signal is digitized with appropriate sample rate (>2KHZ) and stored on computer disk files. The electrocardiogram signal is also digitized simultaneously for reference, as described in the previous chapter. A digital plot of the stored heart sound data is obtained and the first and second heart sound signals are identified by visual inspection of the digital plot. The desired heart sound is extracted for analysis by multiplying the heart sound signal data file with a smoothing window positioned appropriately.

Figures 3.1 a & c present the data file before and after it has been windowed by a Hamming type window (0.54 + 0.46 cos θ) (figure 3.1b). Windows are weighting functions applied to data to reduce the spectral leakage associated with finite observation intervals. Windows are used in spectral analysis to reduce the undesirable effects related to spectral leakage [Harris, 1978]. By applying a window to a data file, the data are brought to zero at the boundries. The windowed data file is shown in figure 3.1c ready for FFT analysis, and the resulting FFT spectrum is shown in figure 3.1d.

3.3 Use of moving window for heart sound analysis

The heart sound signals contain bursts of cardiac structural vibrational energies associated with distinct events in a cardiac cycle. As mentioned in the introductory

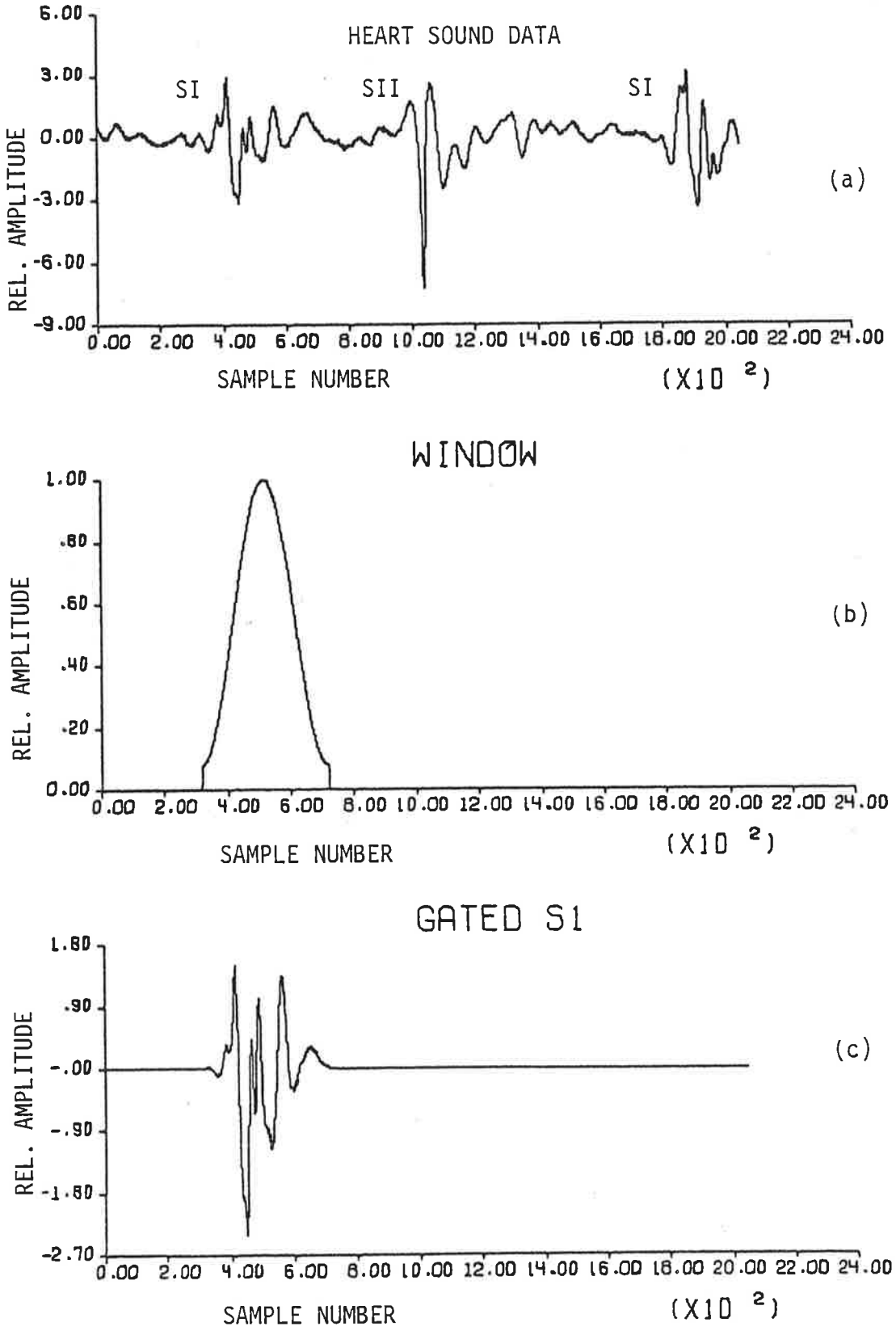

FIGURE 3.1 (a):PHONCARDIOGRAPHIC RECORD. (b):HAMMING WINDOW
(c):WINDOWED DATA

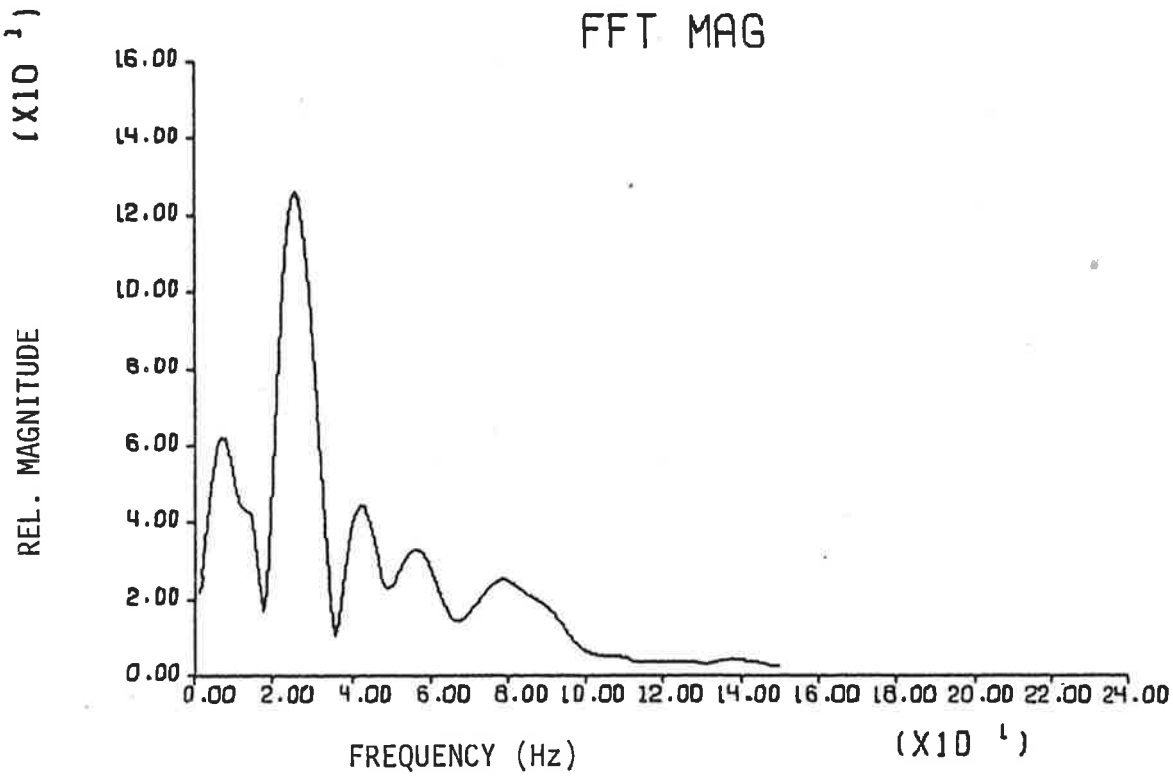

FIGURE 3.1(d) MAGNITUDE SPECTRUM OF FIRST HEART SOUND

chapter, the main concern will be on the two main complexes of heart sounds viz: first heart sound and second heart sound. Many cardiac elements vibrate at different instances of time contributing to the production of the first and second heart sounds.

The Fourier transform method (using FFT technique) has been applied to look at the spectral components of each heart sound. The spectra have shown reproducible peaks at certain frequencies. But there is no information on the precise correlation of the time of occurrence of the auscultatory signals with the spectral resonances.

For example the first heart sound is produced following the closure of mitral and tricuspid valves. The characteristics of the first heart sound are governed by the chronological sequence of events occurring during early ventricular systole. Hence, if the spectral peaks formed in first heart sound could be identified in terms of its time of occurrence, then a correlation could be made with the geometry and dynamics of cardiac elements contributing to the production of the sound in that time interval. This would enable identification of the physics-based genesis of the heart sound and thereby determine the physical properties of the vibratory cardiac structure, and correlation of the properties with the pathologies.

A possible method to extract some information on the time of occurrence of some of the frequency resonances found in the heart sound spectrum is to use a moving window. Using a

fixed width window and applying it to the heart sound data at appropriate locations to analyse the desired heart sound (first or second), by moving the window along the data record over a fixed number of samples successively. For each position of the window, a FFT can be performed to obtain a spectrum. The spectra could be displayed and the frequency peaks could be compared and related to the time of positioning of the window. The processing steps involved in this method are shown in figure 3.2. The sampled heart sound data is processed to remove any d.c. and normalised with respect to the RMS value.

The analysis of the digitized heart sound data is carried out as per the block diagram indicated in figure 3.2. Firstly the selection of an artifact-free segment of the phonocardiogram is accomplished by visual inspection of the time signal on the computer graphics screen. Digital Equipment Corporation's GT40 graphics processor has been used for this display. The next step is to select by visual inspection a starting point for analysis of the first or second heart sound. Then a time segment of the signal, with width of 200 samples (of approximately 80 m.seconds), beginning with the selected starting sample, is gated with a Hamming type window. Zeros are added to extend the signal file to a width of 1024 samples.

A fast Fourier transform of the windowed data is then obtained using the FFT algorithm available from the International Mathematics and Statistical Library (IMSL).

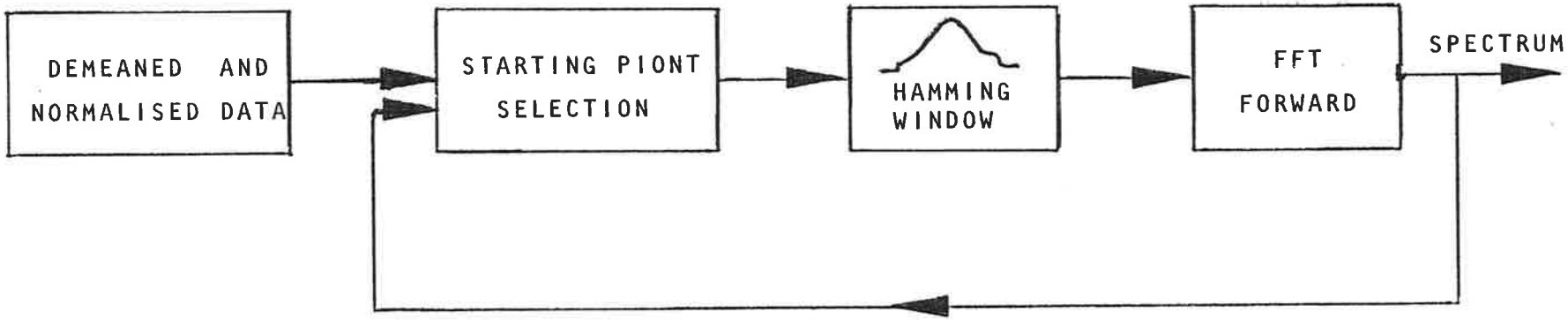

FIGURE 3.2 HEART SOUND PROCESSING STEPS

The IMSL library is available on the Adelaide university's CYBER 173 disk. The signal processing steps are carried out on the Cyber 173 computer interactively with a graphics terminal GT40. The window is then shifted in the time domain a distance of 30 samples (12 msecs) from the original starting point, and again multiplied with the data signal. The window signal is then processed as described above. The procedure is repeated until the required heart sound has been processed completely.

An interactive FORTRAN 66 program is developed to perform the FFT analysis based on the processing steps indicated in the schematic diagram of figure 3.2. The starting point, window width, number of samples over which the window has to be moved each time and number of window shifts are input interactively. The program performs the FFT analysis for each amplitude spectra for all the window positions.

Figure 3.3 shows a typical heart sound signal (of a normal adult) and the spectra for 15 positions of the window applied on the first heart sound (SI) starting at sample number 2350, as displayed on the G.T.40 graphics screen. The spectra clearly display a variation in amplitudes of frequency peaks. Figure 3.4 is the digital plot of the file containing the spectra for 15 window positions. The FFT is performed on the 1024 point data as discussed earlier. The FFT returns 512 coefficients corresponding to a maximum frequency of half the sample rate. The sample rate used in

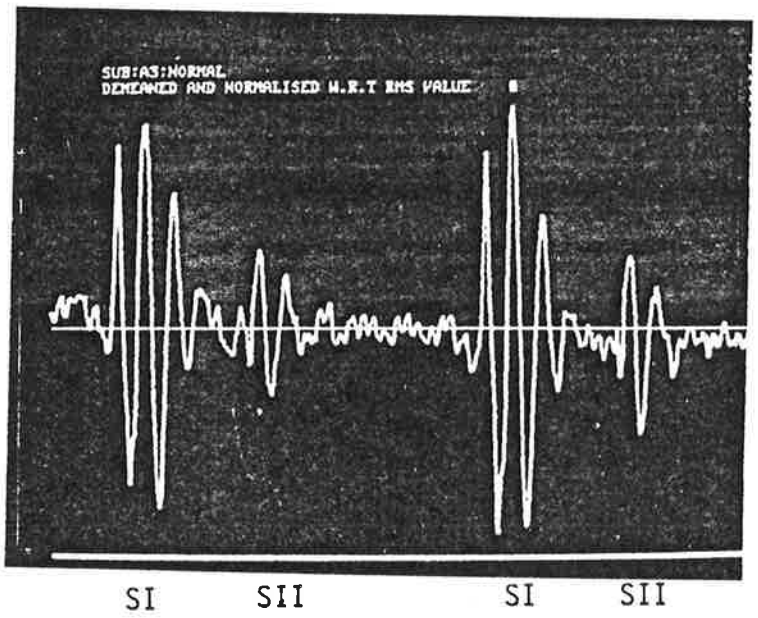

(a)

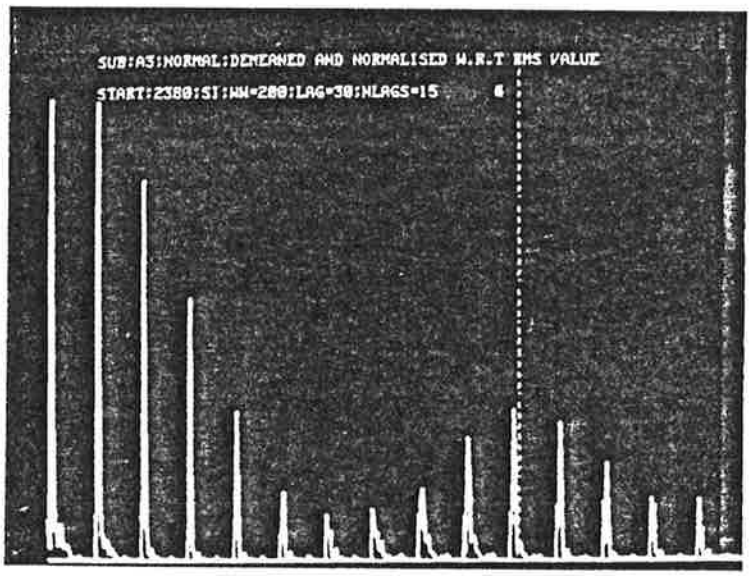

(b)

FIGURE 3.3 (a):HEART SOUND SIGNAL (NORMAL SUBJECT)

(b):SPECTRA OF FIRST HEART SOUND FOR MULTIPLE WINDOW POSITIONS. WINDOW WIDTH:200 SAMPLES

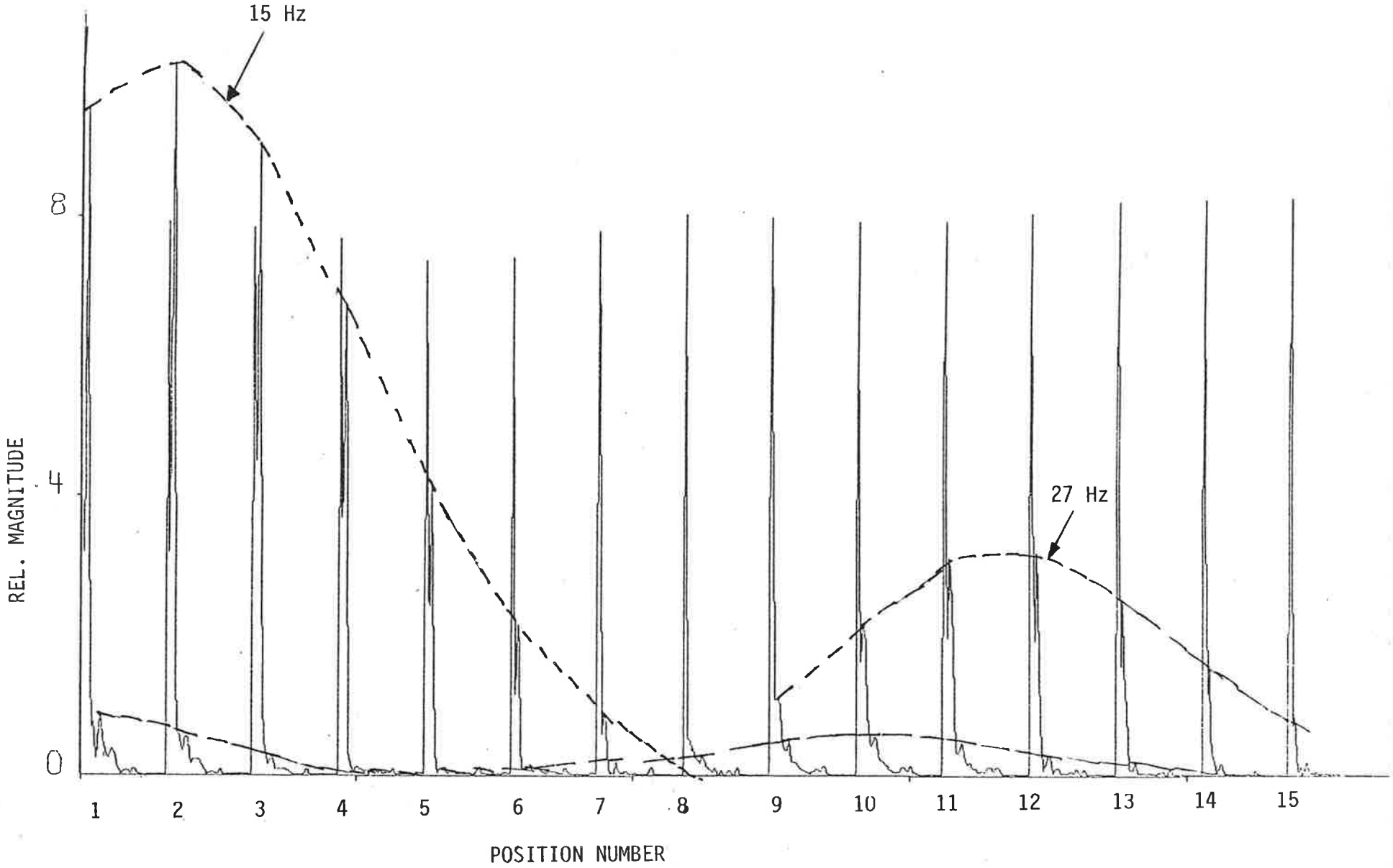

FIGURE 3.4 SPECTRA FOR 15 WINDOW POSITIONS

PRINTED IN AUSTRALIA 7/80 CHART No. JS220

the present case is 2500HZ. Therefore the frequency resolution is approximately 2.44HZ/coefficient.

Figure 3.5 shows the graphics display of the spectra, for different positions, indicating the frequency peak variations. The time difference between two successive window positions is 30 samples, i.e. 12 milli-seconds (msecs) approximately. The dotted line in figure 3.4 represents the contour of the same frequency peaks. Some of the window positions in figure 3.4 are displayed much better in figures (3.6) and (3.7), by plotting the data using a digital plotter.

Figure 3.8 shows the frequency spectra of the first heart sound for another normal subject, obtained by using a moving window of the same width and shape as in the previous case. This clearly indicates the occurrence of a low frequency resonance around 15 HZ during the onset of SI. This resonance disappears approximately 50 msecs later and is followed by the appearance of two resonances around 24HZ and 43 HZ. These resonances grow in amplitude for about 40-50 msecs before they start decreasing in amplitude. The 43 HZ oscillations persist somewhat longer than the 24 HZ as indicated in the figure 3.8.

The second heart sound spectra are represented in figure 3.9 for 8 successive window positions. This indicates clearly a 24 HZ resonance throughout and a 35 HZ resonance starting approximately after 25 msecs and disappearing much earlier. Frequency peaks in the low frequency range have

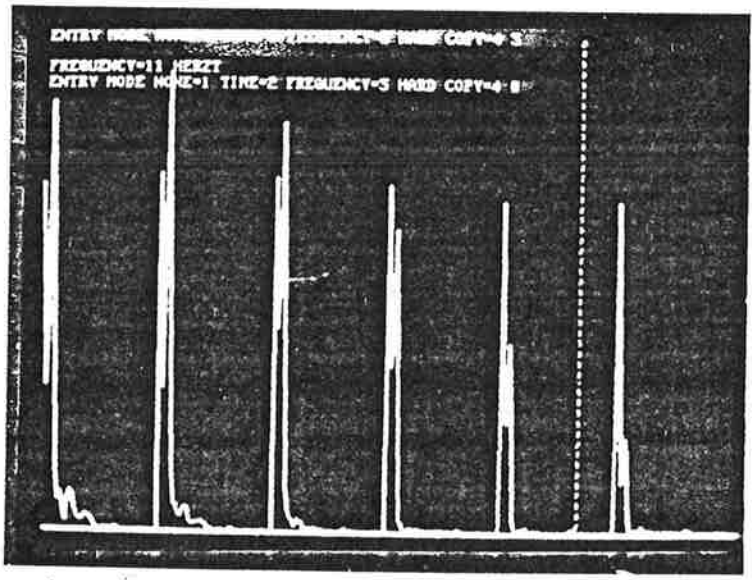

1 2 3 4 5 6

(a) WINDOW POSITIONS 1-6

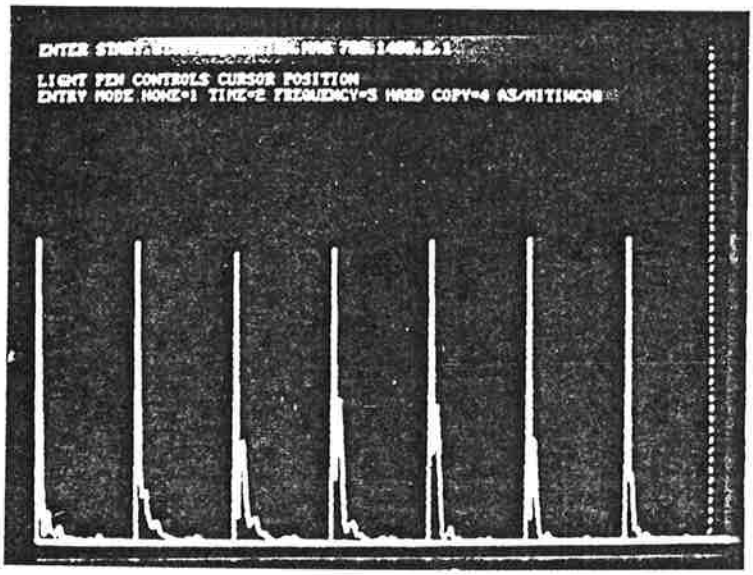

8 9 10 11 12 13 14

(b) WINDOW POSITIONS 8-14

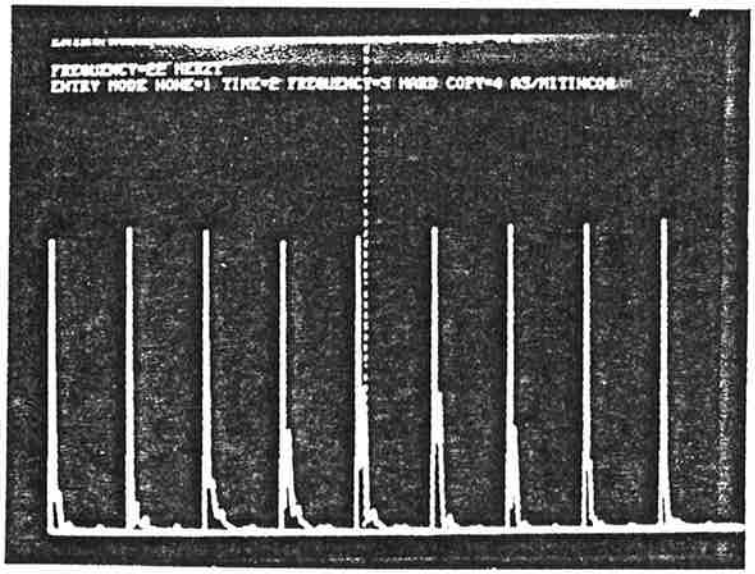

7 8 9 10 11 12 13 14 15

(c) WINDOW POSITIONS 7-15

FIGURE 3.5 COMPUTER GRAPHICS DISPLAY OF SPECTRA OF SI FOR MULTIPLE WINDOW POSITIONS.

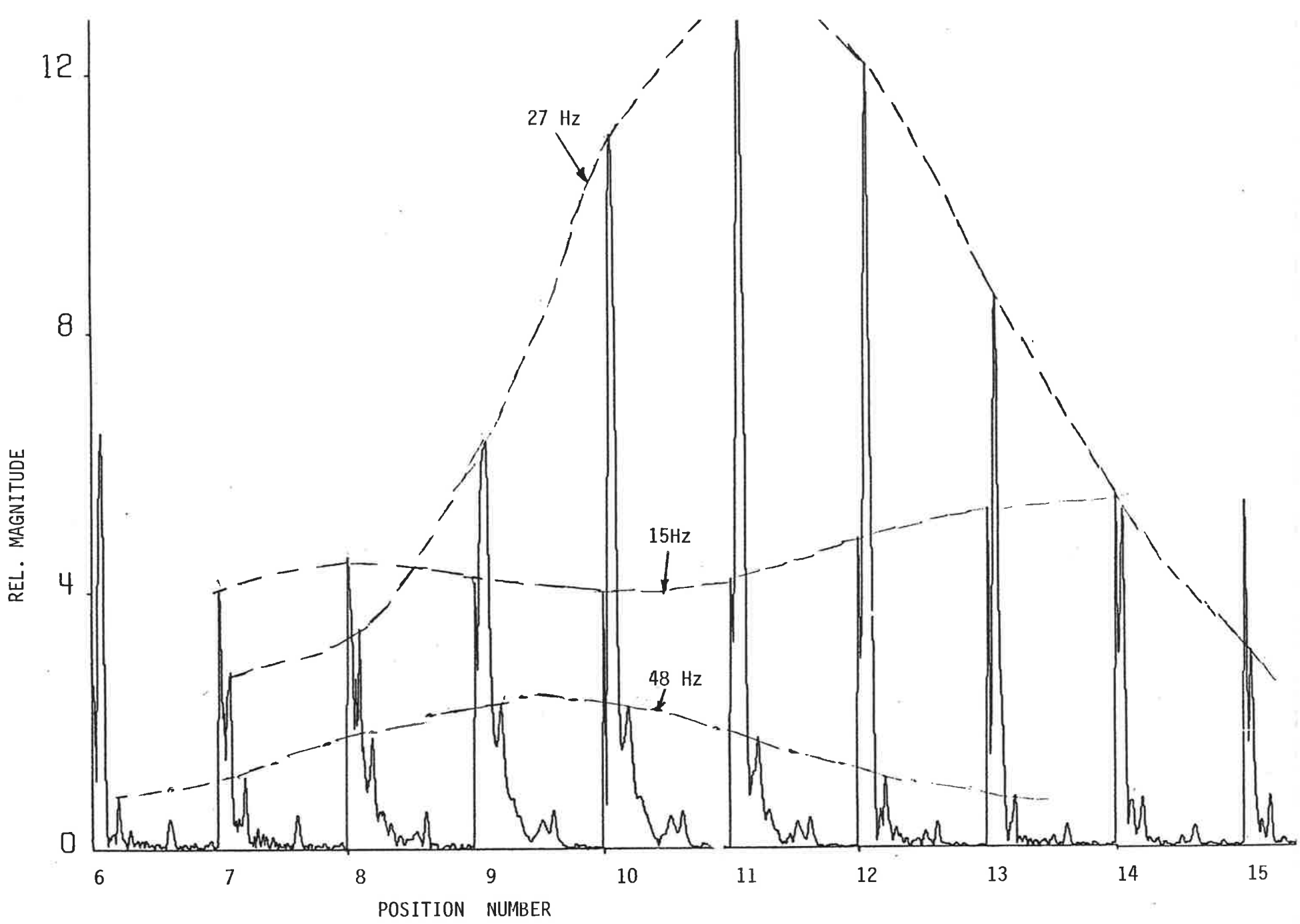

FIGURE 3.6 SPECTRA FOR WINDOW POSITIONS 6- 15

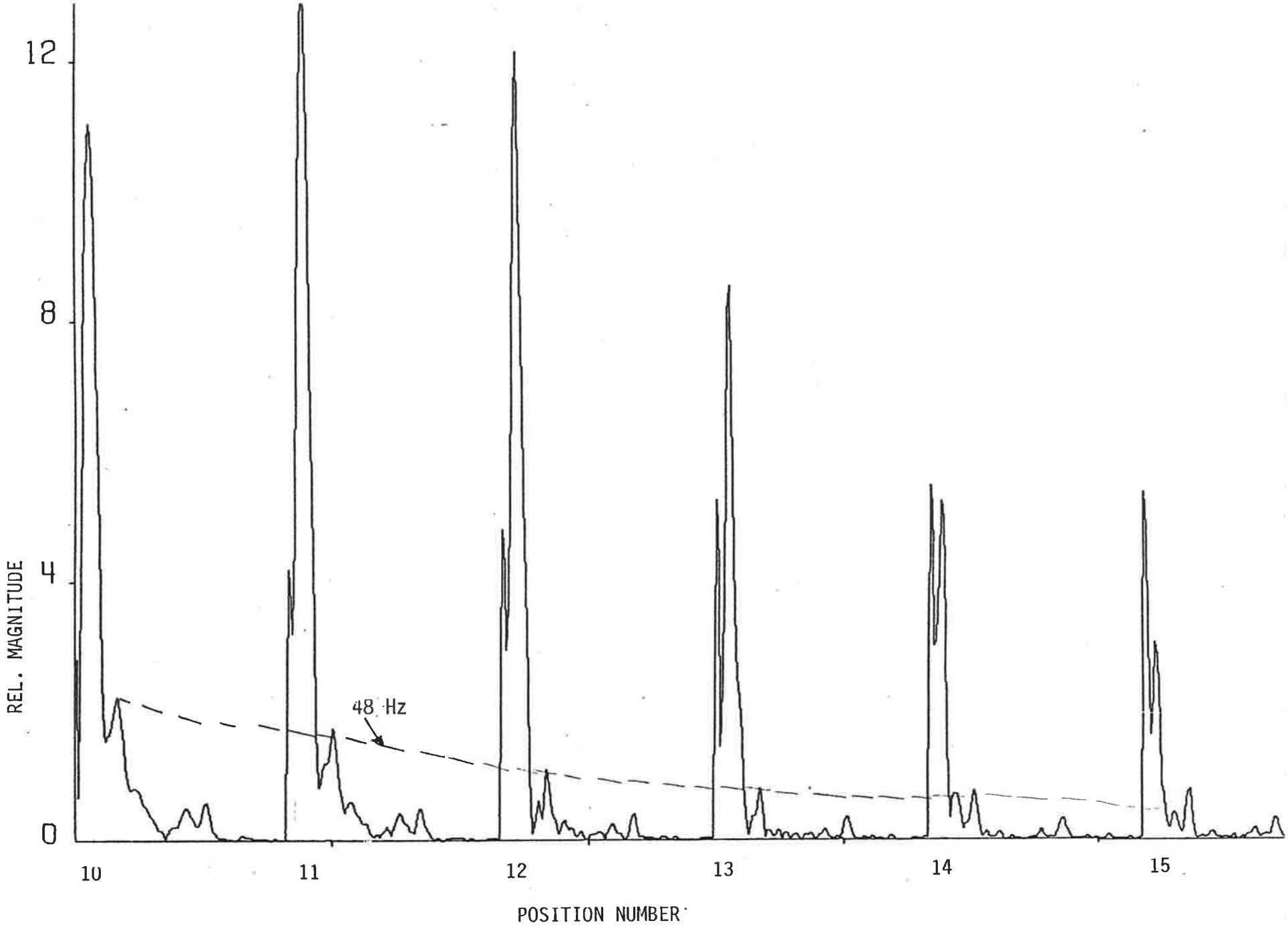

FIGURE 3.7 SPECTRA FOR WINDOW POSITIONS 10 - 15

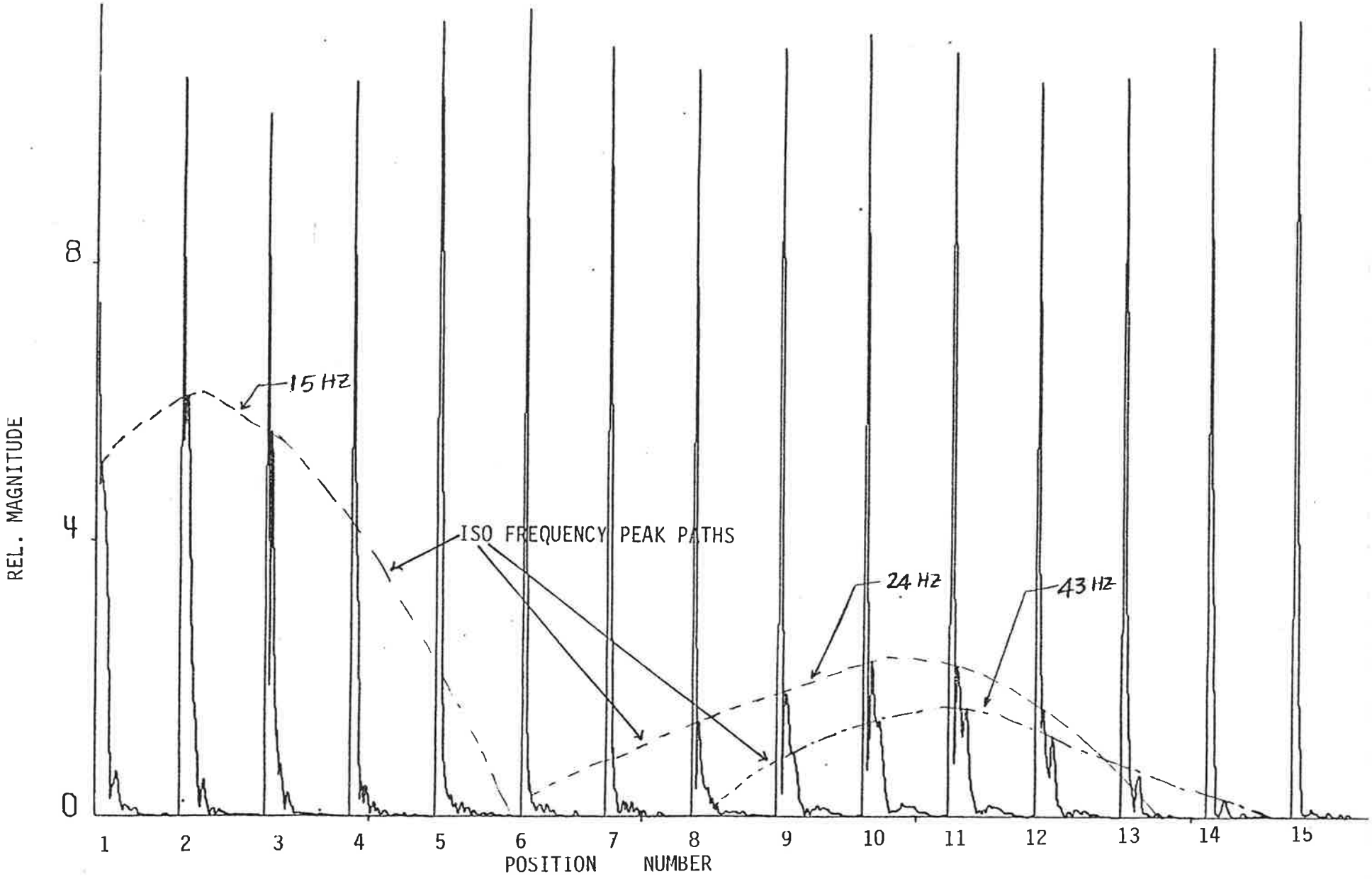

FIGURE 3.8 FREQUENCY SPECTRUM OF S_1.

SPECTRUM FOR EACH SUBSEQUENT WINDOW POSITION SHOWN. NUMBER OF POSITIONS: 15

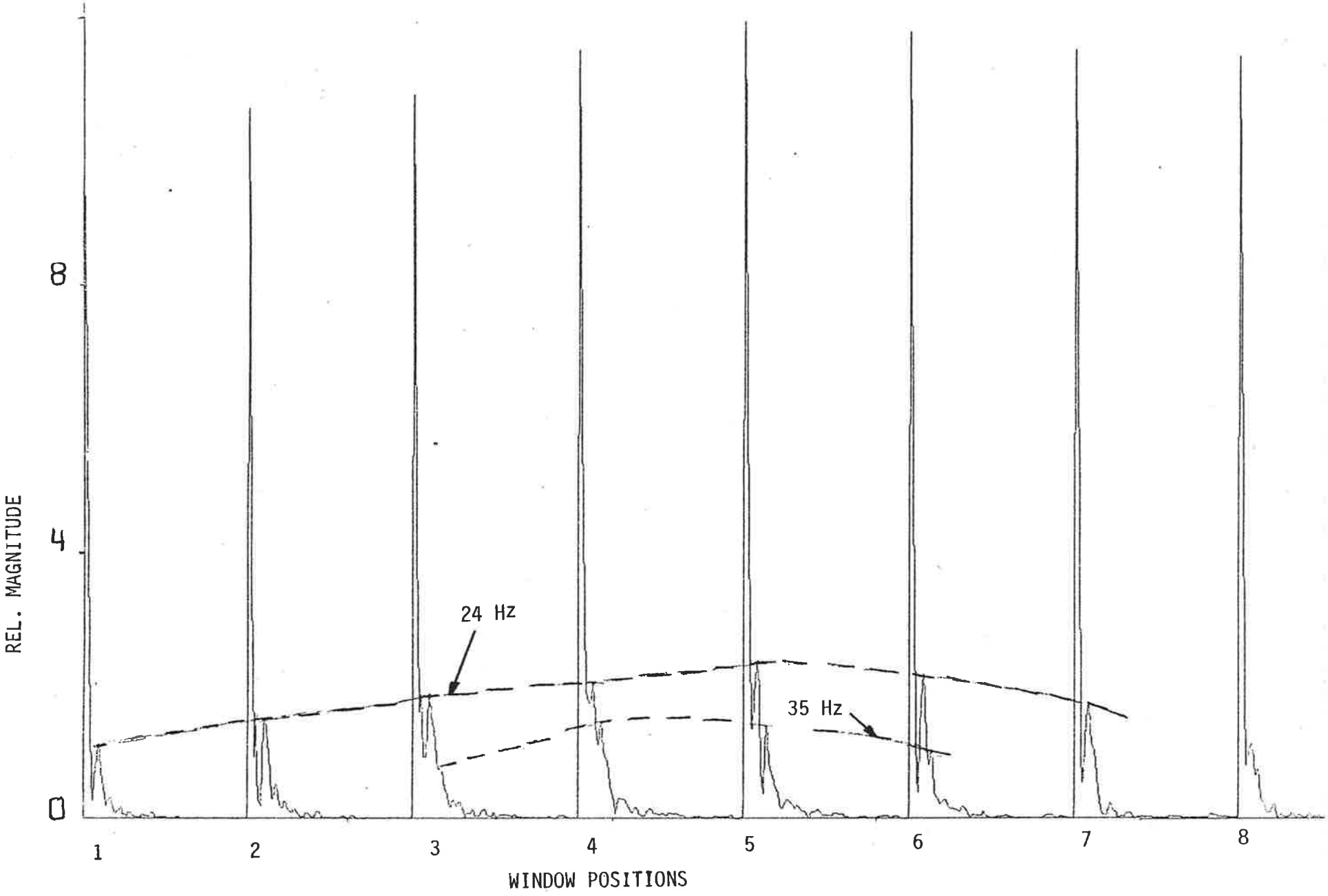

FIGURE 3.9 SPECTRA OF SECOND HEART SOUND USING MULTIPLE WINDOWS

been observed by previous investigators [Yoganathan, et al, 1976; Hearn, et al., 1979] but the exact origins of these resonances are as yet undetermined. Using the technique described here, it may be possible to say when a particular peak appears and disappears. This information may definitely be valuable in determining the time of occurrence of a particular resonance in relation to the cardiac cycle, and when correlated with associated hemodynamic events taking place during that phase of the cardiac cycle could provide insights into the etiology of these heart sounds.

3.4 Three dimensional spectral representation of heart sounds:

By tracking the spectral peaks as they develop with time one can thus examine the appearance and disappearance behaviour of the various frequency components in the time domain. Instead of displaying spectral data obtained from moving window analysis, as indicated in figures 3.6 to 3.8, where the spectra has been displayed successively on a two dimensional axis, one could provide the information more resourcefully in a three dimensionsal space of amplitude, frequency and time. Figure 3.9 shows the 3-dimensional plot of spectral distribution of the first heart sound (SI) for the same subject. Figure 3.10 indicates distinct resonances by a dominating frequency at different instants. The time difference between the two observed peak resonances in figure 3.10 is approximately 45 msecs. Figure 3.11 exhibits a similar trend for SII in another subject.

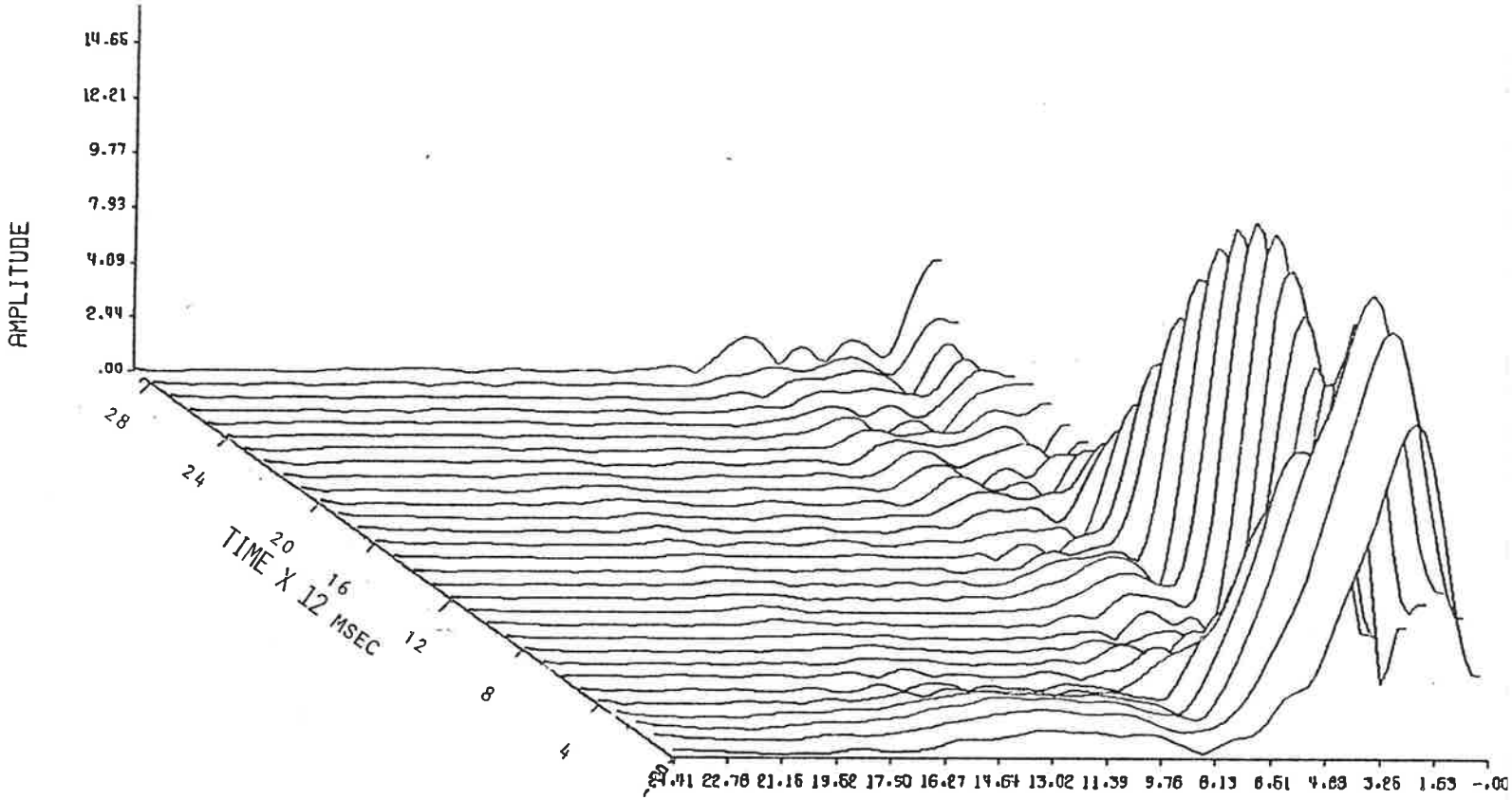

FIGURE 3.10 3-DIMENSIONAL SPECTRAL DISTRIBUTION OF SII
(SUBJECT 1)

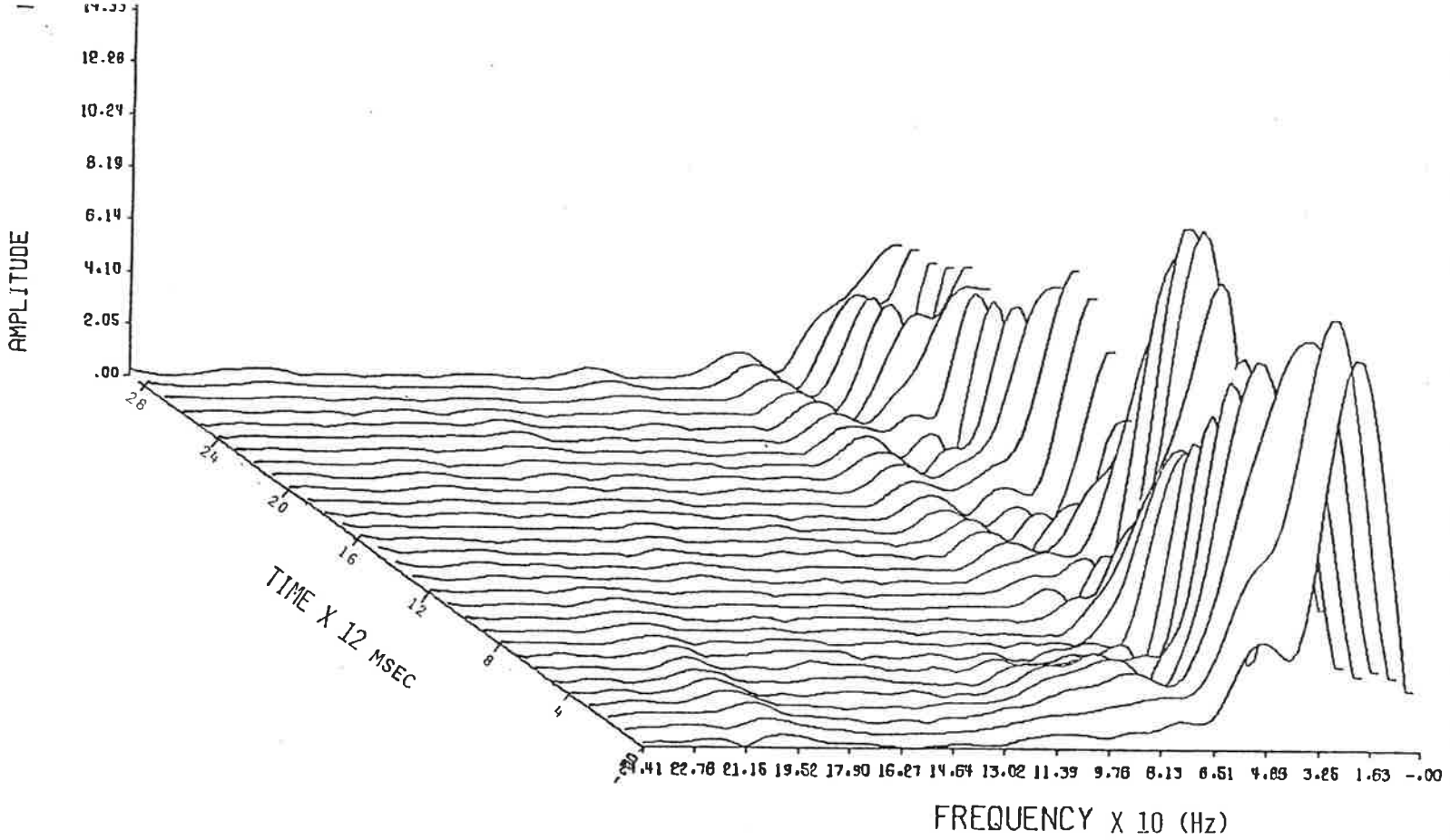

FIGURE 3.11 3-DIMENSIONAL SPECTRAL DISTRIBUTION OF SII (SUBJECT 2)

An interesting spectral distribution of SII is seen in figure 3.12 for a subject with ejection clicks. This pattern appears quite different from other subjects studied by this technique. This 3-dimensional representation of the spectra of successive time segments of first and second heart sounds may yield interesting features characteristic of specific cardiac abnormalities. The mechanisms involved in the production of sounds can be studied by (i) first correlating these resonant frequencies with those derived from vibration analyses of cardiac structures deemed to contribute to the heart sound production (ii) identifying the vibratory structure with the heart sounds resonant frequencies, and then (iii) obtaining their time of vibration by the above described technique of peak frequency tracking.

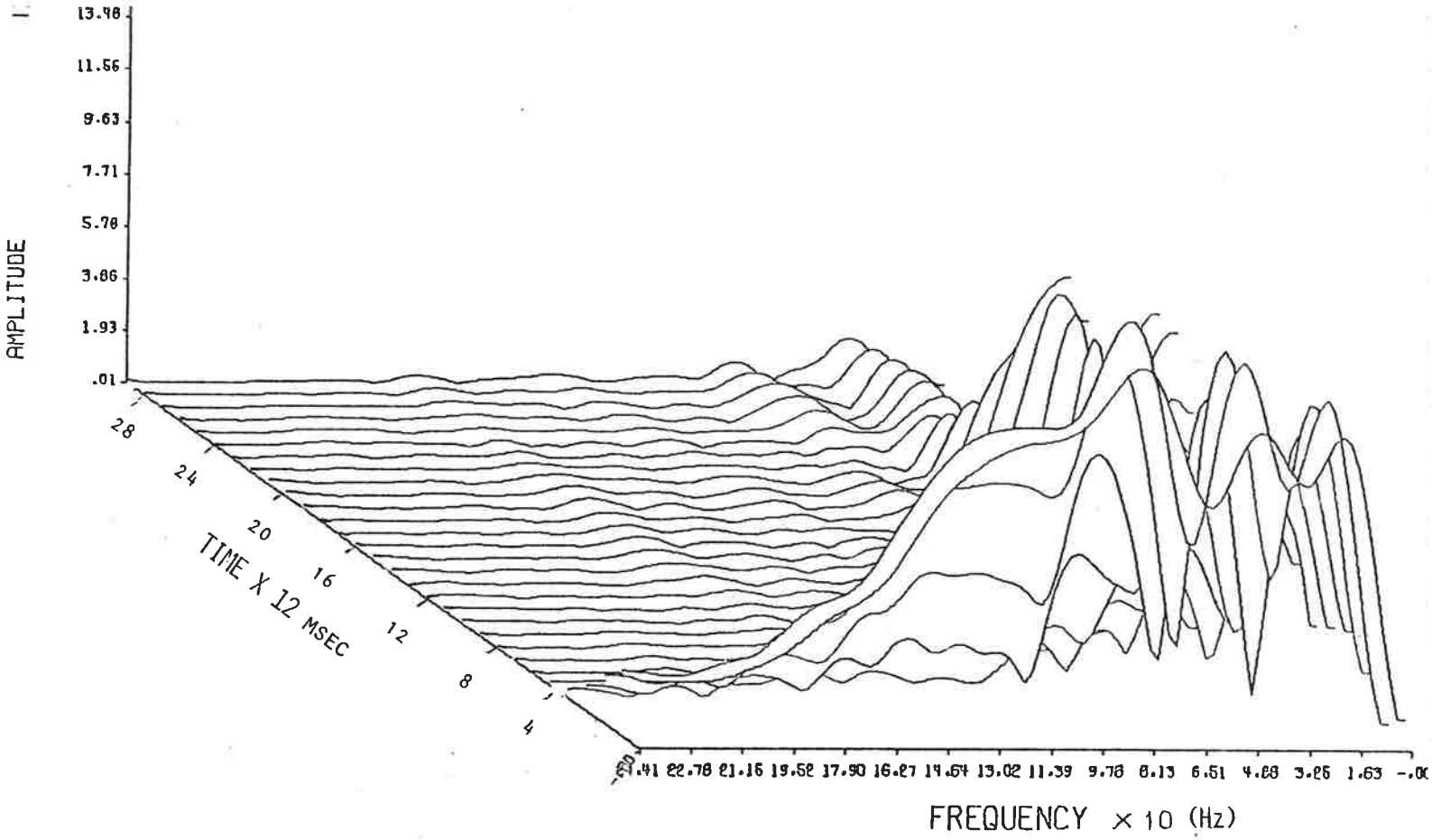

FIGURE 3.12 3-DIMENSIONAL SPECTRAL DISTRIBUTION OF SII (SUBJECT 3 PATHOLOGICAL)

CHAPTER 1V

LINEAR PREDICTION TECHNIQUE APPLIED TO HEART SOUND ANALYSIS

4.1. Introduction

Linear prediction is an aspect of time series analysis. In Biomedical Engineering, it has been extensively used for the analysis of speech signals, vocal tract modelling etc. [Atal and Hanauer, 1971; Haskew, et al., 1973; Markel and Gray, 1976]. The use of linear prediction filters (LPF) has enhanced the detectability of narrow band signals in broad band noise [Alexander and Zeile, 1977]. Linear prediction technique has also assumed its importance in data compression and transmission. In this chapter, the application of linear prediction to heart sound analysis will be discussed.

The underlying philosophy of linear prediction rests on the idea that a signal sample can be estimated by a weighted linear sum of past samples. The weights are known as linear prediction coefficients and they are estimated by a least squares minimization of the error between the actual signal sample and linearly predicted signal sample for a suitable time period of observation.

The exposition of linear prediction in the spectral analysis of speech is due to Makhoul [1973, 1975]. The formulation of linear prediction in speech processing is well documented in the literature [Saito and Itakura, 1978]. The

linear prediction spectrum has been found to be superior in comparison with other spectral analysis methods [Rabiner and Schafer, 1978].

4.2 Linear prediction coding (LPC)

The linear prediction analysis technique is also known as linear prediction coding (LPC). In LPC, a time series 'S_n' is predicted from a linearly weighted summation of its past values. If 'S_n' is the predicted value of the n^{th} sample, then,

$$\bar{S}_n = a_1 S_{n-1} + a_2 S_{n-2} + \ldots + a_i S_{n-i} \qquad \ldots\ldots(4.1)$$

where $1 \leq i \leq P$, P is the predictor order

'a_i' s are the predictor coefficients.

This means to predict any particular sample of a given time series, we need only the past values of the time series and each predicted sample is a summation of weighted past 'p' values. The error between the predicted and the actual sample is given by:

$$e_n = S_n - \bar{S}_n = S_n - \sum_{i=1}^{P} a_i S_{n-i} \qquad \ldots\ldots(4.2)$$

The total error "energy" 'E' is obtained by summing up the error energies,

$$E = \sum_n e_n^2 = \sum_n (S_n - \sum_{i=1}^{P} a_i S_{n-i})^2 \qquad \ldots\ldots(4.3)$$

The criterion for obtaining the weighting factors (the 'a 's) is that 'E' is a minimum. This is achieved by
i
equating the first partial derivative of 'E' with respect to each predictor coefficient to zero. This leads to a set of P equations in P unknowns which can be solved for 'a '(s).
i

$$\text{putting } \frac{\partial E}{\partial a_k} = 0, \quad 1 \leq k \leq P \qquad \ldots\ldots(4.4)$$

$$\text{i.e., } \sum_{i=1}^{P} a_i \sum_n S_{n-i} S_{n-k} - \sum_n S_n S_{n-k} = 0 \qquad \ldots\ldots(4.5)$$

$$\sum_n S_{n-k} S_n = \sum_{i=1}^{P} a_i \sum_n S_{n-i} S_{n-k} \quad \text{for } 1 \leq k \leq P \qquad \ldots\ldots(4.6)$$

for $-\infty \leq n \leq \infty$, equation (4.6) becomes

$$R(k) = \sum_{i=1}^{P} a_i R_{(k-i)} \quad \text{for } 1 \leq k \leq P \qquad \ldots\ldots(4.7)$$

$$\text{where } R(k) = \sum_{n=-\infty}^{\infty} S_n S_{n+k}$$

is the autocorrelation of signal 'S '
n

Two major methods of linear prediction coding have been developed, based on the range of summation in the above equations, to evaluate the predictor coefficients. These methods are known as autocorrelation and covariance methods. Makhoul and Wolf [1972] have discussed these techniques in detail, and since then several attempts have been made to

develop computational algorithms to implement the above two methods.

In the autocorrelation method, the range of summations is $-\infty < n < \infty$; in the covariance method, the range is $0 \leq n < N-1$. The signal S_n does not require special definition outside the range $-P < n \leq N-1$. The autocorrelation and covariance methods of evaluating the predictor constants are described in the appendix C.

Expressing equation (4.2) in the 'Z' domain, we have

$$E(Z) = S(Z) \left[1 - \sum_{i=1}^{P} a_i Z^{-i}\right] \qquad \ldots\ldots(4.8)$$

If the predictor order 'P' is sufficiently large, then substantially all correlation is removed from the error e_n, and this yields a white (constant spectrum) signal. The system,

$$H_I(Z) = \frac{E(Z)}{S(Z)} = 1 - \sum_{i=1}^{P} a_i Z^{-i} \qquad \ldots\ldots(4.9)$$

defined from equation (4.8), is an inverse filter whose spectral transformation is the inverse of the generating filter $H_G(Z)$ that would produce $S(Z)$ by filtering a white signal,

i.e.

$$H_G(Z) = \frac{1}{H_I(Z)} = \frac{S(Z)}{E(Z)} = \frac{1}{1 - \sum_{i=1}^{P} a_i Z^{-i}} \qquad \ldots\ldots(4.10)$$

The structure of this signal generating filter is shown in figure 4.1.

Therefore, once the predictor coefficients are evaluated for any given signal, the LPC spectrum is simply obtained from the response of the generating filter indicated in figure 4.1.

4.3 Linear prediction in heart sound analysis:

LPC has been used earlier in other areas, such as industrial time series analysis [Box and Jenkings, 1970) and in the analysis of seismic signals [Robinson 1967]. In the Biomedical area, the LPC has found its use in speech processing as well as in the analysis of electroencephalogram (EEG) signals [Gersch, 1970; Fenwick et al., 1971]. Spectral analysis of cardiovascular sounds based on the autoregressive model has been attempted by Campbell [1978]. Linear prediction analysis has been used successfully to detect the first and second heart sounds in cases of noisy environments by tracking the spectral levels [Iwata, et al., 1980].

The heart sound production mechanism has a similarity to that of speech production mechanism, in the sense that the resulting acoustic signals are due to the resonance of various anatomical structures. In speech, the vocal tract with varying structural cross-sectional area resonates to glottal excitation, whereas in heart sounds the various structures of the heart such as the heart valves,

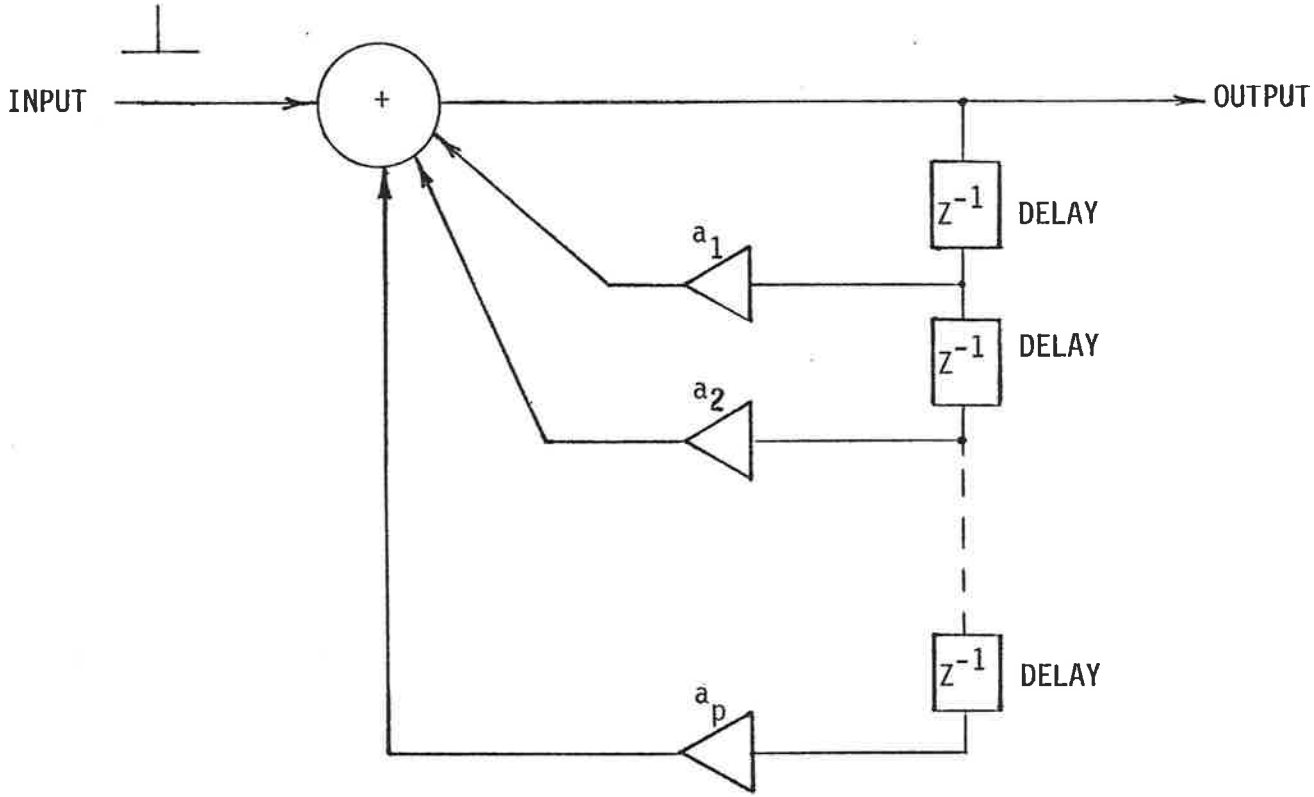

FIGURE 4.1: DIGITAL STRUCTURE OF GENERATING FILTER

heart muscles and chamber walls, resonate at different instances to pressure excitatory functions.

As the linear prediction analysis is found to be more useful in extracting spectral characteristics [Rabiner and Schafer, 1978], an attempt has been made here to apply this LPC technique to process the heart sound signals. The autocorrelation method has been used to solve for the predictor coefficients in this study; Durbin's algorithm [1959] is used to compute the 'a_i's.

It is necessary, for valid LPC spectral analysis, that the spectrum of the heart sound signal occupy a substantial part of the Nyquist frequency range of '1/2 T' HZ, where 'T' is the sampling rate. Before developing a procedure for the LPC spectral analysis of heart sounds, consideration must be given to the following factors: spectral range, sampling rate of the heart sound signals, the duration of the desired heart sound segment (ie first or second heart sound), the effects of windowing, requirement of preprocessing and most importantly, the choice of predictor order. These factors are discussed below.

The spectral range of the heart sound signal has been discussed in the earlier chapters. Heart sound frequency peaks are found in the frequency ranges up to 500 HZ. In this study, a sample rate of 2042 HZ has been used which is much higher than the Nyquist frequency. The sampling rate of the data files can be reduced if necessary by retaining only one from N signal samples and discarding the remaining N-1

samples. This expands the effective frequency range by N. This would in fact enable the LPC analysis to be applied over a desired frequency range of the signal spectrum. For example, the first heart sound has reproducible frequency peaks in the range 20-150 HZ. In order to evaluate the spectrum in this range, the sample rate has to be reduced so that the inverse filter can use all of its coefficients to represent the desired portion of the spectrum. In a later chapter, a different method is discussed to estimate the spectrum in selected frequency ranges without having to reduce the sampling rate.

The duration of the desired heart sound signal segment can vary from subject to subject, depending on the age and other physiological conditions of the subject. The desired heart sound signal is normally extracted by applying an appropriate window as discussed in chapter 3. The window width is selected by visual inspection of the desired heart sound to be analysed. Pre-processing of the signals, as discussed in chapter 3, is a general requirement to make the data samples more suitable for analysis.

As regards the choice of predictor order, it is desirable to have as few poles as possible. The effect of varying the predictor order is discussed in a later section. The number of poles required for an exact spectral modelling of the signal would depend on the number of frequency resonances. In the case of vocal tract modelling using speech signal, it has been possible to evaluate the predictor order based on

the length of vocal tract, velocity of sound in the vocal tract and the sample frequency [Atal and Hanauer, 1971; Wakita, 1973]. In the case of heart sounds, the acoustic signal is transmitted to the chest from more than one source. The heart sound signals do not travel through a confined tube. It is rather difficult to determine the choice of the predictor order quantitatively.

The predictor order for the heart sounds may be estimated from the expected number of frequency resonances below the folding frequency [Rabiner and Schafer, 1975; Makhoul and Wolf, 1972]. One complex pole pair is required to represent each frequency peak. It may be supposed, if there are only six resonant peaks in the frequency range 20-120 HZ of the first heart sound, that a predictor order of 12 would normally be enough to represent the first heart sound signal in this frequency range. However, the choice of predictor order to represent the spectra of the first or second heart sound should be based on the statistical average of a number of peaks seen in the spectra of respective sounds.

4.4 Pole enhancement

In the spectra of systems that have low-Q (high bandwidth) poles, it is often difficult or even impossible to distinguish visually between several peaks. In the case of a myocardial infarction, it was found that the spectral peaks get flattened [Renner and Renner, 1979]. This means the resonant peak would have a low-Q. It has also been observed

that the quality (Q-factor or fractional bandwidth) of the spectral peaks of the first heart sound has a high correlation with the severity of infarction due to inhomogeneity of the myocardial structure in the case of infarction [Renner and Renner, 1979]. In this situation, the simplest way to enhance the dormant peaks of the spectrum is to change the radius of the unit circle, i.e. to evaluate the Z-transform on a unit circle closer to the poles of the spectral model. Markel and Gray [1976] have indicated a technique to enhance the poles. This is achieved by replacing each predictor coefficient a_i by $a_i r^i$, where $r = e^{-\pi B_o T}$ (B_o being the bandwidth reduction of each resonance and T the sample interval).

4.5 LPC spectral analysis procedure

Once the phonocardiographic data is available on the CYBER 173 computer disk (as described in chapter two), this data file (stored on computer disk) is plotted for visual inspection or displayed on the GT40 graphics terminal along with the corresponding ECG signal. The desired heart sound is identified and then extracted by multiplying the data file with an appropriate window function. A Hamming window has generally been used in this study.

The windowed heart sound data is selectively filtered so that the signal contains frequency components in the frequency range of interest. The selective filtering is done by simply performing a forward discrete Fourier transform

(DFT) operation on the windowed data, discarding the coefficients outside the frequency range of interest and then performing a reverse DFT. The selectively filtered data file is then used in the LPC analysis.

The predictor coefficients are extracted from the filtered data. This is the next step. For a specified predictor order, the LPC coefficients are computed from the filtered data using the autocorrelation method. Once the predictor coefficients are estimated from the filtered data, then performing Fourier transformation on the data $1 + \sum_{i=1}^{P} a_i$ yields an inverse spectrum of the signal. Pole enhancement may be performed by modifying the predictor coefficients as described earlier. The signal processing steps involved in this procedure are indicated in figure 4.2. The magnitude spectrum of a typical second heart sound, obtained using conventional FFT technique, is indicated in figure 4.3; this spectrum is plotted for a frequency range up to 200 HZ.

Figure 4.4 shows the magnitude spectrum of the same second heart sound signal obtained through LPC analysis. The predictor order used was 19. The effect of pole enhancement is demonstrated in figure 4.5. The solid line shows the log magnitude spectrum for a second heart sound signal obtained using a predictor order of 22. The dotted line (with symbols $\triangleright$) demonstrates the LPC spectrum for the same signal with order 22, with the predictor coefficients modified to

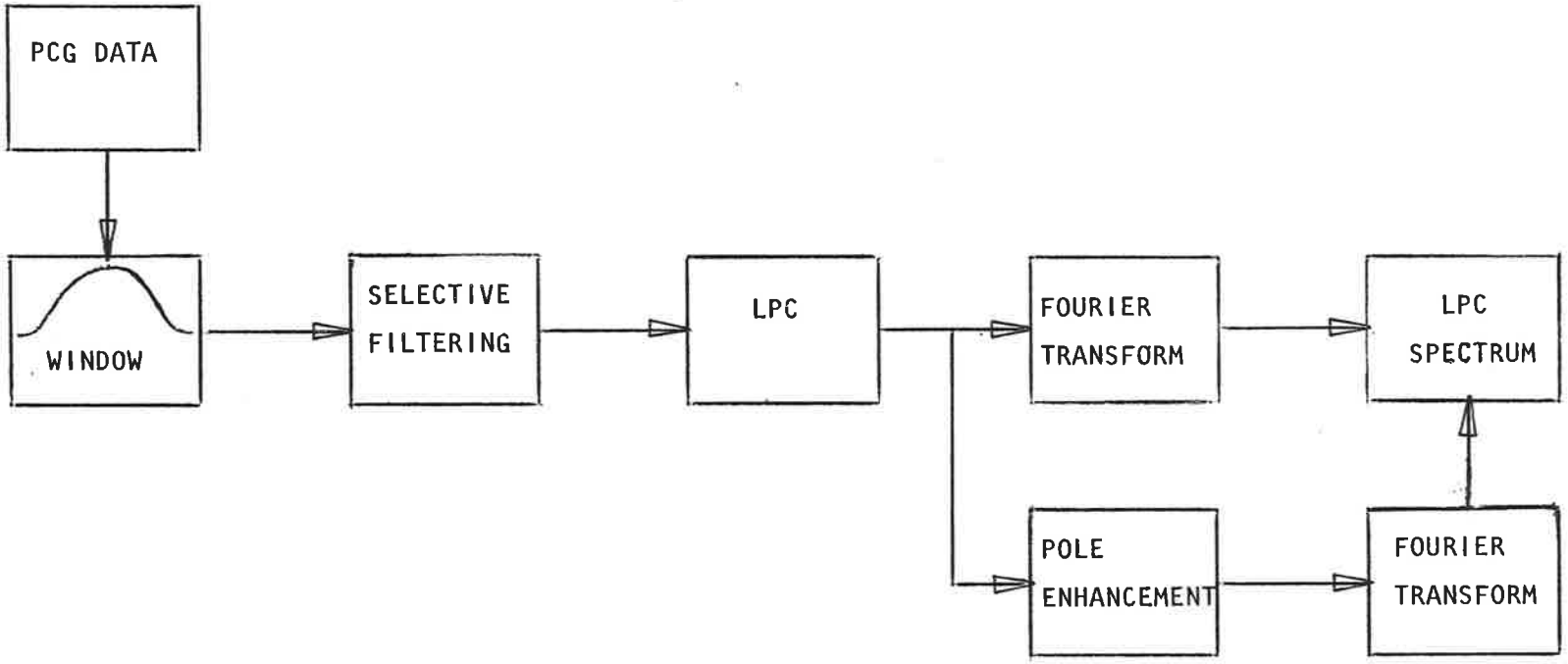

FIGURE 4.2: LPC SIGNAL PROCESSING PROCEDURE

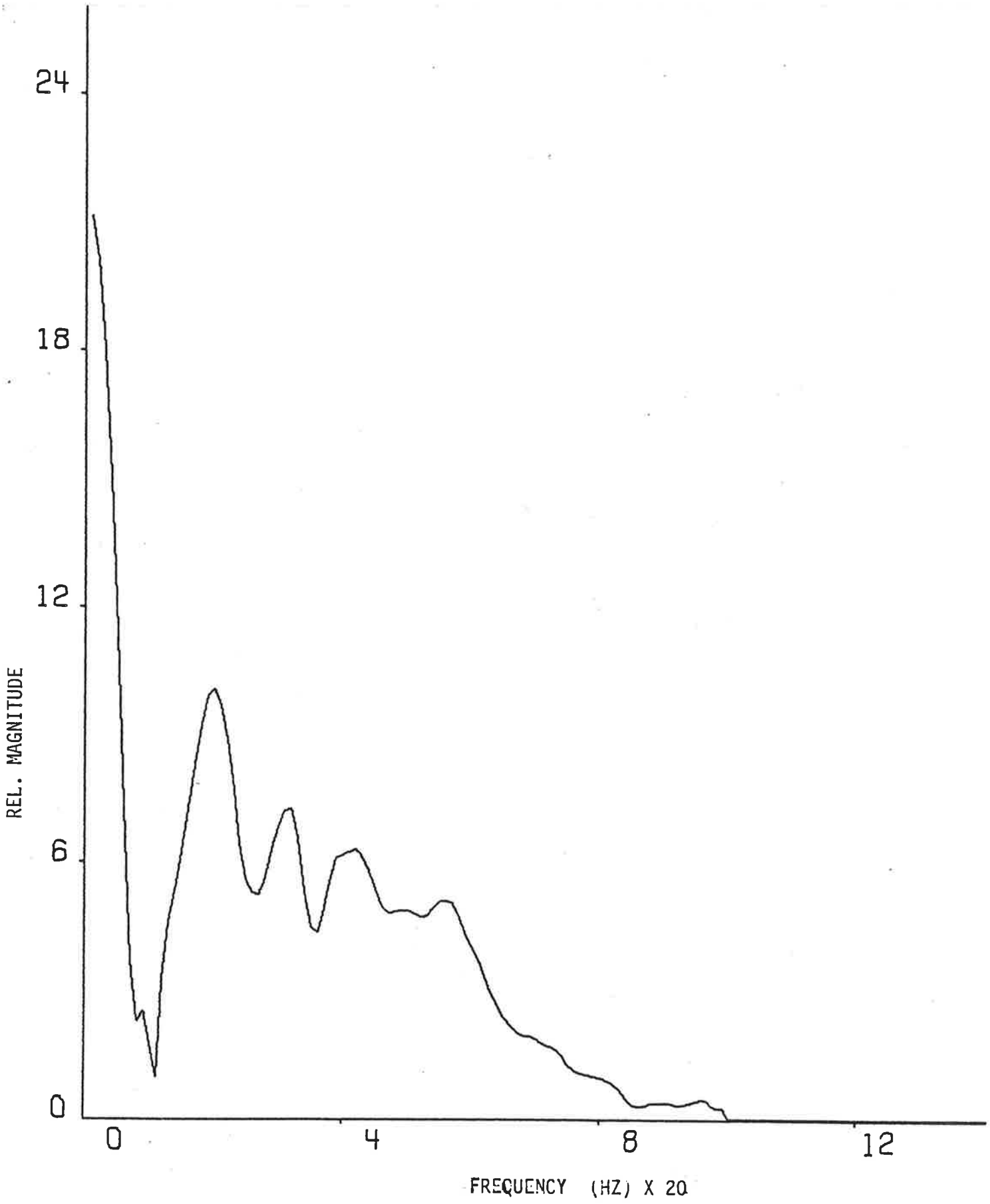

FIGURE 4.3 MAGNITUDE SPECTRUM

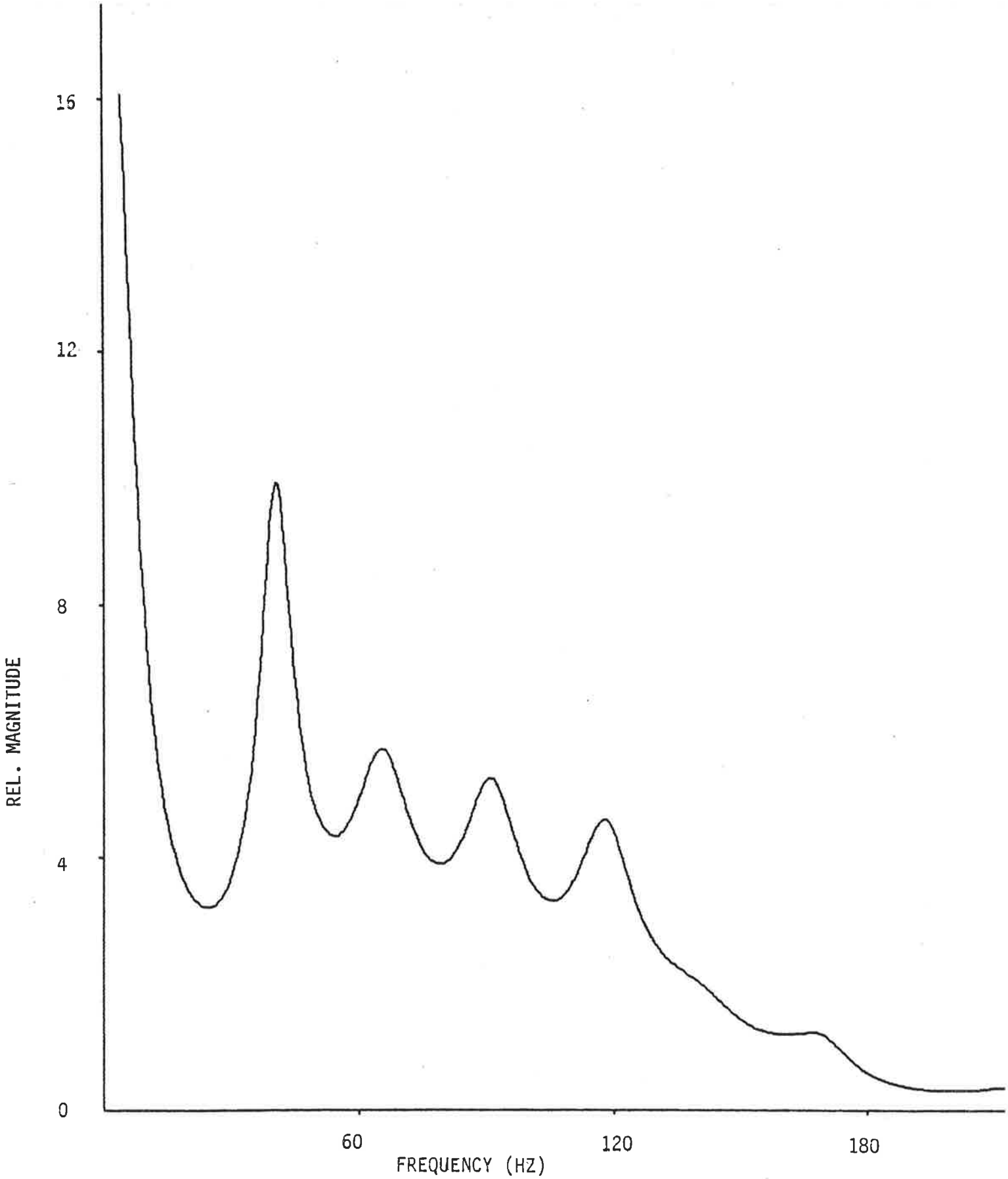

FIGURE 4.4 LPC SPECTRUM

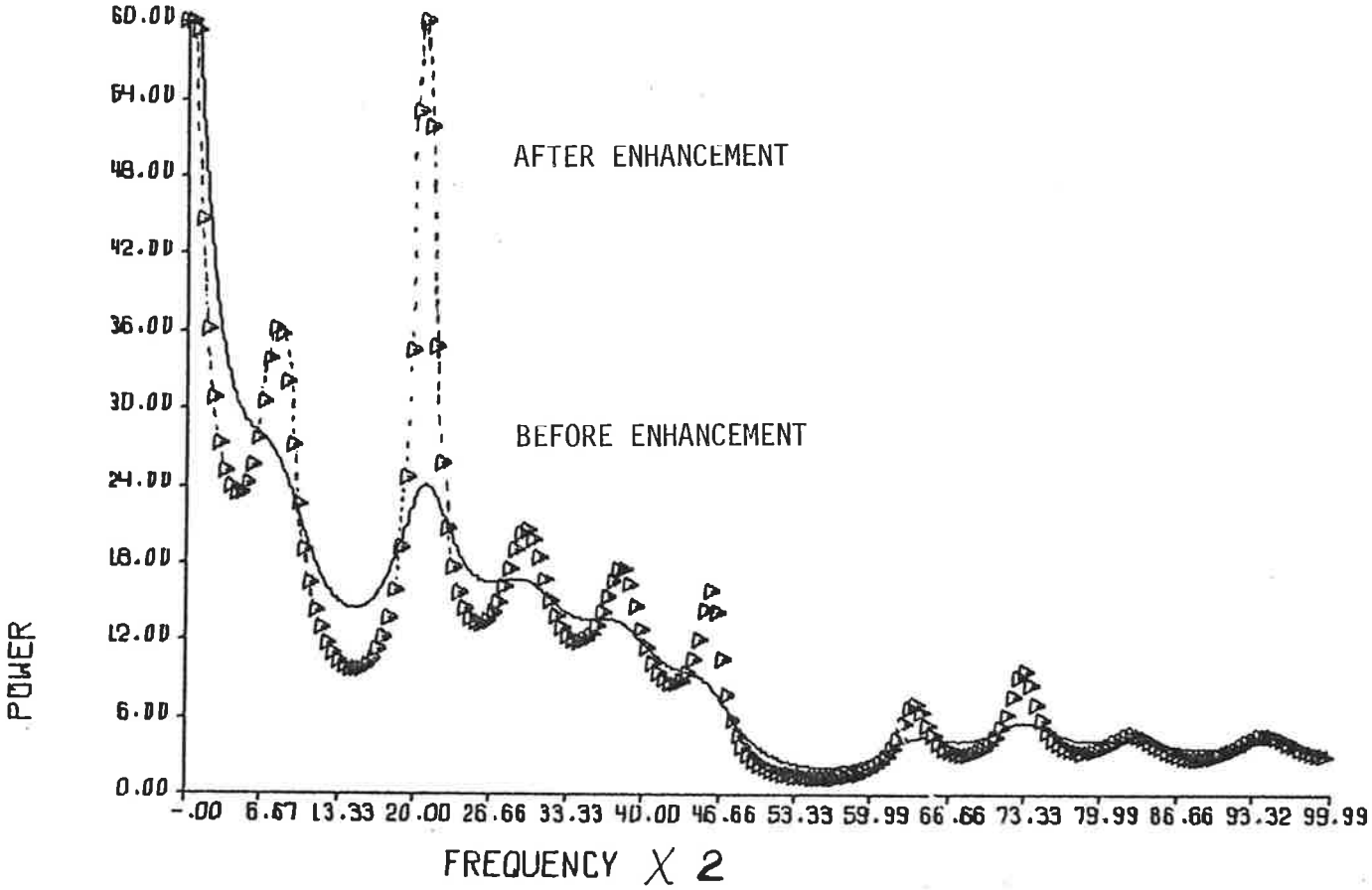

FIGURE 4.5 EFFECT OF POLE ENHANCEMENT

produce pole enhancement as discussed earlier; herein, the unit circle radius used in the evaluation of Z transform is 1.07.

4.6 Problems

With the selective filtering, although a frequency window is introduced to look at the spectral range of interest, the frequency resolution is not improved. The folding frequency or the Nyquist frequency is still half the sample frequency. Moreover, the LPC model may use some of its poles to model the filtered portion of the signal. As seen in figure 4.4, a high predictor order (19) is used to model the signal with relatively fewer frequency peaks. In this situation, a choice for the exact predictor order necessary to model the signal is not easy. It has been observed that a large predictor order (say 28) is necessary to model the signal so as to include comparatively fewer resonant peaks (Nandagopal, et al., 1981]. A modified LPC analysis technique known as selective linear prediction technique will be discussed in the next chapter to rectify some of these problems.

CHAPTER V

SELECTIVE LINEAR PREDICTION

5.1 Introduction

Heart sound spectra are found to have frequency peaks in the low, medium and high frequency ranges as defined by previous researchers [Yoganathan et al., 1979]. For example, in the case of the second heart sound the low, medium and high frequency ranges are 10-80 HZ, 80-220 HZ and 220-400 HZ respectively. The peaks observed in a particular frequency range are attributed to resonant frequencies of cardiac structures. In the LPC analysis described earlier, these ranges can be defined by selective filtering. But in this method, the signal information above the range of interest is sharply filtered. This increases the dynamic range of the spectrum and results in greatly decreased spectral flatness. Also, the inverse filter will use many of its coefficients to represent the filtered portion of the spectrum.

In order to overcome the problems in the LPC analysis of heart sounds and to obtain a sharper spectrum, a selective linear prediction (SLP) technique as proposed by Makhoul [1975] is employed. In this technique, the analysis can be carried out for any desired frequency range (low, medium or high), while employing a low predictor order.

The basic idea in the selective linear prediction method is to obtain the autocorrelation coefficients which are

necessary to compute the predictor constants from a selected portion of the signal power spectrum, so that the selected frequency range spans the angular range 0-π along the unit circle in the Z-plane.

5.2 Selective filtering versus filtering by SLP

The selective filtering, as discussed earlier, in general involves sharply filtering the signal to remove information above a certain frequency; the problems encountered in LPC analysis due to selective filtering of the data have been discussed earlier. Figure 5.1 indicates the processing steps involved in selective filtering, while figure 5.2 demonstrates the effect of such filtering on the spectrum.

Makhoul's selective linear prediction involves the translation of the selected portion of the signal spectrum to the angular range 0- on the unit circle. Consider a signal sequence S(n) having 'N' samples. A data file for analysis is made by adding zeros to the signal sequence S(n), so that the data file length is I samples (where I is a power of 2 and $I \geq N + P$; P is the predictor order).

The FFT of the data series can be computed as:

$$\text{FFT}\{S(n)\} = S(e^{j2\pi kI}) = \sum_{n=0}^{I-1} S(n)e^{-j2\pi nk/I} \quad \text{.....(5.1)}$$

$$\text{for } k = 0,1,2,.....I-1$$

The power spectrum of the data series is given by:

$$P(e^{j2\pi k/I}) = |S(e^{j2\pi k/I})|^2 \quad \text{.....(5.2)}$$

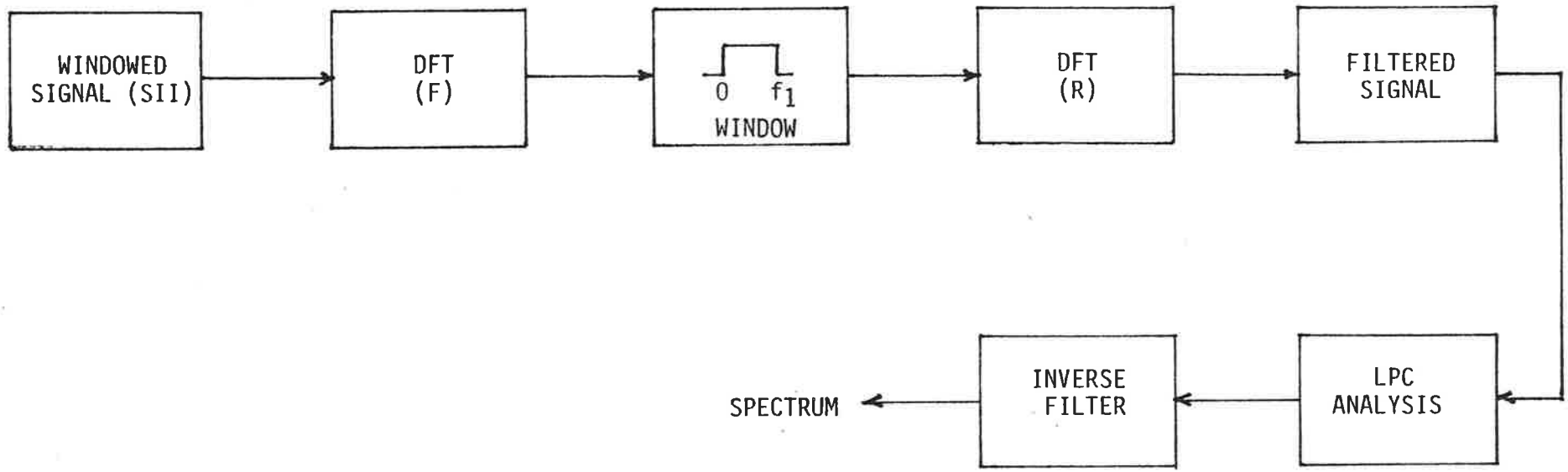

FIGURE 5.1 LPC ANALYSIS STEPS USING SELECTIVE FILTERING

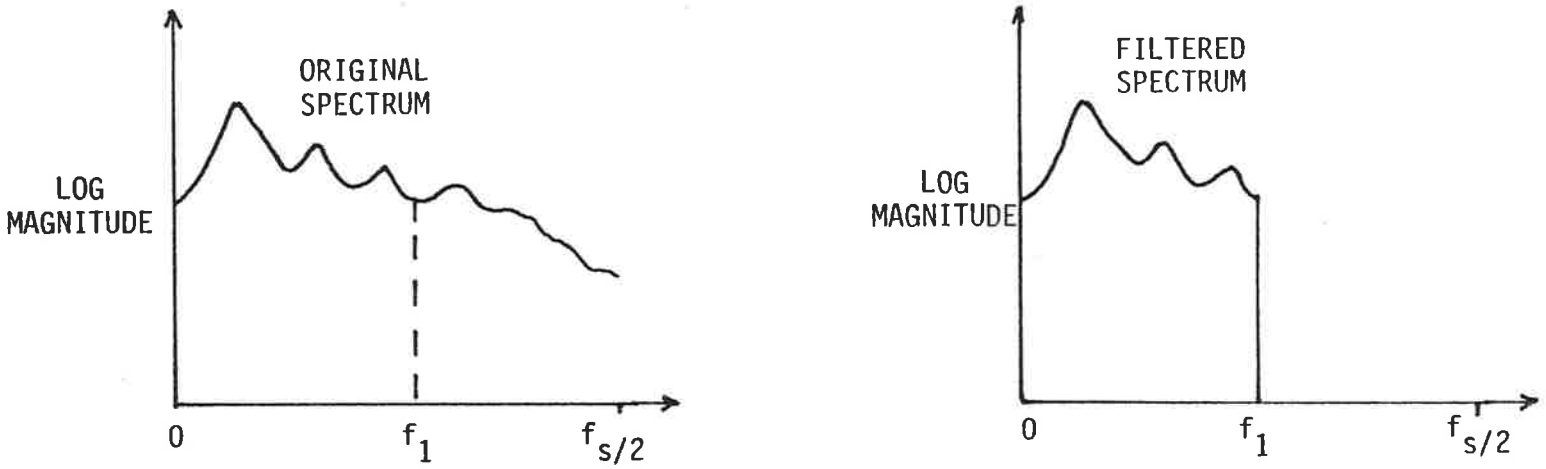

FIGURE 5.2 EFFECT OF SELECTIVE FILTERING ON SPECTRUM

With being the folding frequency; half of the sampling frequency as indicated in figure 5.3.

If a frequency range from f_1 to f_2 is desired, then an angular range corresponding to f_1 and f_2 can be ascribed by

$$\theta_1 = K_1 \, 2\pi/I \qquad .....(5.3)$$

$$\theta_2 = (K_1 + 1)2\pi/I \qquad .....(5.4)$$

If K_1 is zero and $l = I/2$, then $\theta_1 = 0$, $\theta_2 = \pi$, thereby giving the full frequency range of the spectrum.

The new spectrum from equation (5.2), based on the selected range θ_1 to θ_2, is given by

$$P_s(e^{j2\pi k/L}) = P(e^{j2\pi(k + k_1)/I}) \qquad ...(5.5)$$

$$\text{for } k = 0,1,2,\ldots l.$$

Where $L = 2l$ or $2l + 1$. This new spectrum definition is described graphically in figure 5.4. The shifted spectrum in equation (5.5) is made even by reflecting it about π as indicated in figure 5.4.b. The shaded portion of the figure 5.4.b is given by

$$P_s(e^{j2\pi k/L}) = P_s(e^{j2\pi(L-k)/L}) \qquad ...(5.6)$$

where $k = l + 1,\ l + 2,\ l + 3,\ldots\ldots L-1$.

Now, this spectrum can be assumed to be the result of an L-point discrete Fourier transform (DFT) operation on some data sequence. Since the spectrum is real and symmetric, the

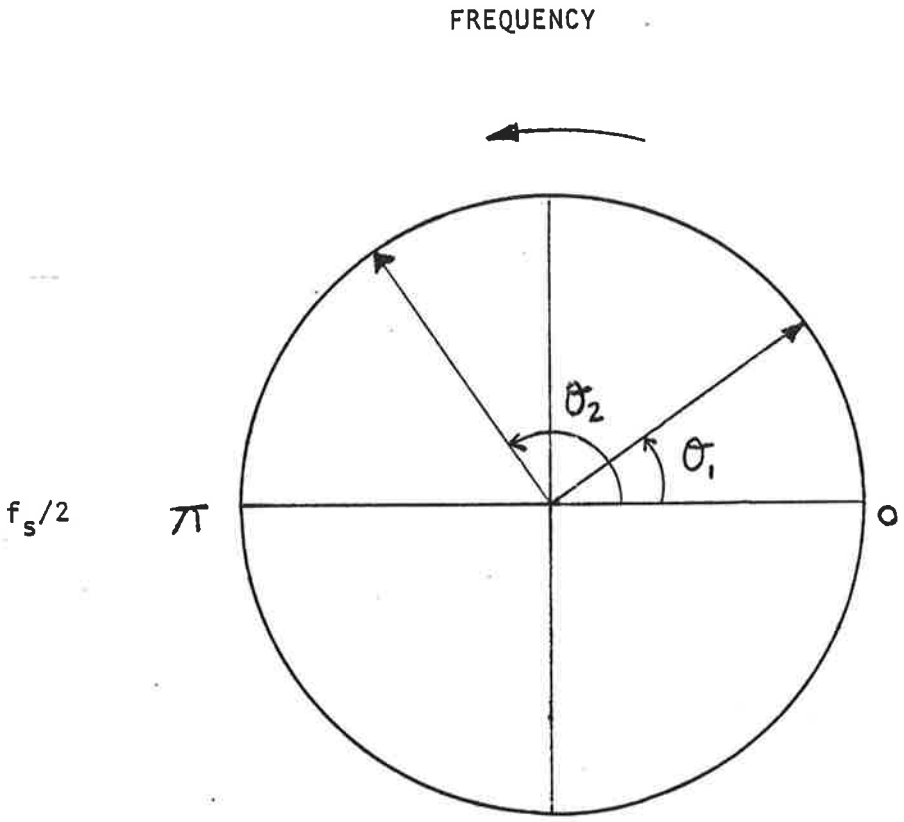

FIGURE 5.3 UNIT CIRCLE IN Z PLANE

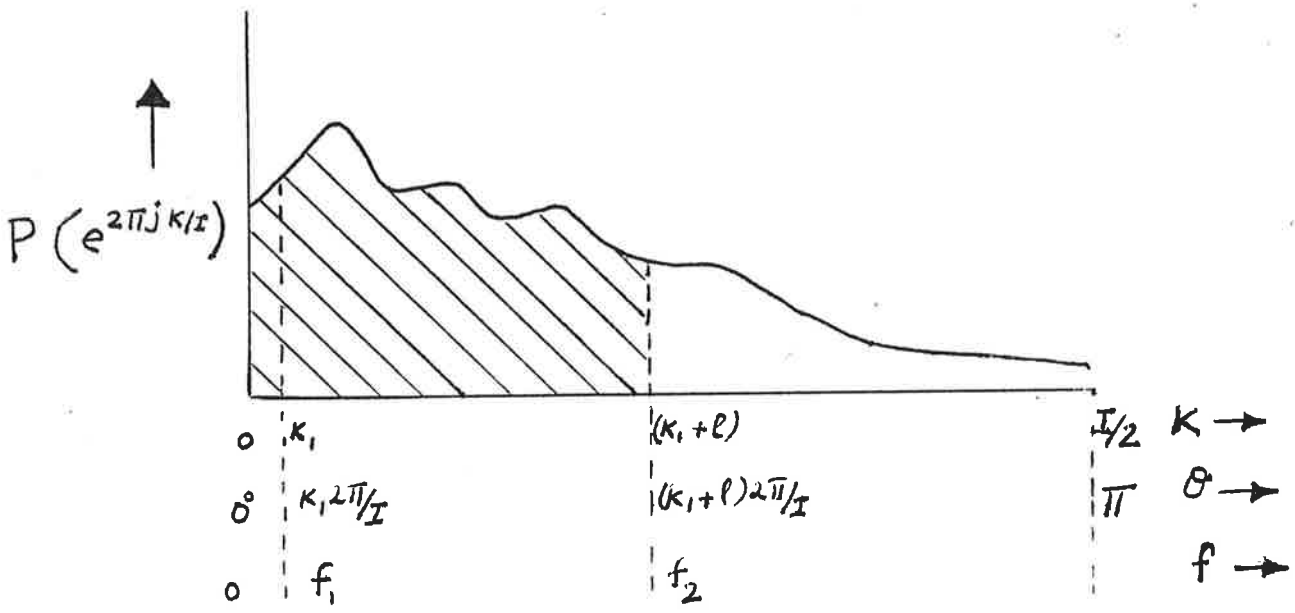

FIGURE 5.4(a) ORIGINAL SPECTRUM. THE DESIRED RANGE IS SHADED

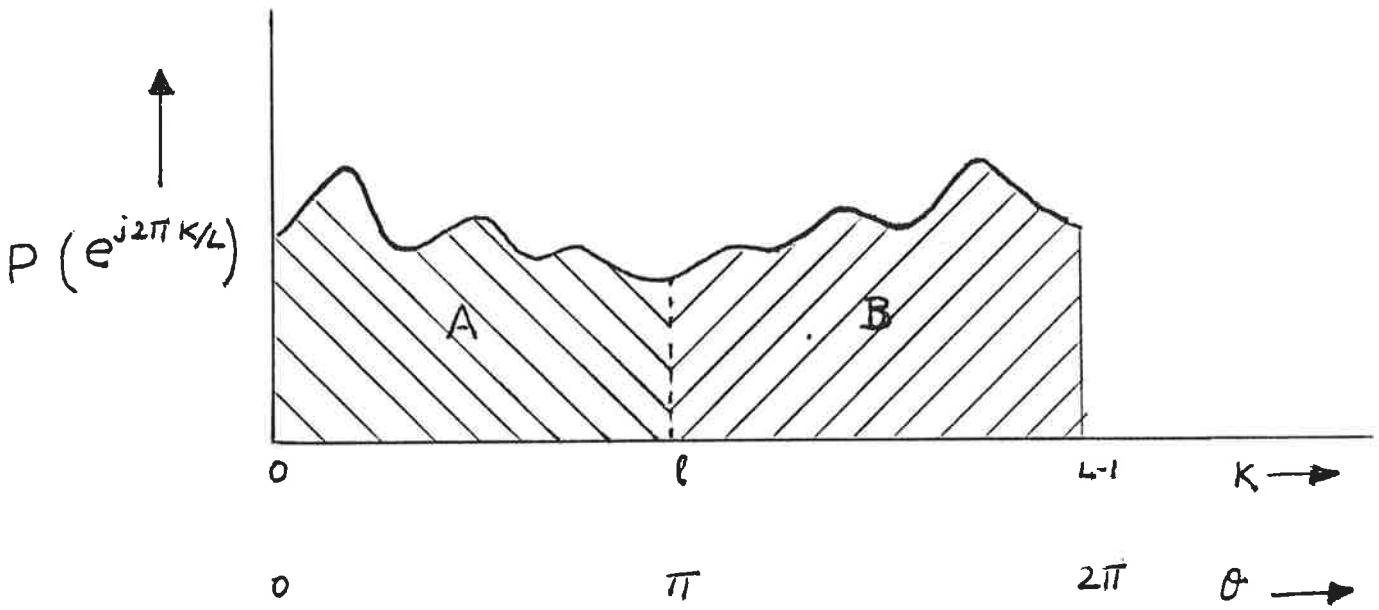

FIGURE 5.4(b) NEW SHIFTED SPECTRUM (PORTION A) AND B IS THE MIRROR IMAGE OF A

autocorrelation coefficients can be obtained by performing a FFT operation scaled by 1/L:

$$R(n) = \frac{1}{L} \sum_{k=0}^{L-1} P_s \left(e^{j2\pi k/L}\right) e^{-j2\pi kn/L} \quad \text{.....(5.7)}$$

where R(n) is the new translated auto-correlation coefficients for n = 0,1,2.....P.

P is the predictor order.

Once the autocorrelation coefficients are evaluated from the translated power spectrum, the predictor constants $a_1, a_2, \ldots a_p$ are obtained as described in appendix C. The digital processing steps involved in the SLP analysis are indicated in figure 5.5.

The frequency resolution of this new spectrum is much higher than the original spectrum. This method enables one to model the signal over a desired frequency range rather than over its entire spectral range. As the spectral range is limited, one needs to use a lesser predictor order than necessary for modelling over a wider range. This approach may be very useful for heart sound analysis, where spectra have frequency peaks in three distinct ranges and each range can be studied separately.

5.3 Application of selective linear prediction in heart sound analysis

As discussed in the previous section, the SLP technique is ideally suited to heart sound spectral analysis in the

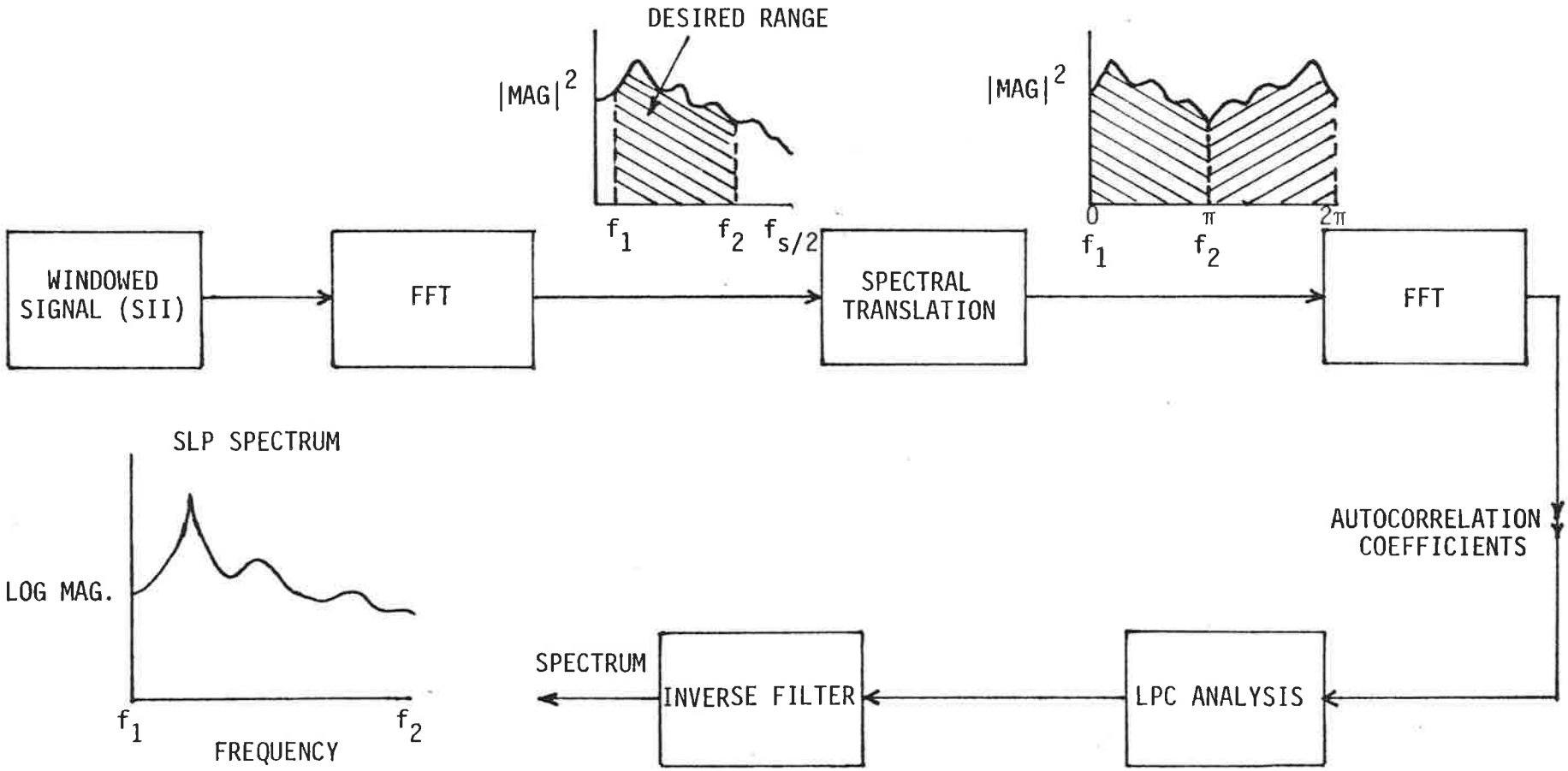

FIGURE 5.5 DIGITAL PROCESSING STEPS FOR SELECTIVE LINEAR PREDICTION ANALYSIS

three basic frequency ranges of interest. The computer program developed (in FORTRAN 66) to analyse heart sounds using the SLP technique was first tested using a synthetic signal. The generated synthetic signal data had five frequency peaks in the range 20 to 300 HZ, a range similar to heart sounds. The purposes of using this test signal were (1) to check the computer program (2) to check the SLP technique in different frequency ranges, (3) to compare the SLP spectrum with the FFT spectrum and (4) to check for spectral reproducibility of the SLP method.

First the synthetic signal data was generated and sampled at 2042 HZ with frequency peaks at 25 HZ, 60 HZ, 110 HZ, 160 HZ, and 215 HZ. The choice for these frequency values is arbitrary. Several segments of this test data were windowed using a Hamming type window with different widths and then analysed using the SLP method. A predictor order of 12 was used for this data. Figure 5.6 shows the spectra of the synthetic signal obtained using the SLP method. The synthetic data file had a length of 1000 samples, hence windowing was possible at different locations.

'SYNSLP1' in figure 5.6 is the SLP spectrum of the test data windowed with the window middle at sample number 300 and a window width of 600 samples while 'SYNSLP2' represents a SLP spectrum when the same window was positioned with the window middle at sample number 500. 'SYNSLP3' and 'SYNSLP4' in figure 5.6 indicate the SLP spectra when the window was

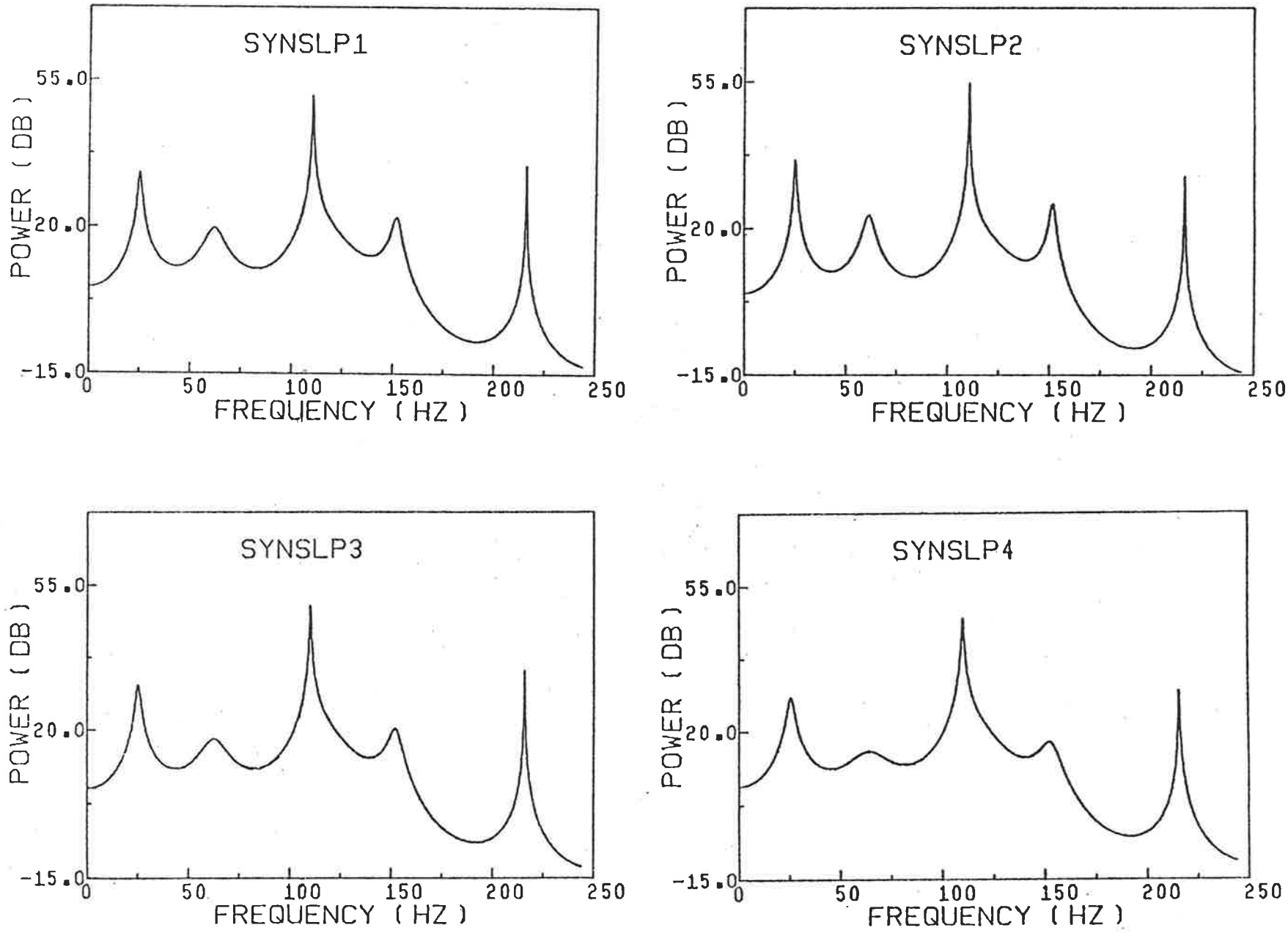

FIGURE 5.6: SLP SPECTRA OF THE SYNTHETIC SIGNAL

positioned about sample numbers 600 and 400 with widths 500 and 400 samples respectively. Thus figure 5.6 demonstrates the reproducibility of the SLP method even when the window width and position changed on the same signal. Figure 5.7 shows the above four spectra drawn to the same scale in the same box to indicate the differences. Several segments of the same heart sound recording were also tried to check the reproducibility of the SLP method. Figure 5.8 indicates the resultant SLP spectra of the second heart sound, clearly demonstrating the reproducibility of the SLP technique.

5.4 SLP and FFT spectra of heart sounds

Figure 5.9 shows the FFT spectrum of a typical second heart sound signal in a normal child. The spectrum is plotted in the frequency range 0-345 HZ. It appears from the spectrum that there are a couple of zeros, indicating that the spectrum is not purely all pole.

Although the SLP method is based on all pole modelling, the heart sound spectrum being not purely all pole, we can still apply the SLP method to obtain the spectrum in the frequency range where there are no zeros. Accordingly the SLP analysis is carried out in the frequency ranges 0-100 HZ, 100-245 HZ and 245-345 HZ with predictor orders 18,19 and 16 respectively. Figure 5.10 shows the SLP spectrum obtained in the above 3 ranges plotted together. Comparison of figures 5.9 and 5.10 shows that the SLP method has reproduced almost all of the information found in the FFT spectrum.

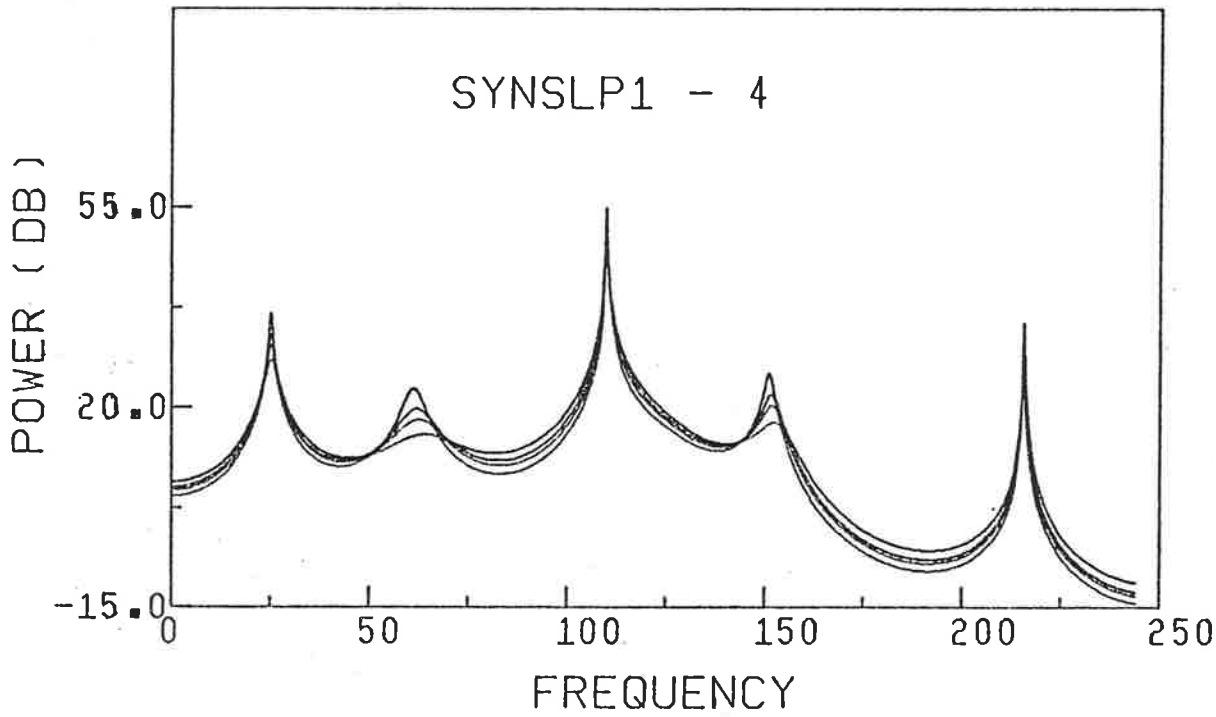

FIGURE 5.7: SLP SPECTRA OF THE SYNTHETIC SIGNAL
(FOR DIFFERENT WINDOW WIDTHS AND POSITIONS)

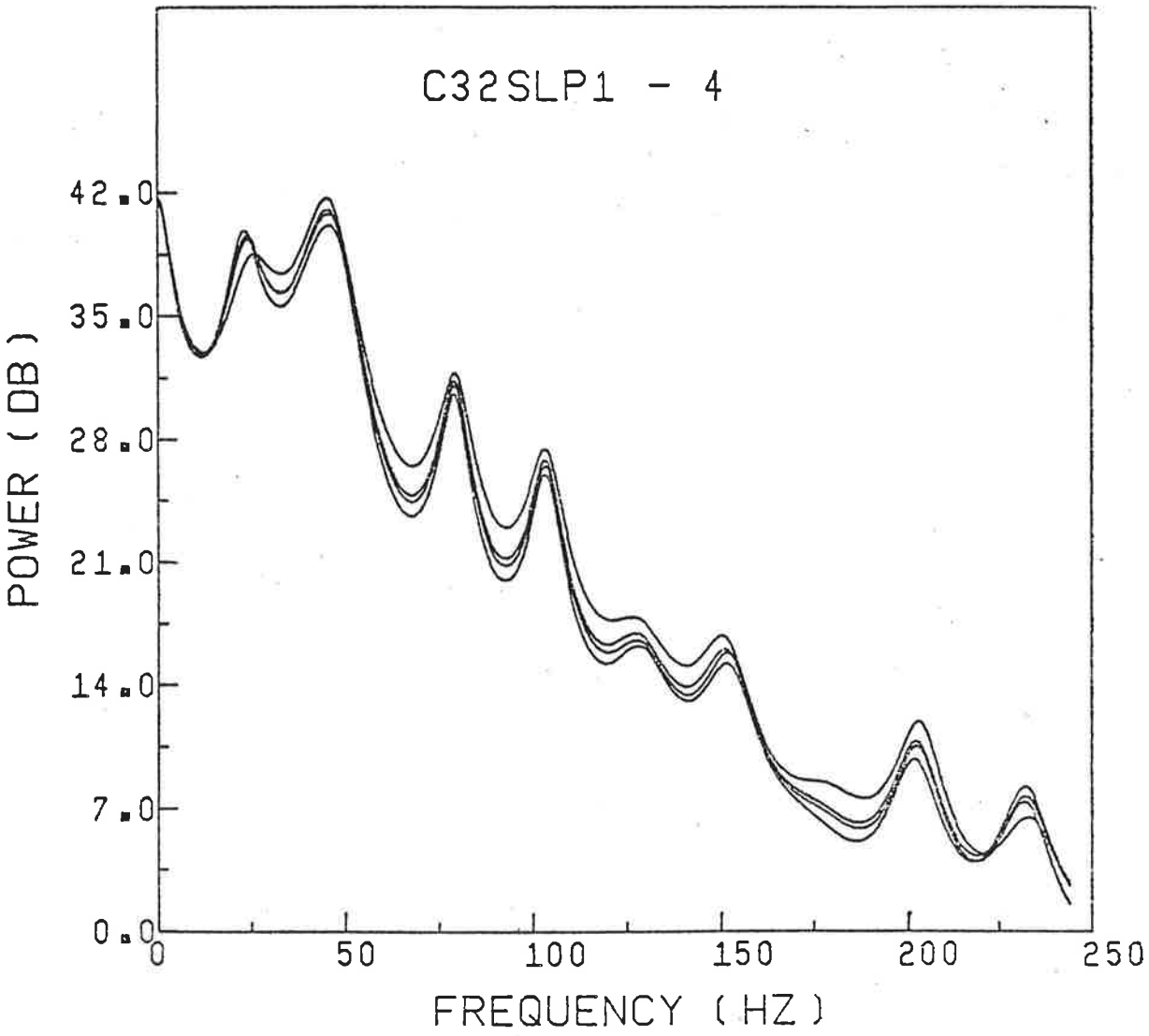

FIGURE 5.8: SLP SPECTRA OF SEVERAL SECOND HEART SOUND SEGMENTS OF THE SAME SUBJECT

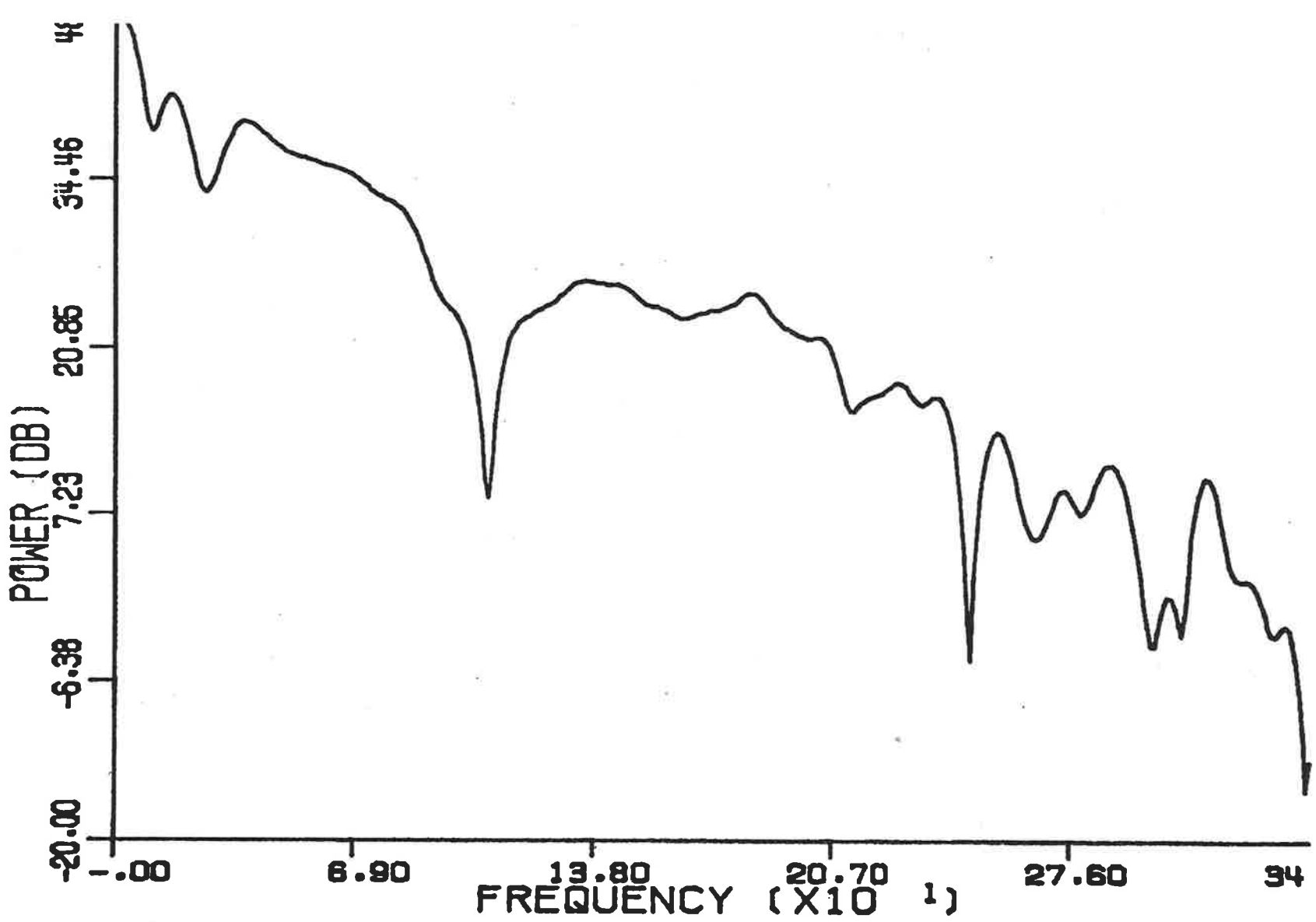

FIGURE 5.9: FFT SPECTRUM OF S11 (SUBJECT C36)
FREQUENCY RANGE 0-345 Hz

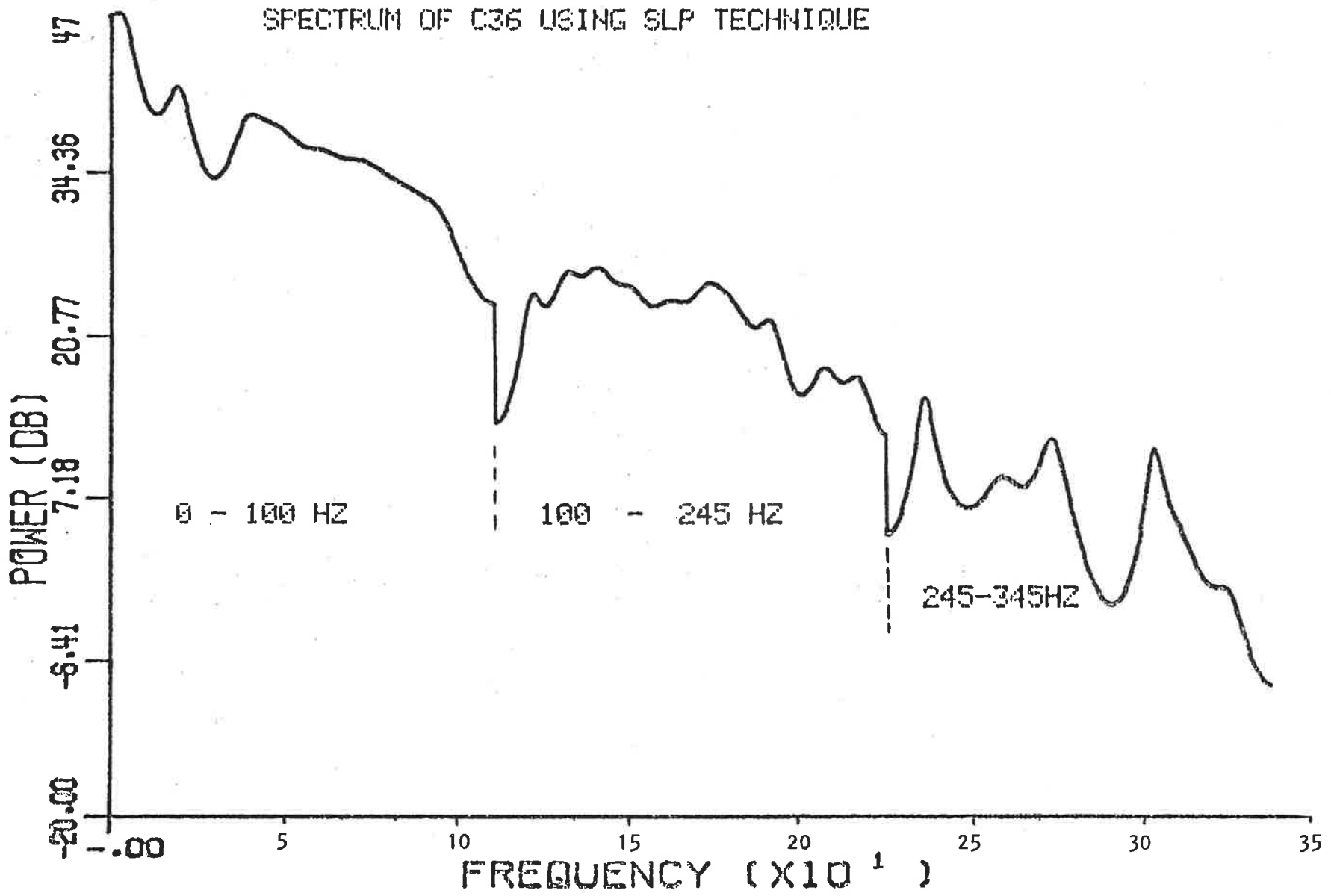

FIGURE 5.10 SLP SPECTRUM OF S11 (SUBJECT C36)

Spectral comparison between the FFT method and SLP analysis can also be made in each frequency range selected. Figures 5.11a and 5.11b show the spectra of the second heart sound (mentioned earlier) in the frequency range of 0-100 HZ, using FFT and SLP methods respectively. The FFT spectrum is defined by 100 points in the frequency scale (figure 5.11a), whereas the SLP spectrum has 1000 points defining the same frequency range. Similarly figures 5.12 and 5.13 define the SLP spectrum in the ranges 100-245 HZ and 245-345 HZ respectively. These clearly demonstrate the efficacy of the SLP method in the production of the heart sound spectral model and its resolution.

5.5 Frequency estimation

The frequency values of various peaks observed in the SLP spectrum can be estimated by knowing the frequency resolution and bandwidth of the selected portion of the spectrum. However, the resonant frequencies can be obtained without actually evaluating the spectrum. This is achieved by simply factorizing the denominator polynomial of the all pole filter (generating filter) transfer function H(Z). If a_1, a_2,...a_p are the predictor coefficients obtained from the SLP analysis, then the denominator polynomial of H(Z) is given by:

$$D(Z) = 1 - a_1 Z^{-1} - a_2 Z^{-2} \ldots\ldots - a_p Z^{-p} \qquad \ldots\ldots(5.8)$$

The roots of the polynomial would provide the pole positions

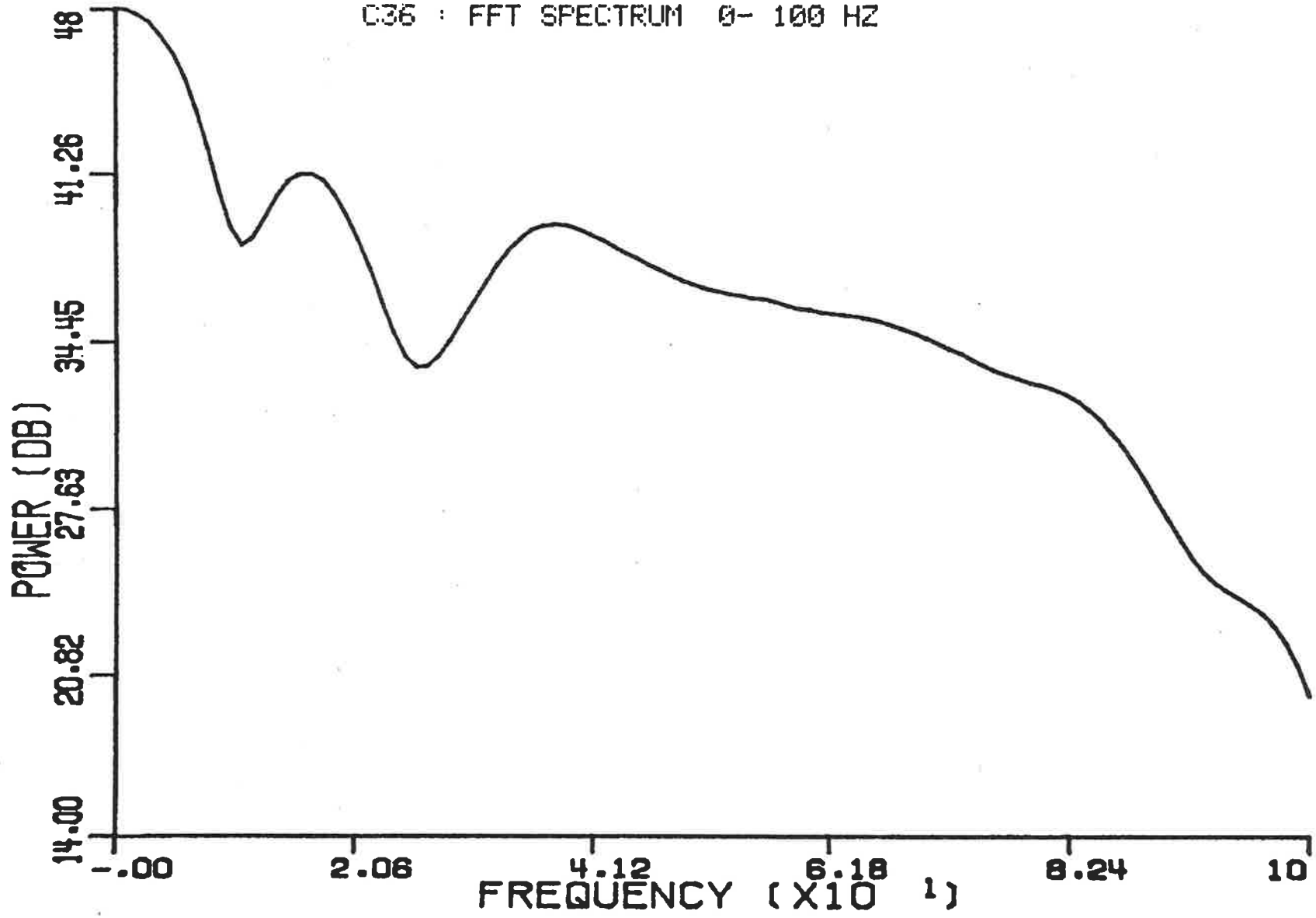

FIGURE 5.11(a) FFT SPECTRUM OF S11 (SUBJECT C36)
FREQUENCY RANGE 0-100 Hz

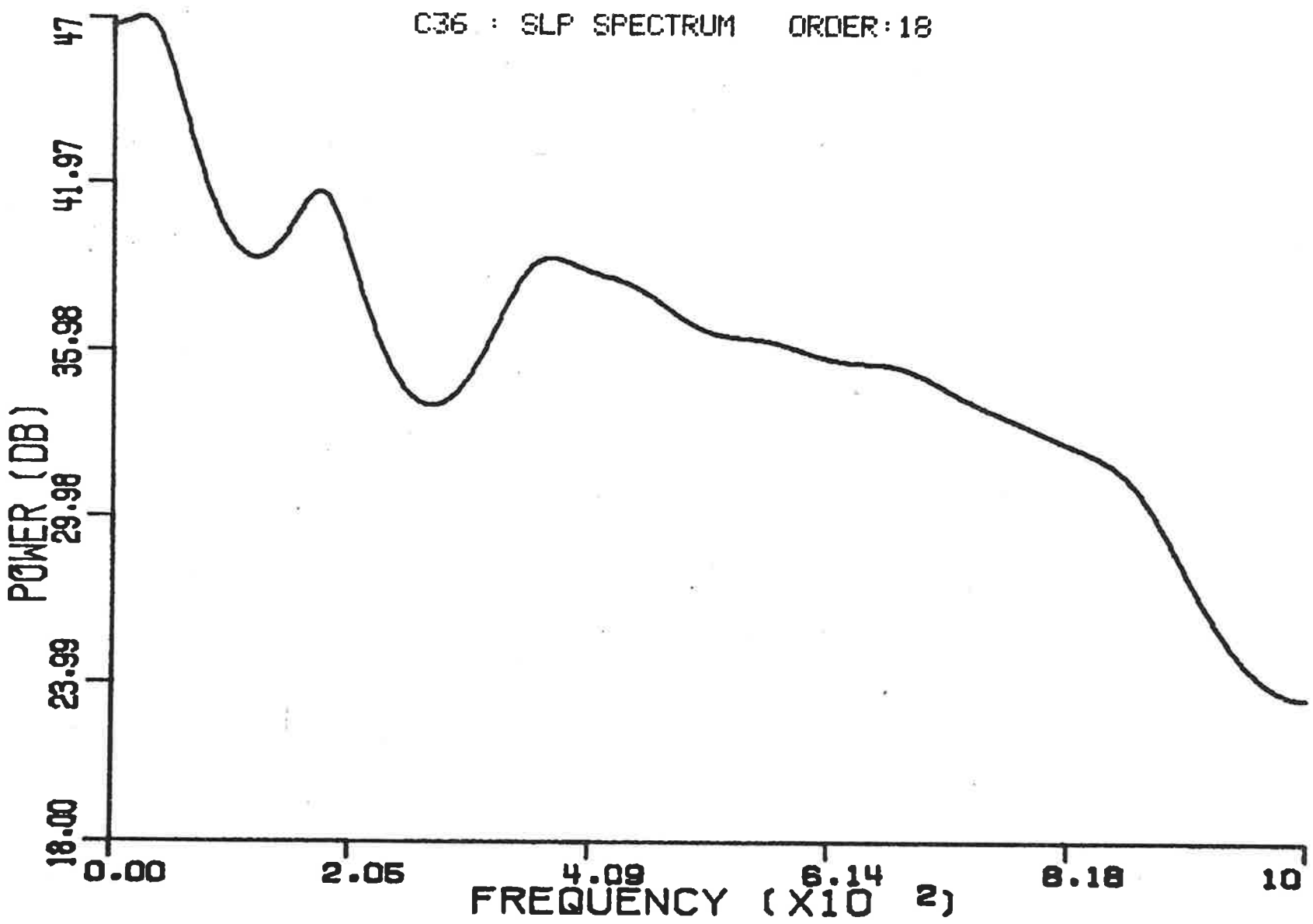

FIGURE 5.11(b): SLP SPECTRUM OF SII (SUBJECT C36)
FREQUENCY RANGE 0-100 Hz

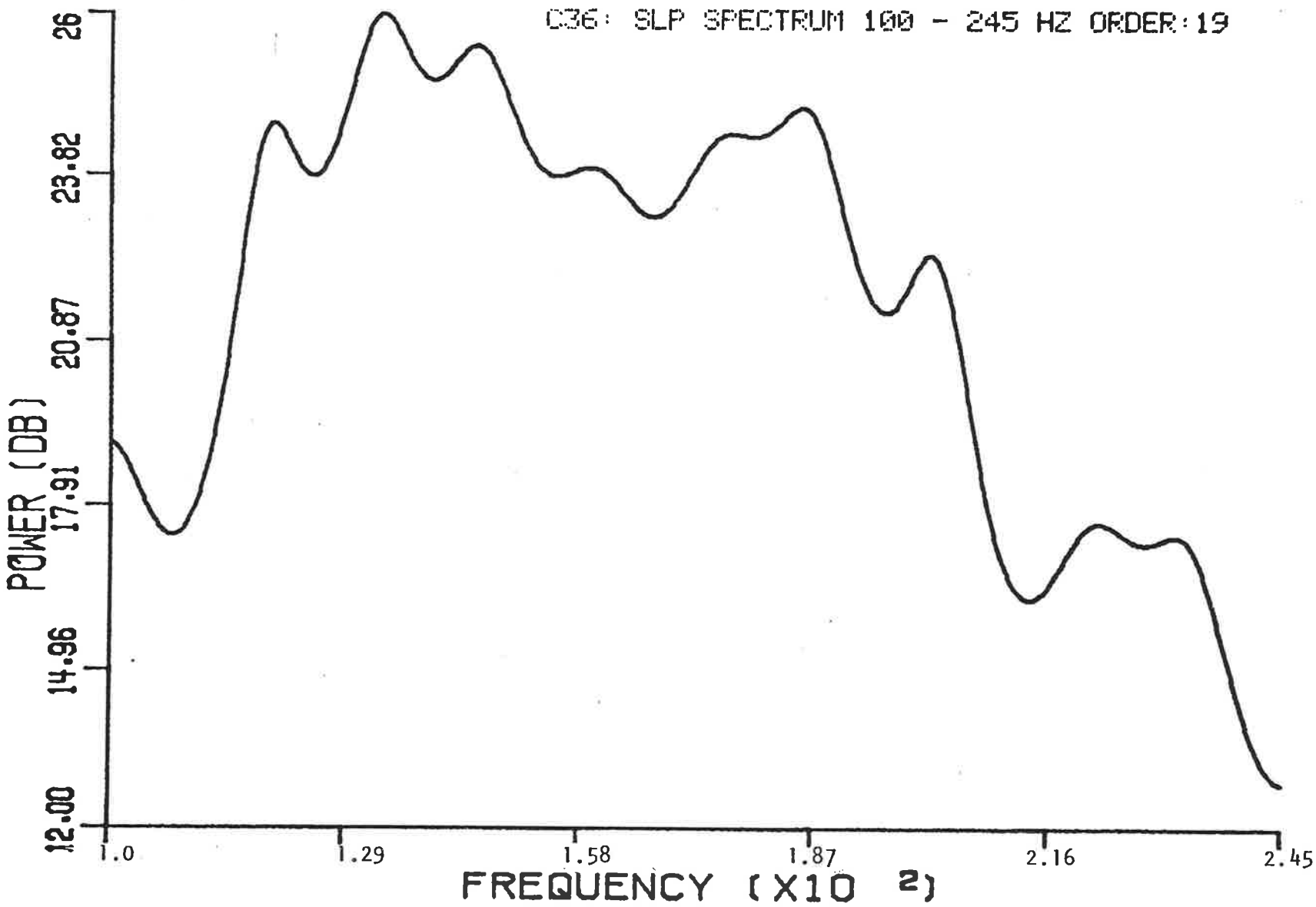

FIGURE 5.12: SLP SPECTRUM OF SII (SUBJECT C36)
FREQUENCY RANGE 100-245 Hz

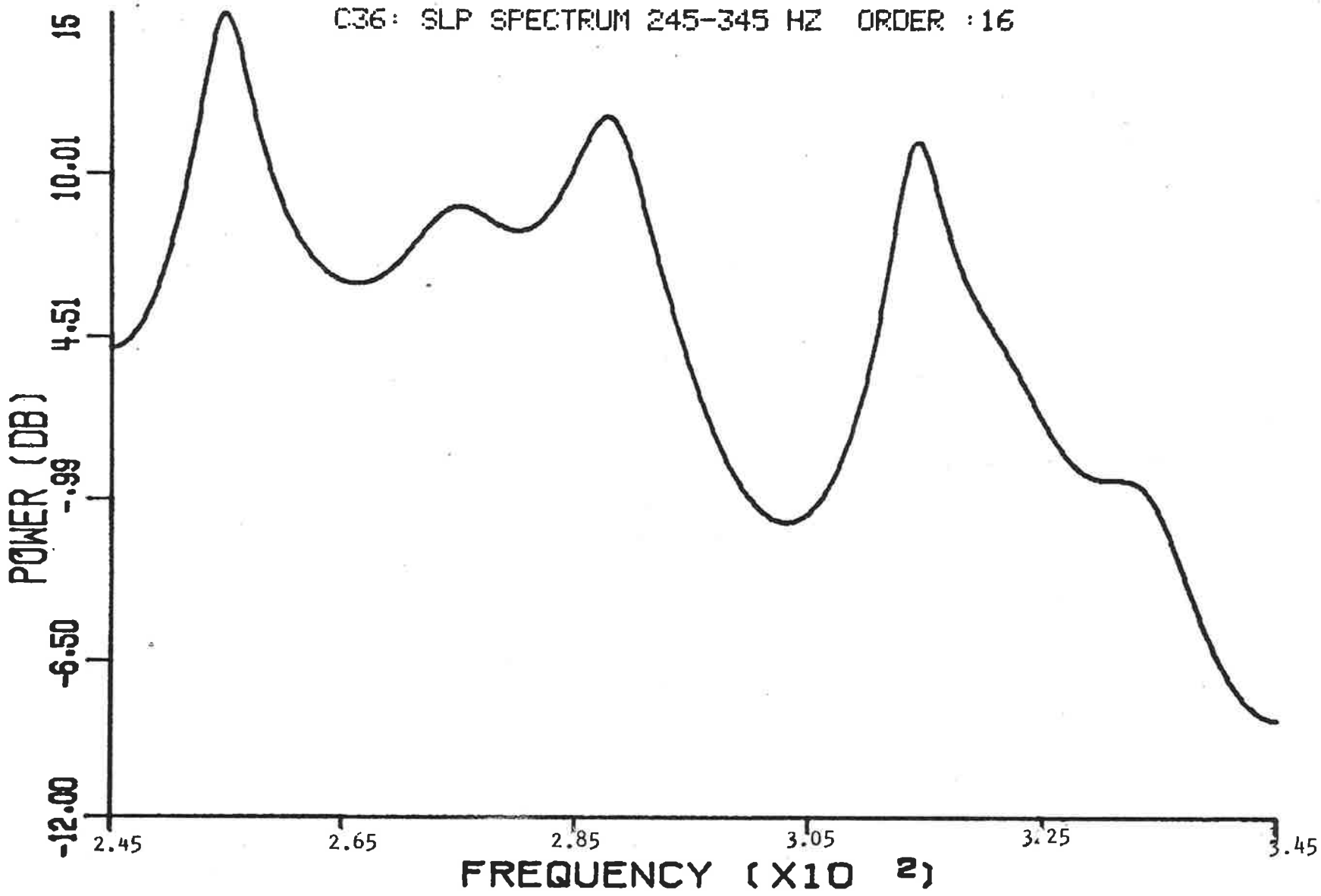

FIGURE 5.13: SLP SPECTRUM OF SII (SUBJECT C36)
FREQUENCY RANGE 245-345 Hz

of the inverse filter and hence the frequency values. Bairstow's method (James, M.L., et al., 1977) can be used to determine the roots of the polynomial. This method is an iterative process for extracting quadratic factors:

$$Q(Z) = (Z^2 + UZ + V) \qquad .....(5.9)$$

of the polynomial D(Z). The starting values for U and V are chosen such that the iteration process converges to the correct values of the U and V. The two roots Z_1, Z_2 are obtained from the first quadratic factor Q(Z)

$$\text{i.e. } Z_{1,2} = \frac{-U \pm \sqrt{U^2 - 4V}}{2} \qquad .....(5.10)$$

The iteration process is repeated to obtain a quadratic factor of the (P-2) degree polynomial, resulting from the extraction of the quadratic factor Q(Z) for the first two roots. Two more roots are then obtained from the second quadratic factor.

This process is repeated until all the roots of the original polynomial are extracted. The roots of the polynomial give the pole positions. If ' r_k ' is the k^{th} complex pole, then the pole frequency is computed by:

$$F_k = \frac{1}{2\pi T} \arctan\left[\frac{Im\ r_k}{Re\ r_k}\right] \qquad .....(5.11)$$

where T is the sampling interval.

The bandwidth of the frequency resonance corresponding to the complex pole ' r_k ' can be computed using the relationship:

$$B_k = -\left(\frac{1}{\pi T}\right) \log_n |r_k| \qquad \text{.....5.12}$$

If the sampling interval 'T' is expressed in seconds, then the units of F_k and B_k will be hertz (HZ).

CHAPTER VI

FREQUENCY ANALYSIS OF SECOND HEART SOUND IN NORMAL CHILDREN USING SELECTIVE LINEAR PREDICTION CODING (SLPC)

6.1 Introduction

The heart muscle and valvular system provide a considerable contribution to the production of heart sounds. It is therefore essential to identify and relate the frequency resonances observed in the spectral distribution of phonocardiograms with the physiologic state of the respective cardiac structures. Mathematical modelling in the study of atrioventricular and semilunar valve vibrations has been an area of increasing interest in the recent past [Ghista and Rao, 1973; Mazumdar, et al., 1978; Blick, et al., 1979]. However, as these models are based on the knowledge of the primary vibrational frequency of valve leaflets, an exact determination of valvular resonances become essential. Studies on spectral phonocardiography in normal and pathological cases have clearly indicated the relationship between the quality of resonant peaks (frequency and sharpness of the peak) and the valvular pathology [Adolph, et al., 1970; Renner and Renner, 1979; Stein, et al., 1980].

It has been observed that due to certain pathological conditions, the dominant frequency component of the second heart sound increases in its frequency value and at the same time the resonance flattens (less sharp) [Sabbah, et al.,

1978; Stein, et al., 1980]. In such cases it becomes difficult to determine the exact frequency of resonance and its quality due to its lossy nature. It is the purpose of this chapter, having established the linear prediction technique in chapters four and five, to study the usefulness of the selective linear prediction coding (SLPC) analysis technique in producing better spectral distribution than the conventional FFT technique. For this a study of the spectral distribution of the second heart sound in normal children using the SLP analysis is made.

6.2 Data Acquisition

Heart sound recordings were made in a sound proof room in the department of Cardiology at the Adelaide children's hospital, under the supervision of Dr. E. Goldblatt. The phonocardiographic recordings were made possible with the assistance of Mr. G.M. Lee and Mr. M. Bentley of the Cardiology department of Adelaide children's hospital.

A block diagram of the data collection system is provided in Chapter 2 (figure 2.6). Lead II electrocardiogram (ECG) and the phonocardiogram (PCG) from the aortic area on the precordium (second right intercostal space) were recorded simultaneously on to a Hewlett-Packard HP 3964A four channel FM tape recorder from seventeen normal children. A contact type microphone HP 21050A was used to pick up the heart sound

signals. The phonocardiogram amplifier had a flat frequency response from 15 HZ to 1 KHZ.

In order to determine the aortic valve orifice size and valve ring (aortic root) diameter, parasternal long axis and short axis views of the aortic valve were recorded for each subject using a two-dimensional echocardiographic machine (Toshiba SSH-10A sonolayergraph) with a 3.4 MHZ transducer. These measurements were used in the phonocardiogram and echocardiogram correlations which will be discussed in Chapter seven.

The preamplified ECG and PCG signals were digitized simultaneously at 2042 HZ by a two-channel 8-bit analog to digital converter controlled by an Intel 8085 microprocessor based system (SDK85) with 8K bytes of memory as explained in chapter two. As the Intel system was interfaced with the University of Adelaide's CYBER 173 computer, the data was immediately transferred to CYBER disks for permanent storage and subsequent analysis.

6.3 Pre-processing of data

The data files were subjected to processing to subtract the mean (d.c. offset that may arise due to biasing conditions in the buffer amplifier and analog to digital converter circuitry). The processed files were then normalised with respect to the root mean square (RMS) value of the respective data files of length 2048 samples. These data files were then displayed along with the ECG signals on the screen of an interactive graphics terminal (either DEC

GT40 or Tektronix 4010 terminals). All the signal processing steps discussed here were performed interactively on the CYBER 173 computer using one of the above two graphics terminals. The second heart sounds were then identified visually from the screen and extracted using a Hamming type window operated on the data-file. The width of the window varied slightly from subject to subject. The window positioning was achieved using the light pen facility available with the graphic terminal to indicate the start and end samples of the second heart sound. The average window width seemed to be around 250 samples. The windowed second heart sounds for each subject were stored as indirect permanent files on the CYBER 173 disk for further processing by the Fourier transform method and SLPC method.

6.4 Fast Fourier transform method

The Conventional fast Fourier transform (FFT) technique was used initially to obtain the spectrum of the second heart sound for all the subjects. An FFT Subroutine available in The International mathematical and Statistical Library (IMSL) on the CYBER 173 disk was used. The signal processing steps involved in the FFT analysis are shown in figure 6.1. FFT spectra for each subject were obtained for several second heart sound segments and an average was obtained in the frequency domain.

6.5 Selective linear prediction coding (SLPC) method

The SLPC analysis technique has been discussed in detail

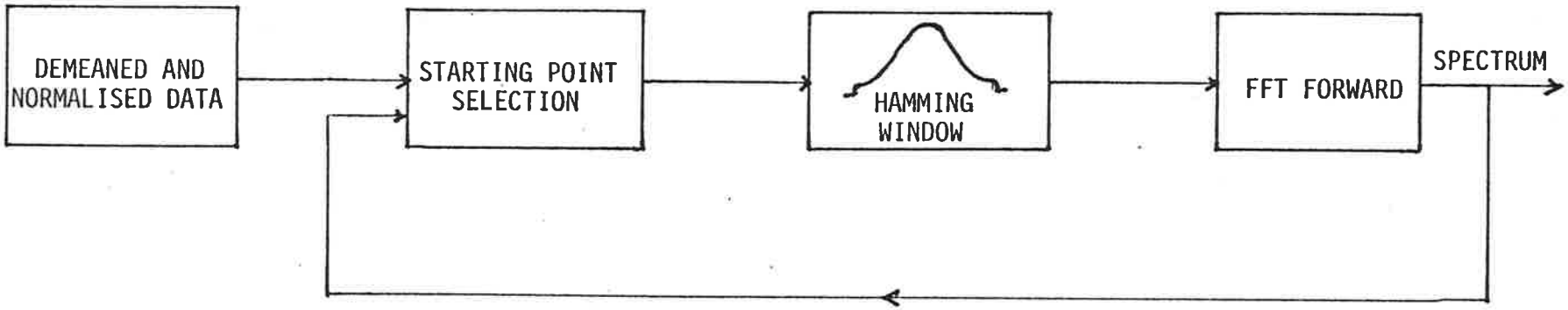

FIGURE 6.1: FFT ANALYSIS STEPS

in the previous chapter. For the SLPC analysis, the same second heart sound data extracted for FFT analysis has been used. The preprocessing and data windowing were common to both FFT and SLPC analysis. The SLPC analysis has been carried out interactively on a CYBER 173 computer as discussed in the previous chapter. A choice was made initially for the predictor order based on the number of resonant peaks seen in the FFT spectrum for a given frequency range. Then the SLPC spectrum was estimated and compared with the FFT spectrum using the interactive graphics screen. The predictor order was changed if necessary. If there are n frequency peaks in the spectrum in the frequency range say, f_1 to f_2 HZ, then a predictor order of 2n + 1 is normally sufficient to model the signal in the above frequency range. The second heart sound spectra were found to have resonant peaks in three distinct frequency ranges: viz. low (<80 HZ), medium (80-220 HZ) and high (220-400 HZ). Accordingly; the SLPC analysis has been carried out in the above ranges. Also, the frequency values of the peaks seen in the three frequency ranges mentioned above, were computed by factorizing the denominator polynomial of the generating filter transfer function H(Z) (Refer chapter IV, equation 4.10). The denominator polynomial is constructed from predictor coefficients as discussed in chapter V. The roots of the polynomial provide the pole positions of the transfer function and hence the frequency values. Bairstow's method as discussed earlier was used to solve for the roots.

6.6 Results and discussion

Spectral distributions of the second heart sound, in 17 normal children were determined using both the FFT and SLPC techniques. The frequency spectrum of SII contains frequency peaks in the low, medium and high frequency ranges as indicated in table 6.1. This table reveals the presence of at least three peaks in the ranges 15-80 HZ and 80-150 HZ for the majority of subjects. Also there are resonant peaks above 150 HZ.

The dominant frequency of SII found by inspection of spectrograms was 30 $\pm$ 5 HZ. It is interesting to compare this frequency distribution in children with the corresponding result in adults. Stein et al., [1980] have reported that the dominant frequency of the aortic component of SII in adult subjects with normal aortic valves to be 53 $\pm$ 3 HZ and in the case of aortic stenosis to be 87 $\pm$ 5 HZ. They have proposed that the increase in the dominant frequency is due to the increased stiffness of aortic valve leaflet as a result of stenosis. The dominant frequency of SII in children in the present investigation seems to be lower than that for adults (even though the valvular dimensions of children are smaller). This would mean, according to Stein's theory, the aortic leaflets in children are less stiff than in adults and hence have lower dominant frequencies.

In the present analysis of the second heart sound, the frequency analysis has been limited to 250 HZ as there was no significant output seen beyond this frequency range. The

TABLE 6.1

Frequency distribution of second heart sound in normal children

Subject No.	Age	Frequency Peaks 10-80Hz	Frequency Peaks 80-150Hz	Frequency Peaks >150Hz
1	8	14,24,44,55,63,75	84,94,113,139	167,198,218
2	5	13,24,34,42,49,58, 68	85,99,104,114,132, 140	
3	11	32,45	83,108,130	
4	14	15,26,63,80	96,108,133	176,212,245
5	4	14,31,42,57,74	91,110,151	173
6	8	14,29,45,66	90,112,137	164,188,208
7	7	14,30,49,69	86,113,137	186,215,233
8	9	37,49,72	96,124	161,188,212
9	6	39,51,71	112,123	170,194,214,234
10	4	19,40,61	94,129	171,209
11	12	19,40,60	83,110,126,142	177,200,224
12	16	21,37,58,78	98,118,145	165,193,213
13	12	39,61	84,100,120,146	168
14	11	26,47,58,69	87,101,115,131,149	170
15	12	23,44,76	102,134	156,200
16	5	18,32,44,58,79	92,107	165,188,214
17	7	16,38,52,68	82,96,121,145	190,235

spectra of second heart sound produced by the SLPC technique seem to contain all the frequency peaks seen in the spectra produced by the FFT technique. Figure 6.2 compares the LPC spectra of SII in four subjects with the corresponding FFT spectra over a limited frequency range. The SLPC spectra provides a better frequency peak definition compared to the FFT spectra. Frequency peak identification becomes easier in the SLPC method.

Figure 6.3b shows the FFT spectra of the second heart sound in Subject C. Note the frequency peaks f_A, f_B,...f_F. On comparison with the SLPC spectra indicated in figure (6.3a) for the same signal, the definition of the frequency peaks f_A, f_B...f_F is much better. This demonstrates the efficacy of SLPC technique in frequency peak delineation.

The frequency resolution in the SLPC technique is much higher than in the FFT technique. In FFT analysis, the data length is 2048 samples, sampled at 2042 HZ. The FFT returns 1024 Fourier coefficients in the frequency domain. The frequency resolution therefore is 0.997 HZ/coefficient. This means that 1024 points are used to represent the frequency range 0-1021 HZ; on the other hand, in the SLPC technique, for the same data length and sample rate, the frequency resolution could vary depending on the frequency range over which the SLPC analysis is carried out. For example, let the frequency range of interest be 0-100 HZ. The number of sample points in the frequency domain is still 1024, but the folding frequency now is 100 HZ. The frequency resolution is

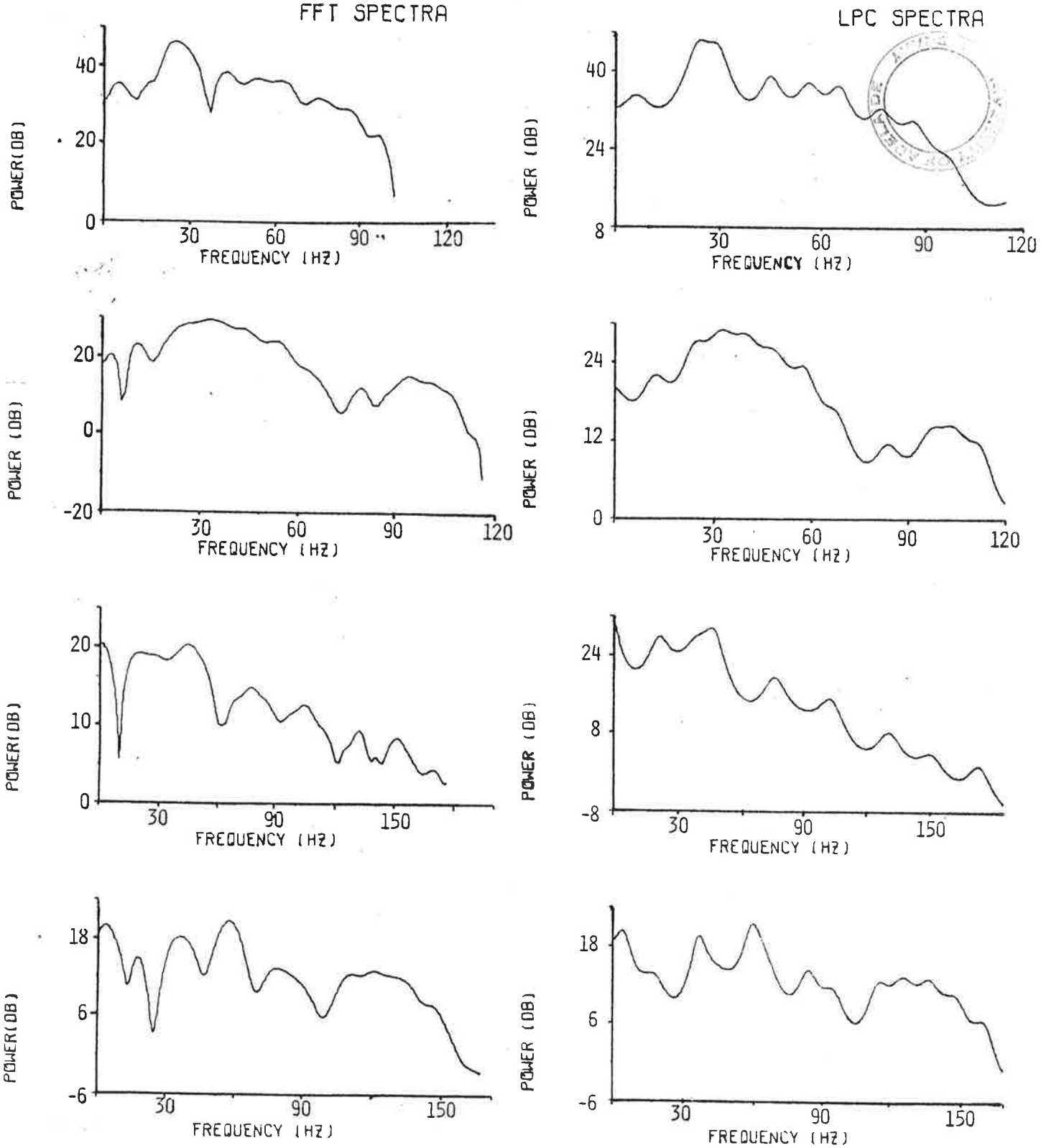

FIGURE 6.2: COMPARISON OF FFT AND LPC SPECTRA
OF SECOND HEART SOUND FOR 4 SUBJECTS

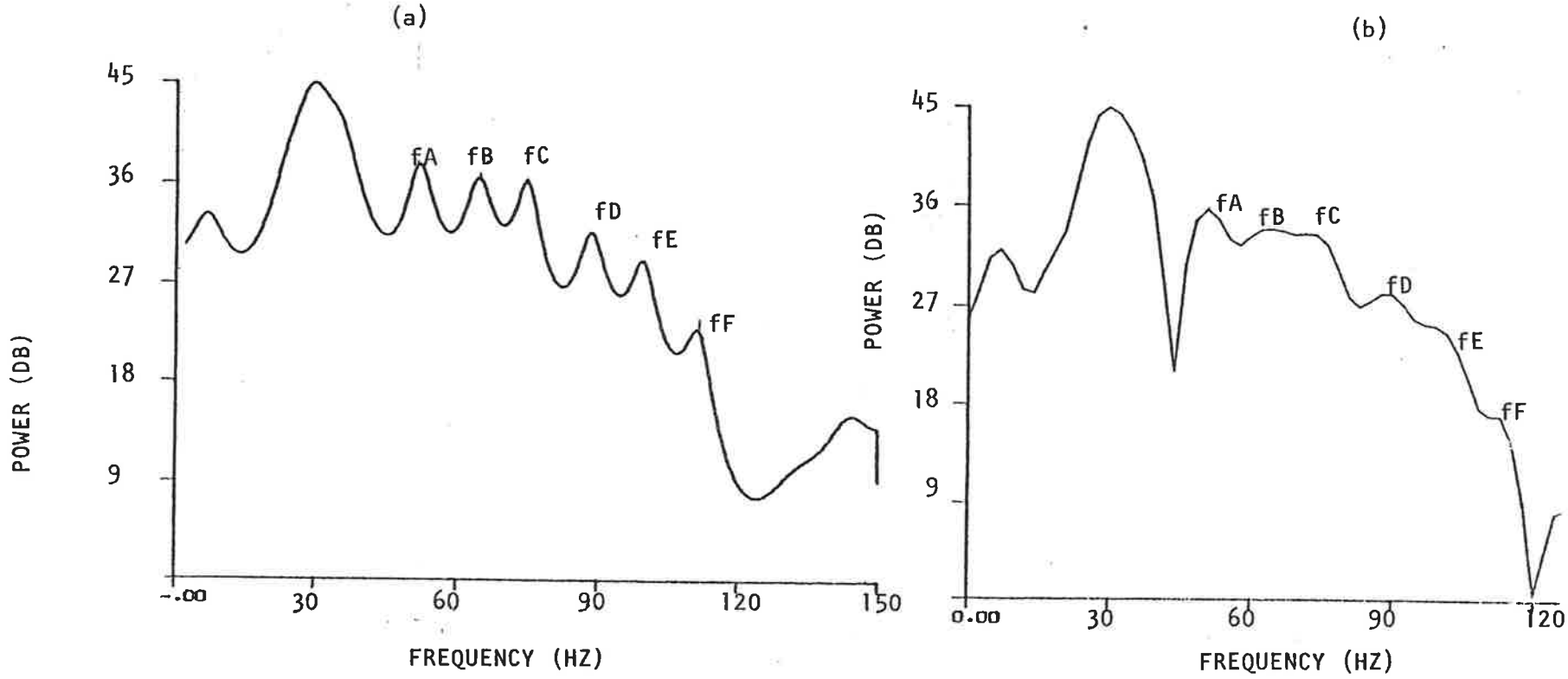

FIGURE 6.3 (a): SLP SPECTRUM
(b): FFT SPECTRUM

higher. The frequency resolution is normally given by $f_s/2^I$ where f_s is the sampling frequency and 2^I is the data length (I is an integer). Zeros are always appended so that 2^I is kept the same for obtaining the data spectrum and SLPC spectrum.

In order to check for the correspondence of the frequency peaks seen in SLPC spectra with those seen in the FFT spectra, the frequency peaks in the SLPC spectra and FFT spectra were estimated for each subject over a limited frequency range and compared. Also pole frequencies were calculated using Bairstow's method as mentioned earlier. The frequency values thus obtained were compared. The relationship between the frequency peaks of the SLPC and FFT spectra is demonstrated in figure 6.4 by plotting the values of frequency peaks obtained from SLPC spectra against the frequency values obtained from FFT spectra. The relationship is linear and the points cluster around a 45 line. The pole frequencies calculated from equation 5.11 of chapter 5 correlate very well with the frequency values obtained from the SLPC spectra. The deviation is only about ± 2 HZ and this is indicated in figure 6.5. This demonstrates that the frequency values of the peaks in the spectrum can be obtained directly from the predictor coefficients without having to estimate the spectrum.

6.7 Conclusion

The selective linear prediction technique has been

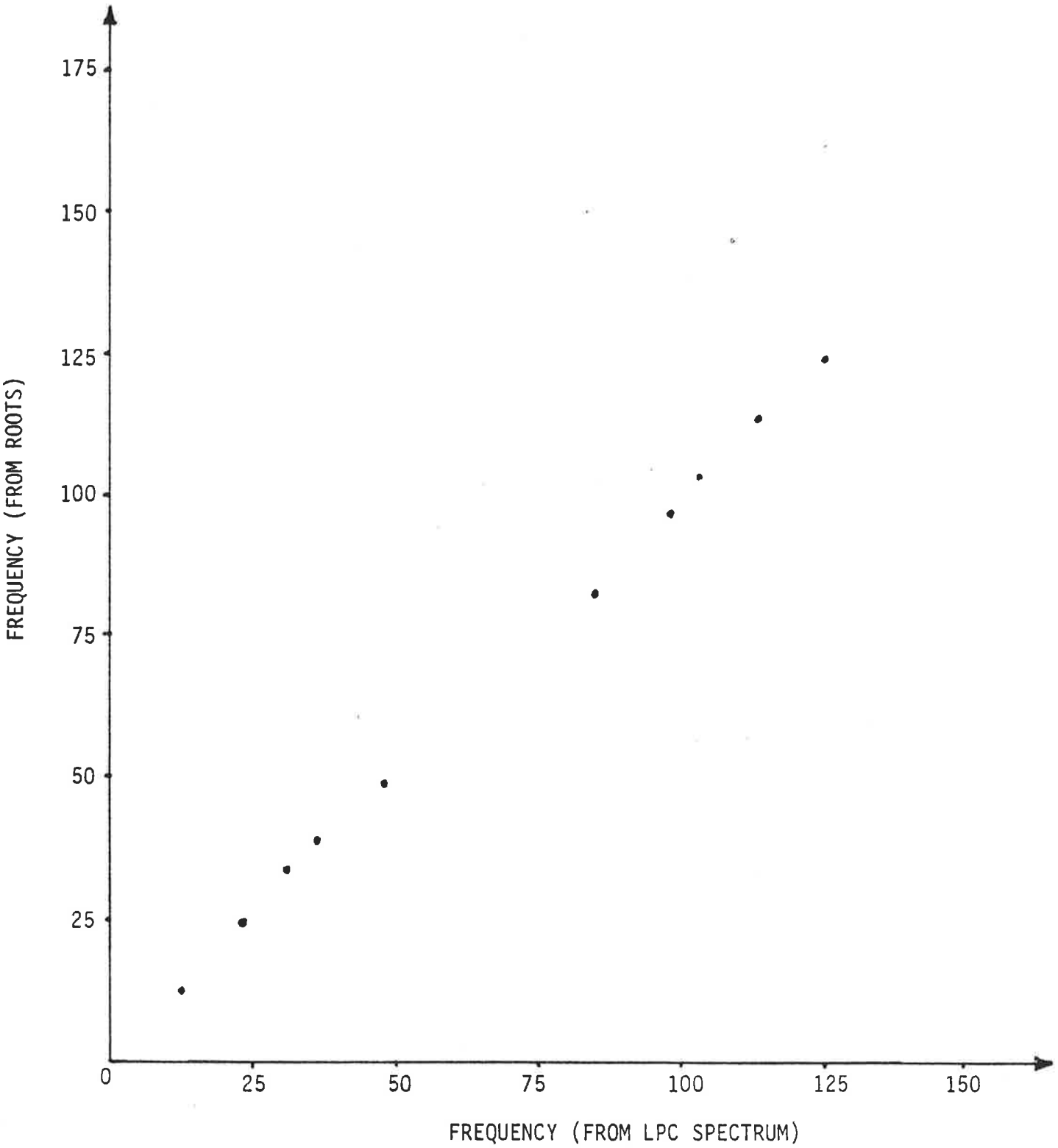

FIGURE 6.4: RELATIONSHIP BETWEEN FFT AND LPC SPECTRAL PEAKS

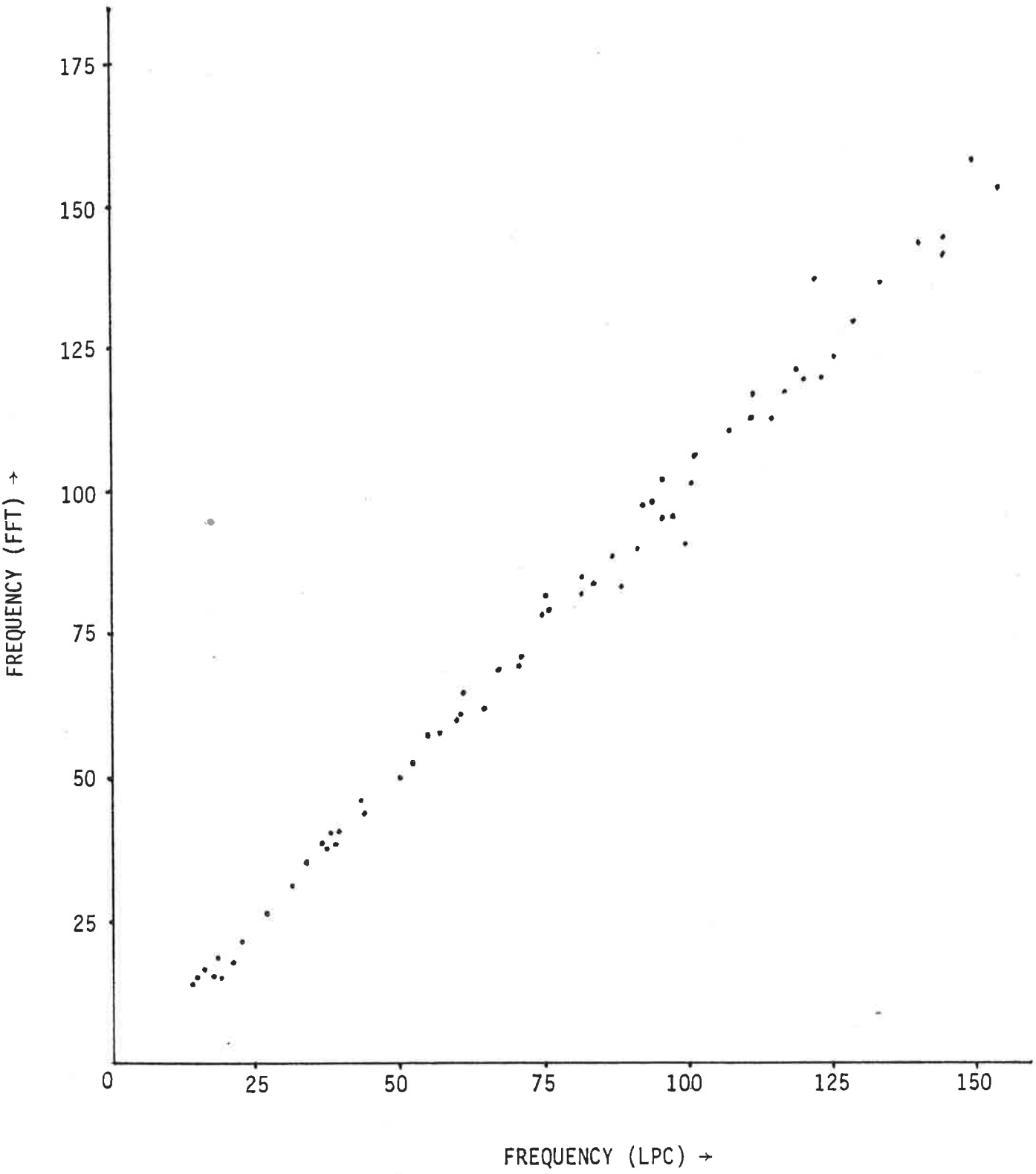

FIGURE 6.5: RELATIONSHIP BETWEEN FREQUENCY VALUES OBTAINED FROM LPC SPECTRUM AND ROOT SOLVING METHOD

applied to obtain the spectral distribution of the second heart sound in 17 normal children. The SLPC spectra have compared with FFT spectra. The efficacy of the SLPC technique in providing better frequency spectra has been demonstrated. The dominant frequency of the second heart sound spectra in children is found to be around 30 HZ which is comparatively smaller than in adults.

The main advantage of using the linear prediction technique is that one has the flexibility of limiting the analysis to a desired frequency range without losing the dynamic range of the spectrum. Also the desired frequency range can be obtained by doing the analysis over subdivided ranges using inverse filters of lower predictor order. The SLPC technique can be viewed as providing a narrow frequency window through which the second heart sound signal can be viewed to determine the spectral characteristics.

CHAPTER VII

SPECTRAL ENERGY CORRELATIONS OF SECOND HEART SOUND WITH ECHOCARDIOGRAPHICALLY DERIVED VALVULAR DIMENSIONS

7.1 Introduction to echocardiography:

Echocardiography is now an established diagnostic procedure in most hospitals throughout the world. This is done in real time, entailing cross sectional imaging of the heart using ultrasonic scanning techniques. The echocardiographic techniques have been used in the present study to obtain aortic valve dimensions for correlation with spectral energy of the second heart sound with a view to understand the contribution of aortic valve vibration to the production of the second heart sound.

Ultrasonic techniques are used for the examination of soft tissue structures in a way complementary to X-Rays employed for imaging hard tissues. Ultrasonic imaging is based on delineation of tissue structural boundaries due to reflection of part of the energy of a pulse of ultrasound when it meets the boundary between two media of different accoustical properties. The ultrasound reflection phenomenon is schematized in figure 7.1. The transducer (piezoelectric crystal) sends a short burst of ultrasound into the object under examination. This short pulse of ultrasound travels from the transmitter and when it reaches a surface between two different media, some of it is reflected producing an

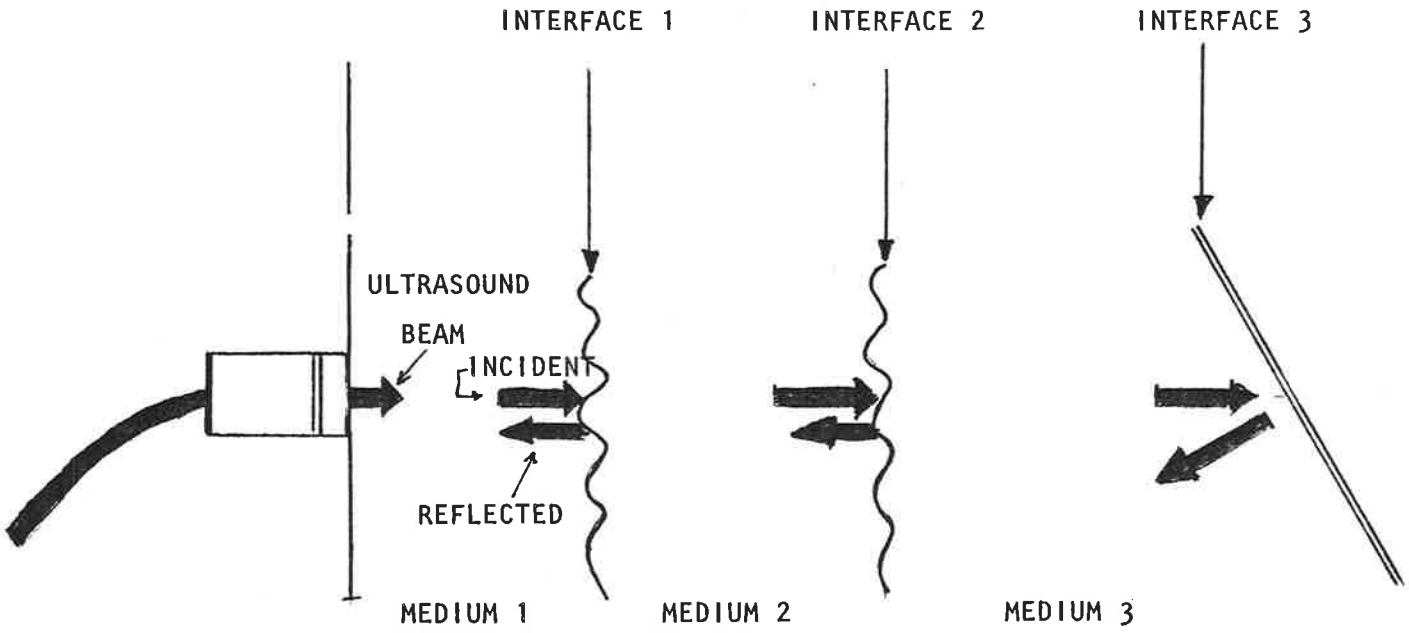

FIGURE 7.1 ULTRASOUND REFLECTION AT VARIOUS INTERFACES

echo and the rest is transmitted into the second medium. Again, an echo is produced at surface 2 and successive surfaces.

The echoes are detected by the receiving elements of the transducer; most often the transmitting elements detect the echoes as well. Echoes are detected only if they travel back to the receiver, i.e. if they are reflected from surfaces which are perpendicular to the beam. As seen in figure 7.1, the echo produced from Surface 3 would not be detected. The amplitude of the detected echo would depend upon a number of factors such as the shape of the reflecting surface, nature of the media and the absorption of the ultrasound by the media.

The time between the pulse being transmitted and the first echo being received may be detected by monitoring the pulses on an oscilloscope. Knowing the velocity of sound in the medium, the depth of the surface causing the particular echo can then be calculated.

$$\text{depth} = \text{velocity of ultrasound} \times \frac{\text{time between the pulse and echo}}{2} \qquad .....(7.1)$$

The velocity of propagation of ultrasound in a medium is given by:

$$\nu = f\lambda \qquad .....(7.2)$$

where f is the frequency of ultrasound and λ is the wavelength. The frequency of ultrasound employed in cardiac imaging varies between 1 and 7 MHZ. The velocity of

ultrasound in soft tissue is assumed to be constant around 1540 m/sec. The higher the frequency of ultrasound, the larger is the attenuation as the ultrasound penetrates the tissue. The detected echoes are processed and displayed to produce real time images of the heart-cross section. In echo-cardiography, two types of techniques are normally used to scan the heart.

1. M-mode echocardiography
2. 2-Dimensional echocardiography

In M-mode echocardiography, the ultrasound pulse is produced by a single transducer and directed along a single line. This gives an image of the heart along a single line with respect to time. The ultrasound beam acuied to pass through various cross sections of the heart is depicted in figure 7.2 and the corresponding reflections from various structures along the beam direction is shown in figure 7.3.

In 2-dimensional echocardiography, multiple transducer elements are used to produce ultrasound beams along seveal lines over a sector of heart. The echoes produced along several lines, when viewed together, produce a 2-D image of the section of the heart. The reconstructed 2-D images are reproduced at a rate of 30/second to give a dynamic real time scan. By varying the position and angle of the transducer, different sections of the heart are imaged.

Various types of ultrasound transducers used to produce 2 dimensional echocardiography are shown in figure 7.4. The phased array scan is probably the most sophisticated technique for obtaining two dimensional images of the heart.

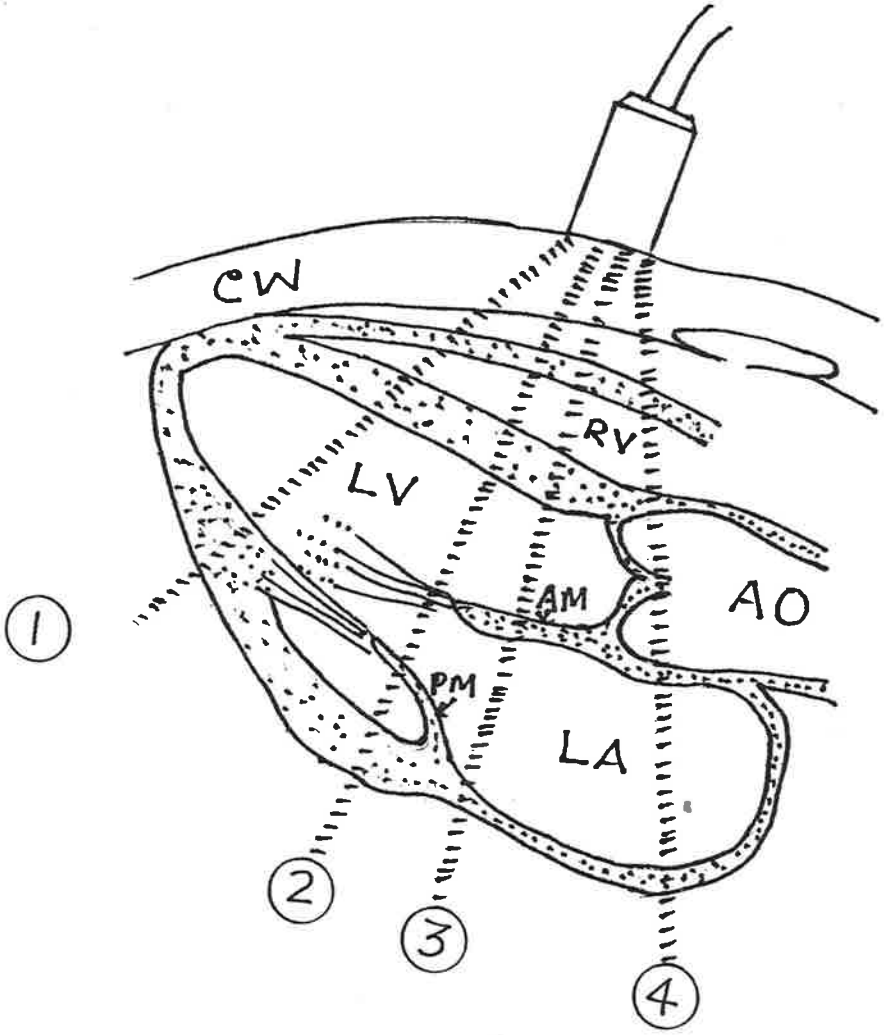

FIGURE 7.2 HEART CROSS SECTION SHOWING ULTRASOUND BEAM DIRECTIONS AS IT IS SCANNED FROM THE APEX TO THE BASE.
CW: CHEST WALL, RV: RIGHT VENTRICLE
LV: LEFT VENTRICLE, AM: ANTERIOR MITRAL
PM: POSTERIOR MITRAL, AO: AORTA
LA: LEFT ATRIUM

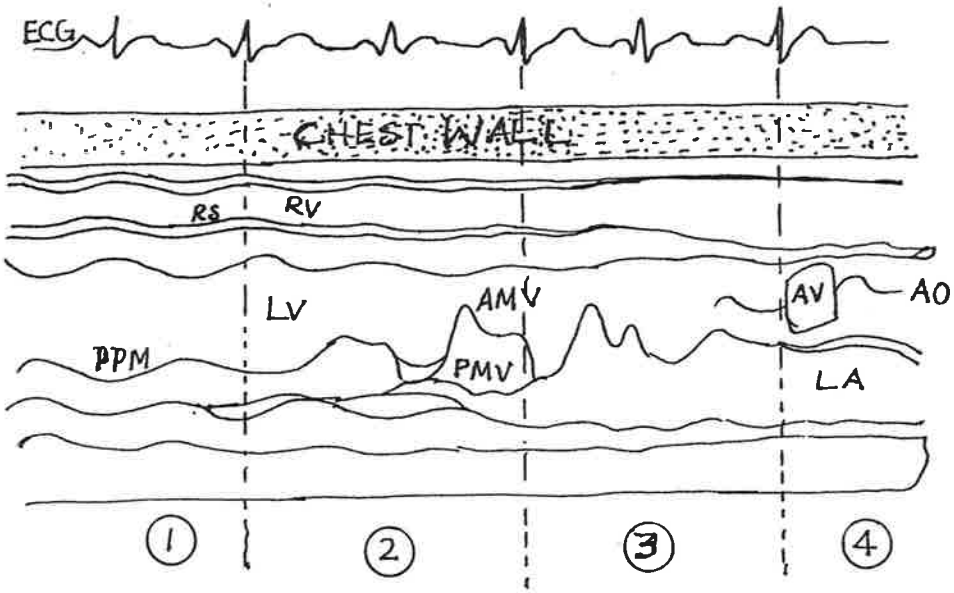

FIGURE 7.3 M-MODE ECHOCARDIOGRAM AS THE TRANSDUCER IS DIRECTED FROM APEX TO THE BASE (POSITIONS 1 THROUGH 4 OF FIGURE 7.2)

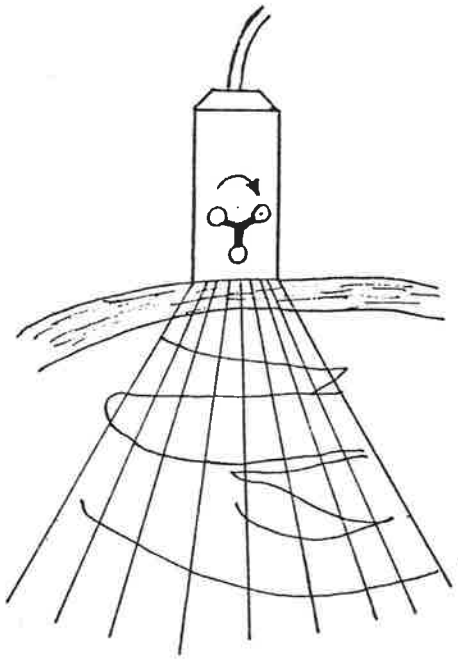

MECHANICAL SCAN

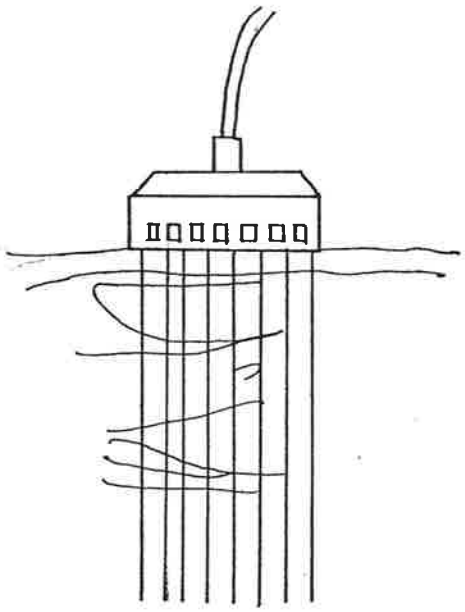

LINEAR ARRAY

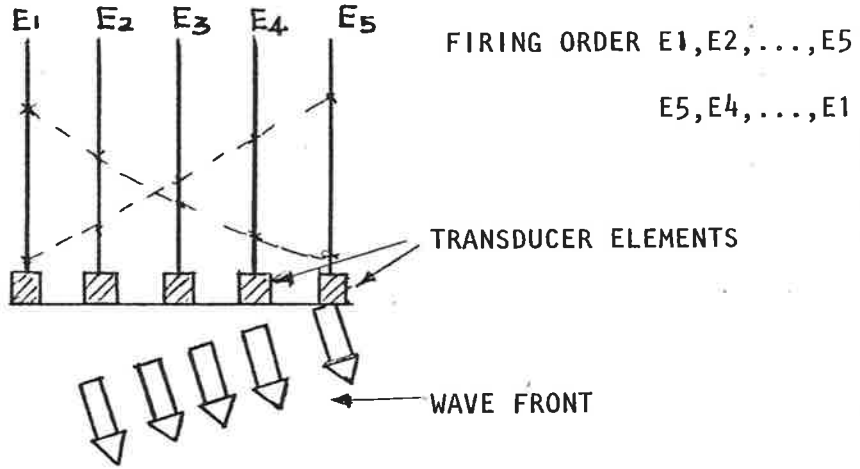

PHASED ARRAY

FIGURE 7.4 ULTRASOUND TRANSDUCERS FOR 2-D ECHOCARDIOGRAPHY

The transducer is normally about 2 cm wide allowing positioning between the ribs. It employs multiple elements (say, about 32) which are activated in sequence with an electronically timed delay so that the ultrasonic wave front is at an angle with the transducer. This electronic scan permits high speed scanning without having to use mechanical moving parts. The Cardiac structure is scanned over a sector as wide as 78°.

7.2 2-dimensional echocardiographic planes

The cross-sectional view of the heart obtained in two-dimensional echocardiography depends on the location and angle of the transducer on the precordium with respect to the heart. Accordingly, a number of planes have been described for 2-D echo imaging and are standardised by the American Society of echocardiography in 1979. Some of the common transducer positions are shown in figure 7.5. The parasternal long axis approach allows the study of the aorta, mitral valve, left ventricle and left atrium. For this long axis view, the transducer is placed in the left parasternal region, usually in the third or fourth left intercostal space. The plane of the ultrasound beam is parallel to the axis of the left ventricle from the apex to the aorta. The corresponding image of the heart in this approach is shown in figure 7.6a. In the parasternal short axis view, the transducer location is as in the previous view, but rotated 90 clockwise so that the ultrasound beam is perpendicular to

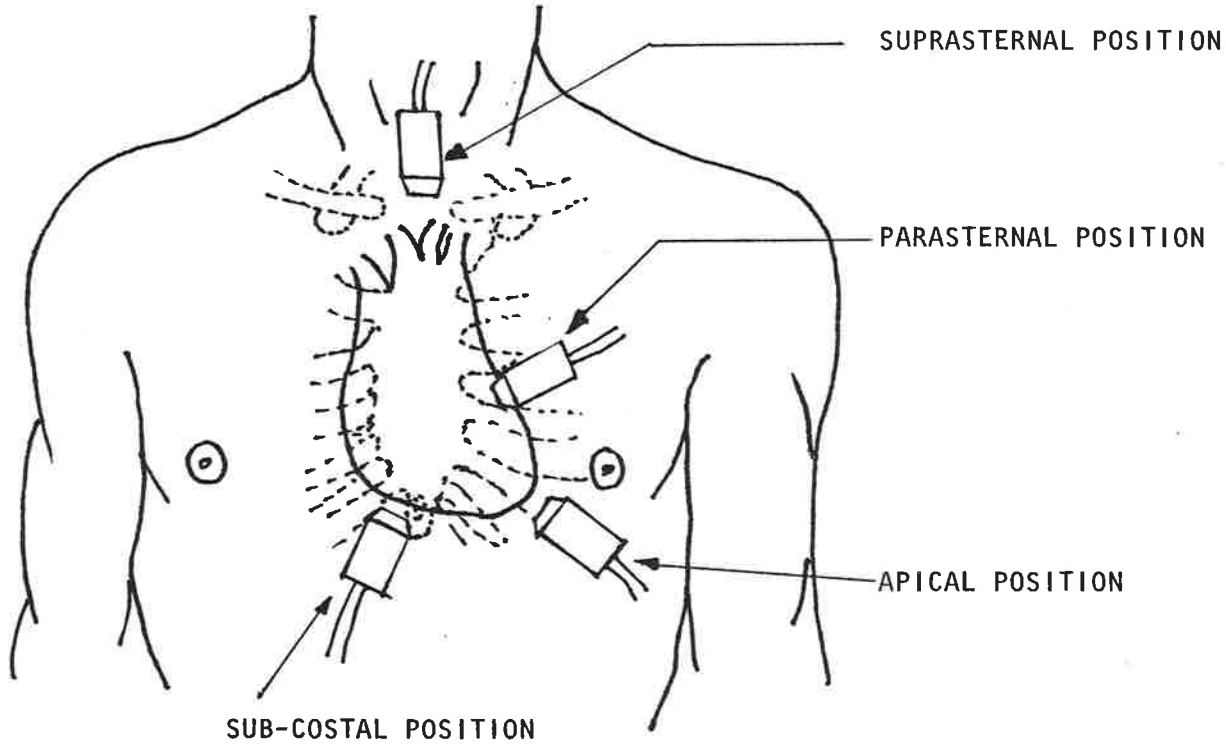

FIGURE 7.5 TRANSDUCER POSITIONS FOR ECHOCARDIOGRAPHIC EXAMINATION

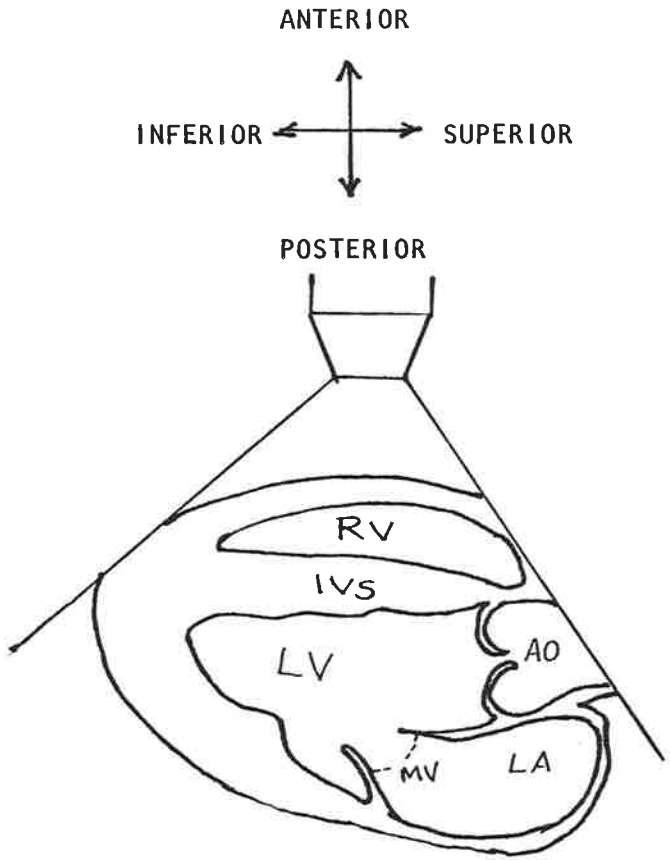

FIGURE 7.6(a) LONG AXIS VIEW

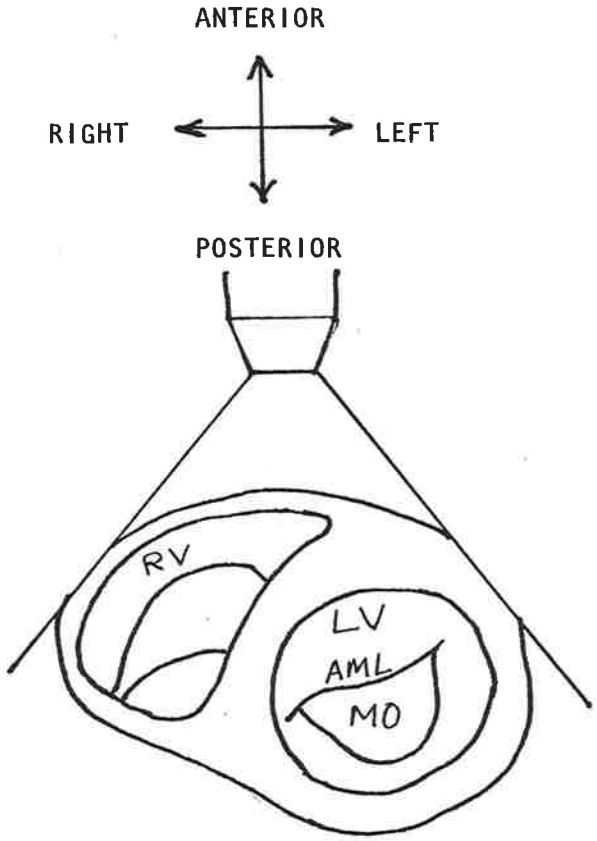

FIGURE 7.6(b): SHORT AXIS VIEW

LEGEND : RV: RIGHT VENTRICLE, IVS: INTER VENTRICULAR SEPTUM, LV: LEFT VENTRICLE
AO: AORTA, LA: LEFT ATRIUM, MV: MITRAL VALVE, MO: MITRAL ORIFICE
AML: ANTERIOR MITRAL LEAFLET.

the long axis. The short axis view is indicated in figure 7.6b. These are the two main views used in this study to obtain the aortic valve size parameters. Depending on the cross section of interest, other echocardiographic planes such as apical and subxiphoid are also used in the routine clinical examination of the heart.

7.3 Heart sound spectral energy distribution

The spectral analysis of heart sounds in general clearly indicates the presence of several resonant peaks believed to be due to the resonance of various cardiac structures. These resonant peaks have different amplitudes as seen in the previous chapters. The knowledge of the energy distribution of heart sounds is important in valvular diagnosis [Rangaraj, et al., 1979].

Most of the spectral analysis studies in cardiovascular sounds have been aimed at providing better understanding of the vibratory origin of the heart sounds and murmurs. In the case of the first heart sound (SI), a number of meticulous studies have suggested that the vibration of the atrio-ventricular valve leaflets may be a contributory factor in the production of SI [Laniado et al., 1973; Prakash et al., 1976; Mills et al., 1976].

As the heart sound data have been collected on 17 normal children and the second heart sound spectra for the above subjects have been determined (refer chapter 6), an attempt is made in this chapter to determine the energy distribution

of second heart sound in the frequency domain. Heart sound energy distribution in the time domain has already been attempted by Rangaraj et al. [1979].

In order to estimate the spectral energy distribution, spectral energies were calculated by computing the areas under the power spectrum over a 20 HZ bandwidth, normalized with the total area under the entire spectrum. The areas are estimated by numerical integration of the power spectrum curve over the desired bandwidth (20 HZ) using a trapezoidal scheme. The energies could also be calculated over 10 HZ or 30 HZ bandwidths. The choice for the bandwidth is purely arbitrary. The average spectral energy distribution in children is represented in the form of a histogram as shown in figure 7.7. The ordinate represents normalized energy or the proportionate energy. It is apparent, from this histogram, that the dominant frequency of SII is in the frequency range 20-40 HZ; more accurately most energy is in this bandwidth.

7.4 Echocardiographic evaluation of aortic valve dimensions

The aortic valve dimensions for children whose spectral distribution was studied earlier, have been evaluated using both M-mode and 2-dimensional echocardiographic techniques. A Toshiba SSH-10A sonolayergraph machine has been used to obtain both the M-mode and 2 dimensional echocardiographs of the left ventricular outflow tract. The 2-D echocardiograph recordings were done at the Adelaide children's hospital

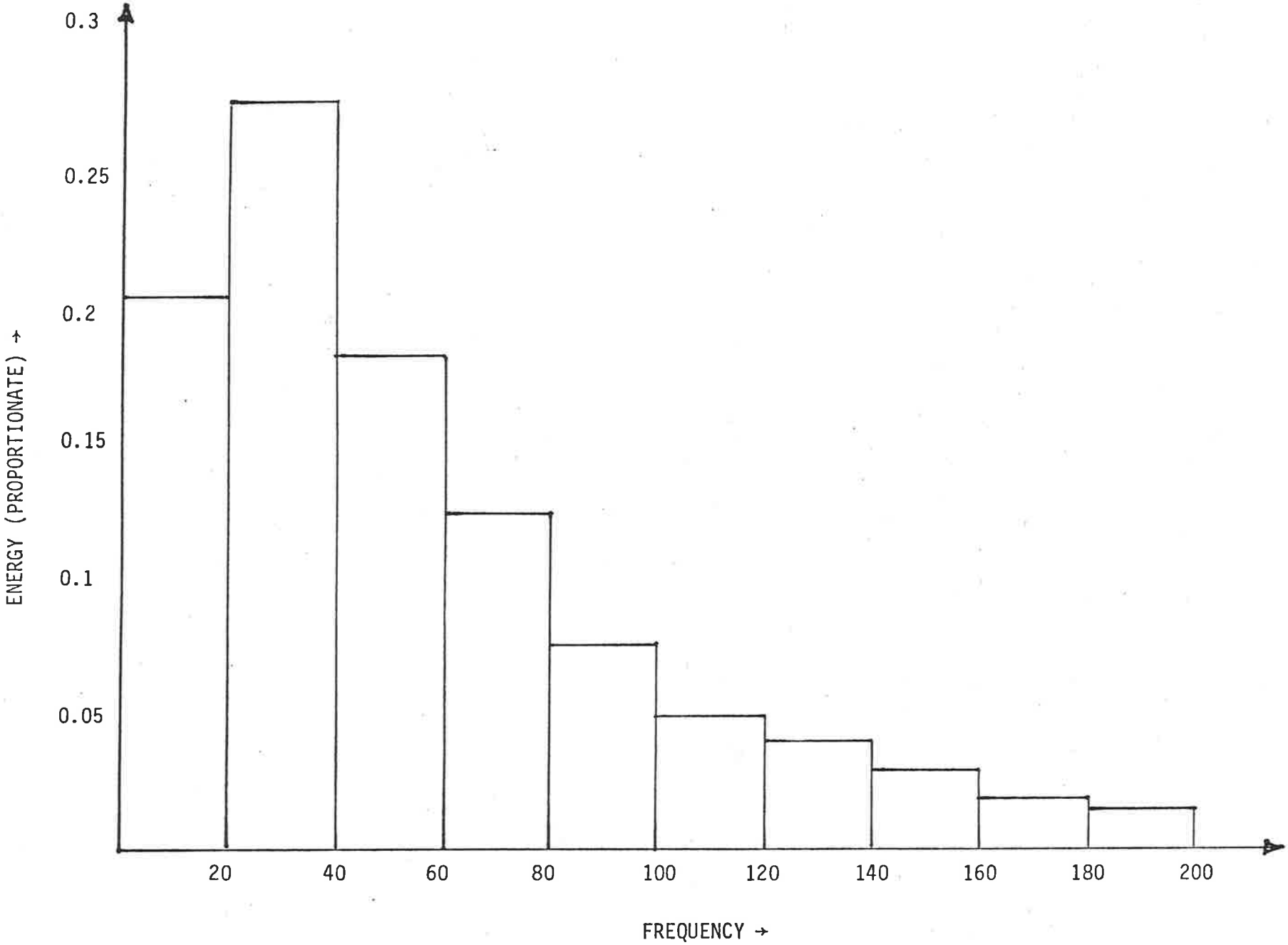

FIGURE 7.7 AVERAGE SPECTRAL ENERGY DISTRIBUTION OF SECOND HEART SOUND IN CHILDREN

along with the phonocardiographic recordings outlined in chapter VI.

Parasternal long axis and short axis views of the aortic valve were used for each subject. A 3.4 MHZ ultrasound transducer was used in these measurements. Two dimensional echocardiograms were stored on 'U' matic 3/4" video tape by using the video recording facility attached to the Toshiba SSH-10A sonolayergraph machine. In order to determine the aortic valve orifice size and valve diameter, stop frame echocardiographic images of the aortic valve in opened and closed positions (along the parasternal long axis and short axis) were taken for each subject. Figure 7.8 shows the stop frame images of the parasternal long axis views of the aortic valve in opened and closed positions.

The aortic valve ring diameter is measured from all these views by tracing from the stop frame images and then digitising the length along the dotted line in figures 7.8 and figure 7.9 using a Hewlett-Packard 9874A digitiser interfaced with a Hewlett-Packard 9830A computer. An average value is obtained from these views to minimize the error in measurement. Also the valve dimensions thus obtained are checked with the corresponding values from M-mode echocardiography. Figure 7.10 shows the M-mode echocardiography when the ultrasound beam is directed through the aortic valve. The electrocadiogram and phonocardiogram are also displayed alongside. It is also seen, from the figure 7.10, that the coaptation of the aortic valve leaflets

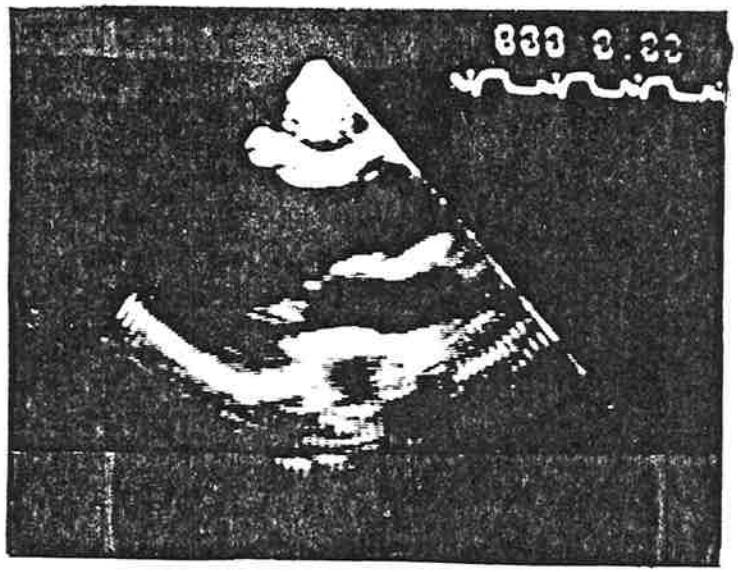

FIGURE 7.8(a) PARASTERNAL LONG AXIS VIEW
AORTIC VALVE OPENED

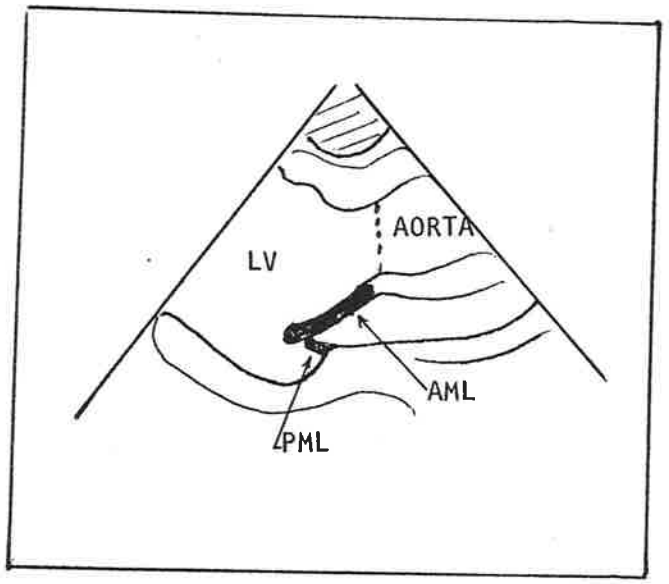

SCHEMATIC OF FIGURE 7.8(a)

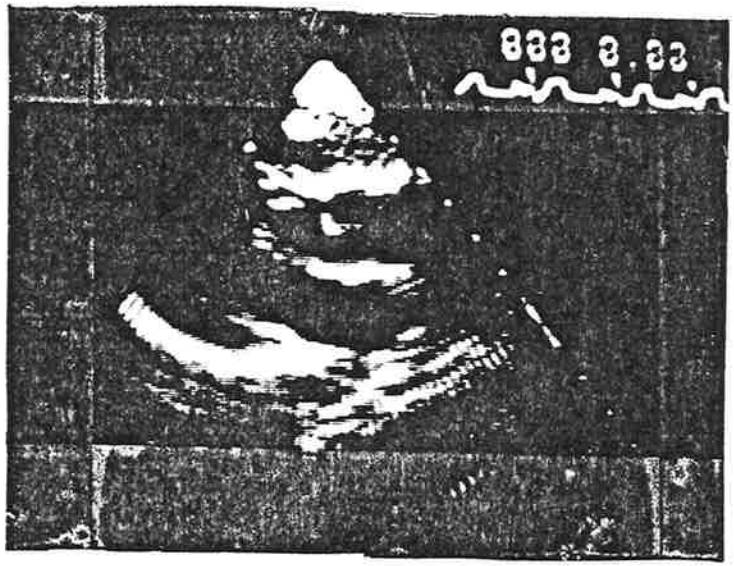

FIGURE 7.8(b) PARASTERNAL LONG AXIS VIEW
AORTIC VALVE CLOSED

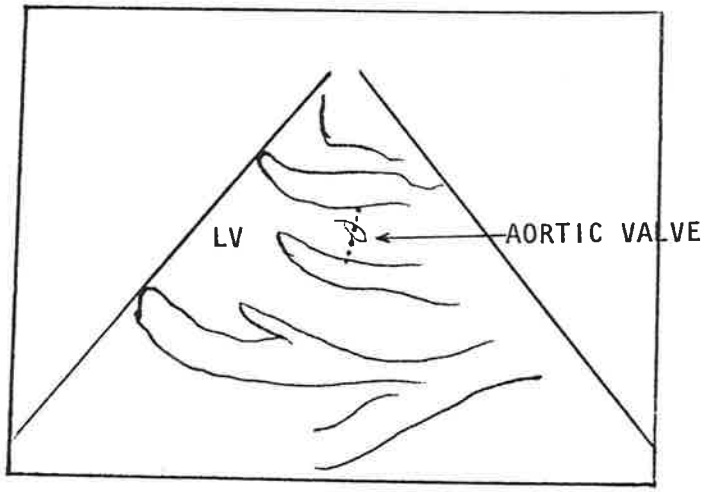

SCHEMATIC OF FIGURE 7.8(b)

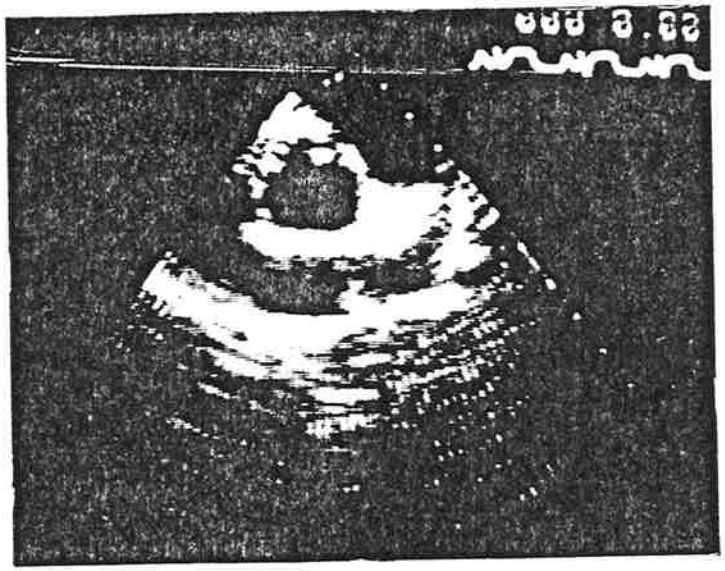

FIGURE 7.9(a) PARASTERNAL SHORT AXIS VIEW OF AORTIC VALVE (OPENED)

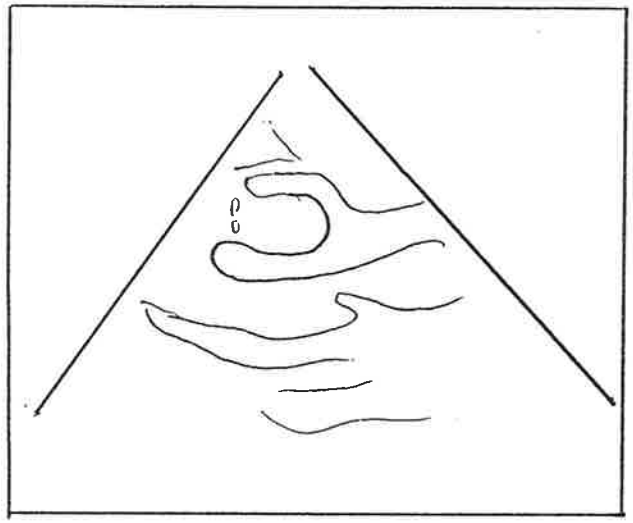

SCHEMATIC OF FIGURE 7.9(a)

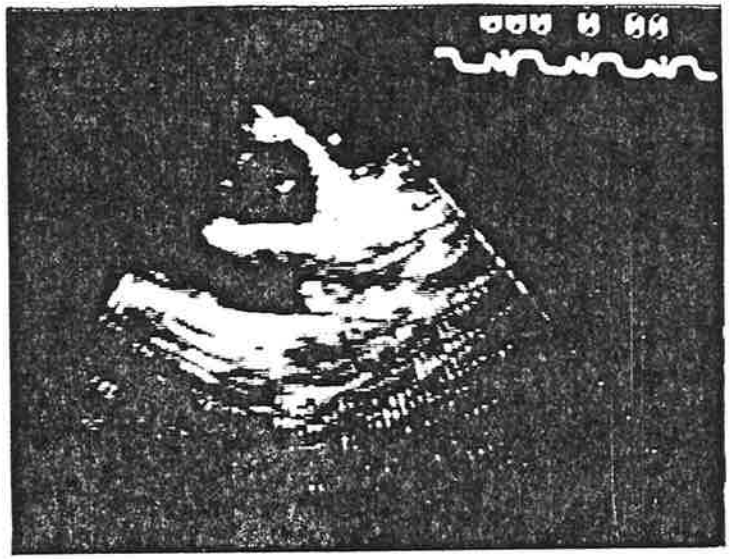

FIGURE 7.9(b) PARASTERNAL SHORT AXIS VIEW OF AORTIC VALVE (CLOSED)

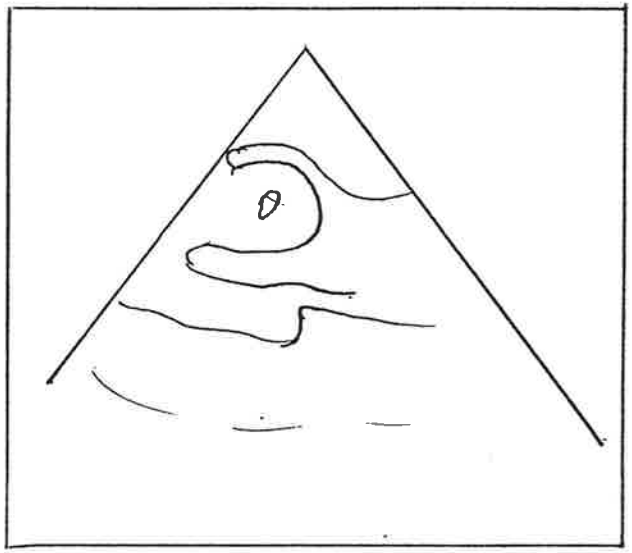

SCHEMATIC OF FIGURE 7.9(b)

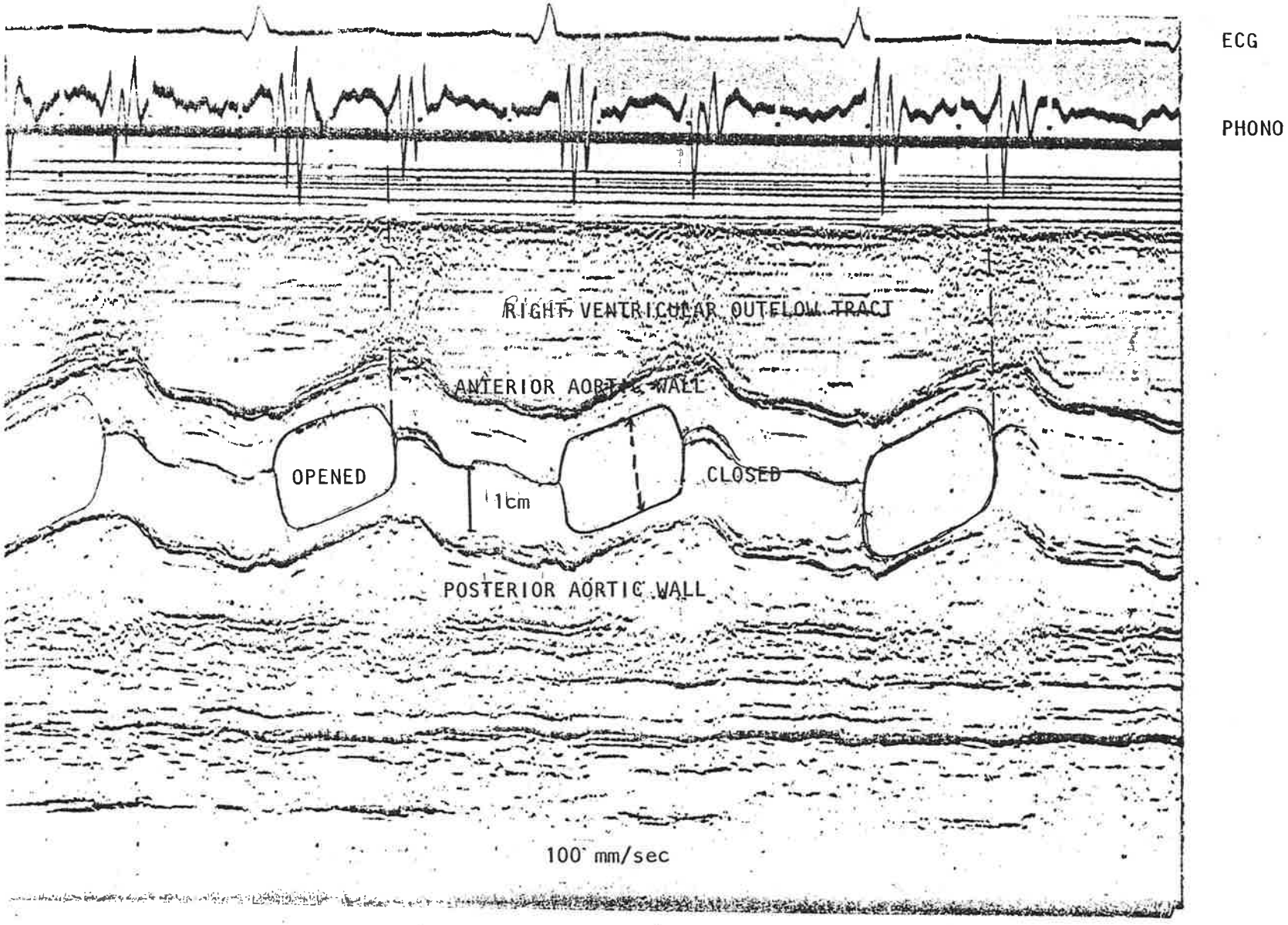

FIGURE 7.10 M-MODE ECHOCARDIOGRAM

is synchronous with the onset of the second heart sound. The aortic valve size parameters were thus obtained for ten subjects. Table 7.1 gives the average diameter of the aortic valve and the average R-R interval for ten subjects.

7.5 Correlation of spectral energy with aortic valve size parameter

Hearn et al., [1982] have demonstrated the existence of a strong correlation between the closing velocity of the anterior mitral leaflet and the first heart sound energy in the frequency bandwidth 30-45 HZ. Further, spectral energy of the first heart sound has been correlated with a mitral valve size parameter and the best correlation was attained in the 30-45 HZ bandwidth [Hearn, et al., 1983]. This may suggest that the frequency peaks seen in the range 30-45 HZ of the first heart sound spectra may originate from the vibration of mitral leaflets.

It is believed that the second heart sound is caused by the vibration of the closed semilunar leaflets immediately after silent coaptation [Stein and Sabbah 1976]. In order to find a relationship between the aortic valve vibration and the second heart sound, an attempt is made to correlate the spectral energies calculated in various frequency bandwidths of SII with the aortic valve dimensions.

The normalised spectral energy contained in 20 HZ bandwidth for each subject is calculated as described in

TABLE 7.1

Subjects	Age/Sex Years	Average diameter of Aortic value cm/sec	Average R-R interval m.secs
C25	12/M	1.8	680
C28	6/F	1.3	720
C29	12/M	1.4	720
C31	11/M	1.71	560
C32B	12/F	1.5	680
C34	5/M	1.2	680
C36	7/M	1.27	720
C1	8/M	1.6	730
C9C	4/M	0.95	640
C13A	9/M	1.4	680

section 7.3. Correlation analysis was performed by correlating the spectral energy contents in 20 HZ bandwidths of the second heart sound spectra of ten subjects with the aortic valve dimension; viz. diameter of the aortic valve ring and the aortic area assuming circular cross section. The Pearsons correlation coefficient γ was used to test for significant correlations [Snedecor and Cochran, 1967]. The correlation coefficient γ is given by:

$$\gamma = \frac{\sigma_{xy}}{\sigma_x \sigma_y} \qquad .....(7.3)$$

where

$$\sigma_x = \sum_{i=1}^{n} x_i^2 - \frac{\left(\sum_{i=1}^{n} x_i\right)^2}{n} \qquad .....(7.4)$$

$$\sigma_y = \sum_{i=1}^{n} y_i^2 - \frac{\left(\sum_{i=1}^{n} y_i\right)^2}{n} \qquad .....(7.5)$$

$$\sigma_{xy} = \sum_{i=1}^{n} x_i y_i - \frac{\sum_{i=1}^{n} y_i \sum_{i=1}^{n} x_i}{n} \qquad .....(7.6)$$

Here, X_i is the array containing spectral energies in 20 HZ bandwidths in various frequency ranges for n subjects and Y_i is the array containing the parameter relating to aortic valve size.

The correlation coefficient γ is calculated for the spectral energy in every 20 HZ bandwidth of the spectra in the frequency range 0-200 HZ using a computer program.

This program first computes the area under every 20 HZ bandwidths of the second heart sound spectra of ten subjects and creates ten arrays containing spectral energies with each array containing spectral energy of 10 subjects in 20 HZ bandwidth of a given range (say 0-20 HZ, 20-40 HZ, etc.). The areas are estimated by numerical integration of the power spectrum curve over the 20HZ bandwidth as explained earlier. Each of the above arrays is correlated with the array containing the valve size prarmeter and a correlation coefficient r is computed.

The Correlation Coefficient obtained by correlating the aortic valve diameter and aortic valve area are indicated in table 7.2. Figure 7.11 shows the correlogram of spectral energies with the aortic valve areas assuming circular cross sections. From the Correlogram it is quite evident that the aortic valve area correlates best with the spectral energies in the bandwidth 120-140 HZ with a Correlation Coefficient of 0.95, implying a relationship between the aortic valve and the second heart sound spectra in the range 120-140 Hz. This may mean that certain modes of vibration of closed aortic valve leaflets may contain frequencies in the range 120-140 Hz. In order to check that this high correlation is not by chance, a cardiac parameter not directly related to second heart sound was chosen for correlation. Accordingly, the average R-R interval for each subject was calculated and correlated. Figure 7.12 indicates that there is no significant correlation in any frequency range.

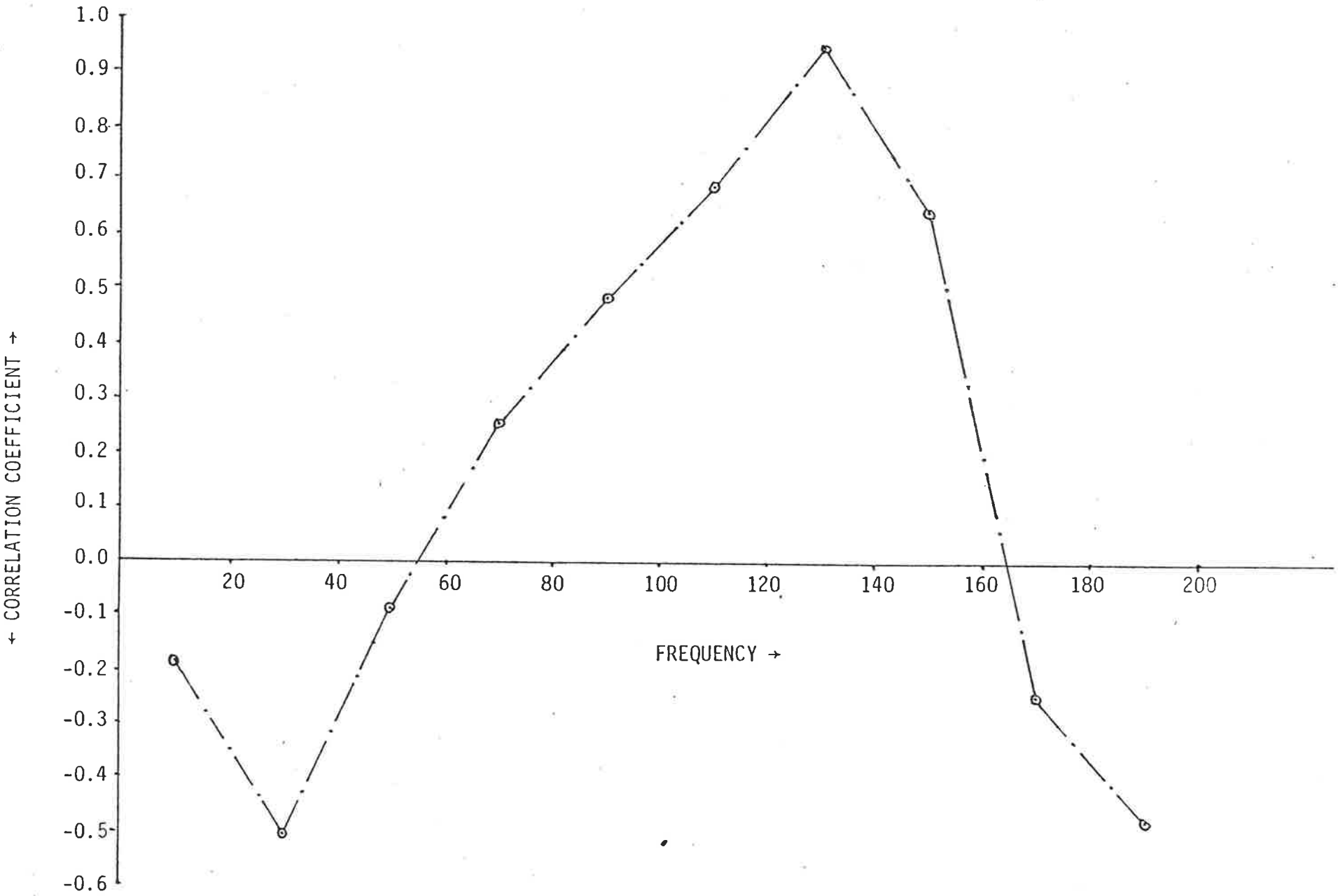

FIGURE 7.11 CORRELOGRAM (SPECTRAL ENERGY WITH AORTIC VALVE AREA)

TABLE 7.2

Correlation coefficients between spectral energy and the aortic diameter and area

Frequency Bandwidth (Hz)	Correlation Coefficient (γ)	
	With the aortic diameter	With the aortic valve area
0 - 20	-0.1931	-0.1943
20 - 40	-0.5272	-0.5132
40 - 60	-0.0986	-0.0890
60 - 80	+0.2229	+0.2096
80 - 100	+0.5196	+0.4895
100 - 120	+0.7234	+0.7059
120 - 140	+0.9458	+0.9501
160 - 180	-0.2991	-0.3027
180 - 200	-0.4581	-0.4721

However, there are a number of factors that govern the characteristics of the second heart sound, i.e. the diastolic pressure gradient across the closed valve, the modulus of elasticity of the valve leaflets, size of the valve(diameter, area of cross section and thickness) and of course, the viscosity of the fluid (blood) surrounding the valve. It has also been observed that the aortic component of SII is caused by physical events that occur after the coaptation of the aortic leaflets [Anastassiades, et al. 1976; Sabbah and Stein, 1976].

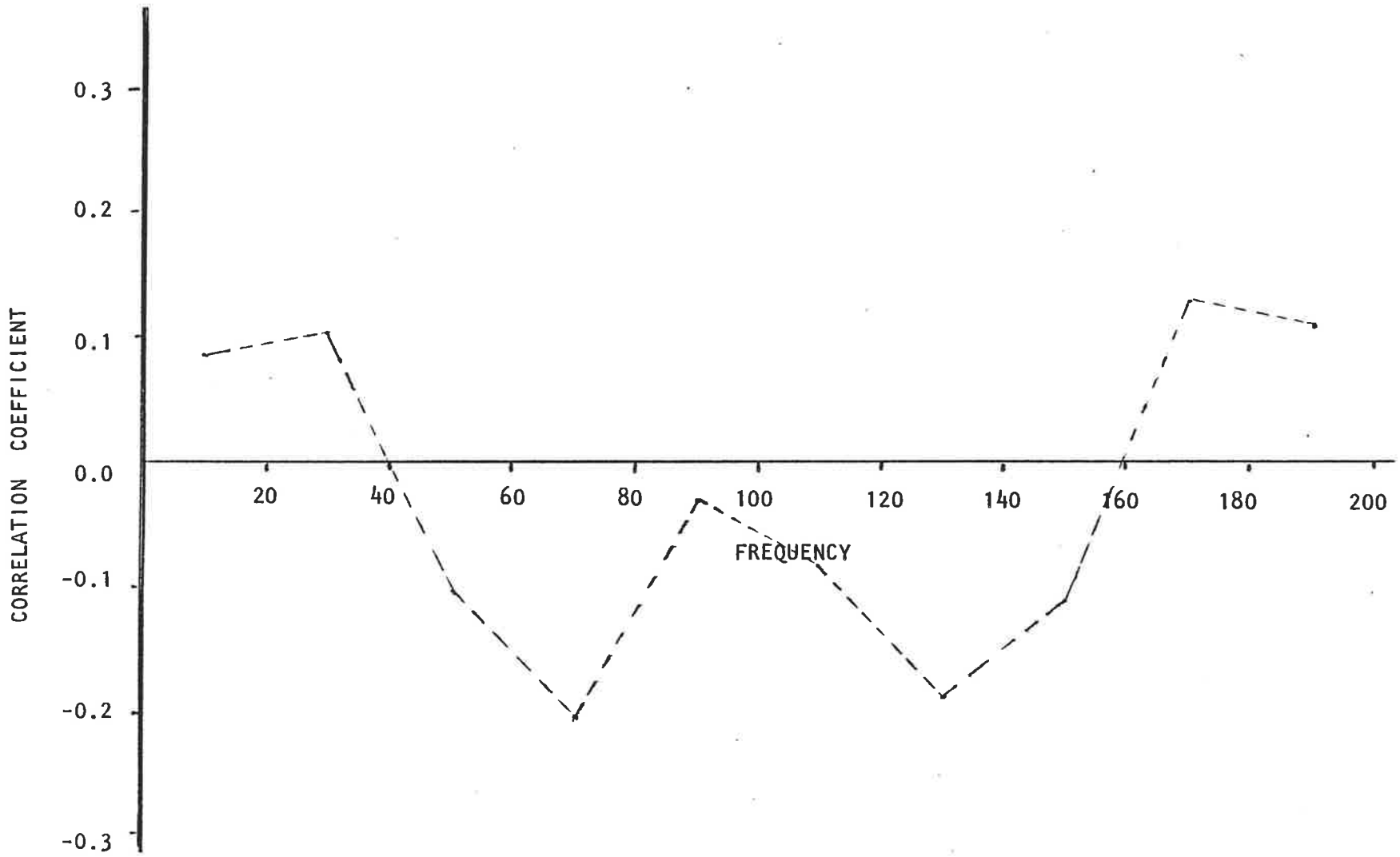

FIGURE 7.12 CORRELOGRAM (SPECTRAL ENERGY WITH R-R INTERVAL)

CHAPTER VIII

TOWARDS QUANTITATIVE DETERMINATION OF VALVULAR CALCIFICATION/MALFUNCTION

8.1 Introduction:

Heart valves, upon coaption of their leaflets, will vibrate when subjected to dynamic pressure loading, corresponding to sudden acceleration or decelerations of intra-cardiac blood columns. Such vibrations have been associated with the occurrence of the first and second heart sounds. Mathematical models to represent the free and forced vibrations of mitral valve leaflets have been developed by Hearn et al [1979]. Assuming semicircular boundary shapes for the leaflets, solutions for the mitral valve frequencies have been obtained by Ghista et al [1972]. Having studied the second heart sound spectral distribution, an attempt will be made in this chapter to model the aortic valve in a simple way proceeding along similar lines to those of Hearn et al [1979]. The maximum energy frequency obtained from the second heart sound spectrum is used in the aortic valve model along with 2-D echocardiographically derived aortic valve dimensions, to designate the vibrational frequency versus valve membrane radius coordinate plane.

8.2 Aortic valve vibrational model

The aim of this analysis is to model the aortic valve

vibrations mathematically so as to determine the primary mode frequencies of the leaflets, and then correlate this vibration with the occurrence of the SII. The boundary shape of the membrane together with the mass of leaflets and the tension in the leaflets will be of major importance for this analysis.

It will be assumed that the curved edges of the aortic leaflets are firmly anchored to rings of dense connective tissue, which in turn are firmly embedded within the musculature of the heart. Thus it is unlikely that the movement of the aortic annulus will accompany leaflet vibrations [Rushmer, 1970]. It has been argued further [Lim et al., 1980] that the absence of regurgitation in the properly sealed valve suggests that the lines of coaption of the individual leaflets may be regarded as fixed. With these assumptions, the closed aortic valve may be modelled as three sectors of a circle as shown in figure 8.1.

It has been pointed out by Lim et al [1980] that the illustrated membrane configuration does not occur as a vibrational mode shape of a vibrating circular membrane. In order to obtain an accurate measure of the vibrational frequencies, each leaflet is considered as a separate membrane and the analysis is carried out in the same manner as Mazumdar [1973].

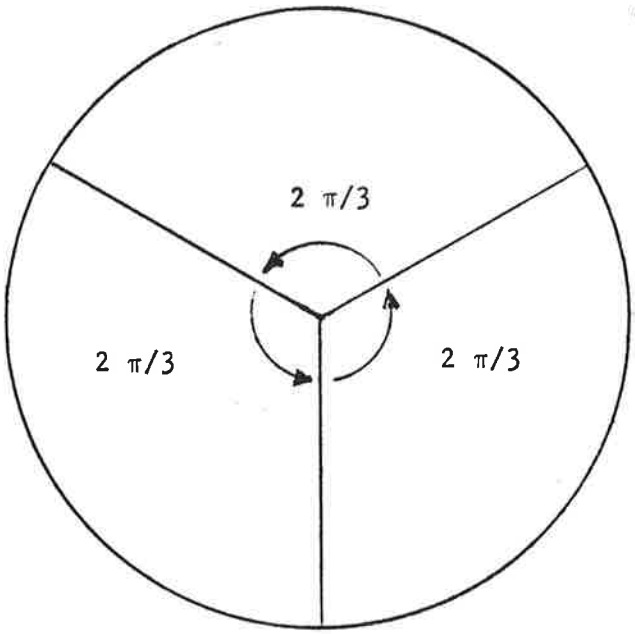

FIGURE 8.1 THREE LEAFLET MODEL OF THE CLOSED AORTIC VALVE

The membrane boundary is represented by a simply connected plane curve C_o enclosing a region Ω_o. The dynamic membrane deflection at any point in the region Ω_o and at any time t, is represented by w(x,y,t). When the membrane vibrates, the profile of the deflection surface at any time may be described by a family of iso-amplitude contour lines, which when projected onto the xy-plane will form a system of level curves

$$U(x,y) = \text{constant}$$

This family of closed curves will be represented by C_u, $0 \leq U \leq U^*$ where C_o represents the boundary of the membrane and C_{u^*} coincides with the point at which the maximum $U = U^*$ is attained. The region bound by C_u is denoted by Ω_u as indicated in figure 8.2.

Small dynamic deflections w of the membrane during vibration will be described by the two-dimensional wave equation.

$$T \nabla^2 w = \rho \frac{\partial^2 w}{\partial t^2} \qquad \text{.....(8.1)}$$

where T is the tension per unit length

ρ is the vibrating mass per unit area

Integrating equation 8.1 over the membrane region Ω_u results in

$$T \iint_{\Omega_u} \nabla^2 w \, d\Omega - \frac{\partial^2 w}{\partial t^2} \, d\Omega = 0 \qquad \text{.....(8.2)}$$

Now introducing $\underset{\sim}{n}$ as an outward normal to the contour C_u, and applying Green's theorem

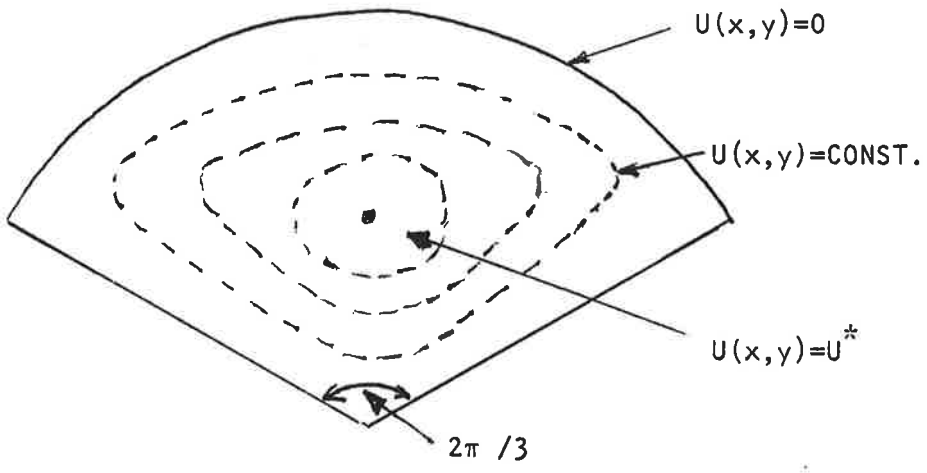

FIGURE 8.2 AORTIC LEAFLET FOLLOWING CLOSURE, WITH ASSOCIATED MATHEMATICAL DESCRIPTION

$$T \int_{C_u} \frac{\partial w}{\partial n} ds - \rho \iint_{\Omega_u} \frac{\partial^2 w}{\partial t^2} d\Omega = 0 \qquad .....(8.3)$$

With the assumption of harmonic vibration,

$$w = W(n)\, e^{j\omega t} \qquad .....(8.4)$$

where ω is the mode frequency and W determines the form of the deflected surface, equation (8.3) reduces to

$$T \oint \frac{dW}{dn} ds + \rho\omega^2 \iint_{\Omega_u} W d\Omega = 0 \qquad .....(8.5)$$

noting that the outward unit normal $\underset{\sim}{n}$ may be described as

$$\underset{\sim}{n} = - \frac{\nabla u}{|\nabla u|} \qquad .....(8.6)$$

and then $\frac{dW}{dn} = \frac{dW}{du}\frac{du}{dn} = \frac{dW}{du} \cdot \nabla u \cdot \underset{\sim}{n}$

$$= \frac{dW}{du} (U_x^2 + U_y^2)^{1/2} \qquad .....(8.7)$$

equation (8.5) may be rewritten as

$$T \frac{dW}{du} \oint \sqrt{\mathcal{T}}\, ds - \rho\omega^2 \iint_{\Omega_u} W d\Omega = 0 \qquad .....(8.8)$$

where $\mathcal{T} = U_x^2 + U_y^2$ .....(8.9)

The double integral in equation (8.8) may be simplified following Mazumder (1971) to yield

$$\frac{dW}{du} \oint \sqrt{\mathcal{T}}\, ds + k^2 \int_{u^*}^{u} W(u)\, du \oint \frac{ds}{\sqrt{\mathcal{T}}} = 0 \qquad ....(8.10$$

where k is given by

$$k^2 = \frac{\rho}{T}\omega^2 \qquad .....(8.11)$$

Differentiating equation (8.10) with respect to U yields

$$\frac{d^2W}{du^2}\oint\sqrt{T}\,ds - 2\frac{dW}{du}\oint_{C_u}\frac{ds}{\sqrt{T}} + k^2W\oint\frac{ds}{\sqrt{T}} = 0 \qquad .....(8.12)$$

which, with the evaluation of the contour integrals, and the introduction of a new variable f given by

$$f^2 = u^* - u \qquad .....(8.13)$$

finally becomes

$$\frac{d^2W}{df^2} + \frac{1}{f}\frac{dW}{df} + 2k^2W = 0 \qquad .....(8.14)$$

Equation (8.14) may be recognized as the zeroth order Bessel equation with the general solution

$$W = A\,J_o(\sqrt{2}\,kf) + BY_o(\sqrt{2}\,kf) \qquad .....(8.15)$$

Where A and B are arbitrary constants.

To avoid infinite displacements, B = 0. Also, since the membrane has zero displacement around the boundary (u = 0),

$$J_o(\sqrt{2u^*}\,k) = 0 \qquad .....(8.16)$$

so that

$$\sqrt{2u^*}\,k = B_i \qquad .....(8.17)$$

where B_i is the i^{th} zero of the zeroth order Bessel function. Thus, for fundamental mode vibration:

$$\sqrt{2u^*}\,k = 2.4048 \qquad .....(8.18)$$

and

$$k^2 = \frac{\rho\omega^2}{T} \qquad .....(8.19)$$

In order to evaluate the frequencies, by employing the eigen values (equation 4.17), it is necessary to specify the value of u*, the maximum value of the iso-amplitude contour function u, based on the size and boundary shape of the membrane. Here, for an idealized membrane subjected to a pressure loading q, the static response W is given by

$$\nabla^2 W = -\frac{q}{T} \qquad .....(8.20)$$

with W vanishing on the membrane boundary.

In the context of the membrane analogy, a cylindrical beam with the same cross-section as the membrane boundary, when under torsion, has lines of constant shearing stress coincident with the iso-deflection contours of the membrane. It has been shown [Jones, et al, 1975] that the function u(x,y) satisfies the same Poisson's equation as does the Prandtl stress function (x,y). Hence,

$$\nabla^2 u = -2 \qquad .....(8.21)$$

with u vanishing on the boundary, and consequently from equations (8.20) and (8.21),

$$u = \frac{2TW}{q} \qquad .....(8.22)$$

Limiting the analysis to the determination of the fundamental mode frequency of vibration (ω), and using equation (8.17), the following expression for the fundamental mode frequency is obtained

$$\frac{\rho}{T}\omega^2 = k^2 = \frac{(2.4048)^2}{2u^*} \qquad .....(8.23)$$

Wherein, u* willl now be specified, using the analogy of the stress function (x,y) of the torsion problem to the u(x,y) of the membrane deflection, by specifying the boundary shape.

In order to specify u*, it is required to obtain the form of u(x,y) or u(r,0) for a sector-shaped membrane. If the boundary shape for an aortic valve leaflet is approximated as a circular sector of angle $2\pi/3$, the fundamental frequencies may be obtained, for a sector-shaped membrane by selecting (in equation 8.18) the appropriate u* corresponding to the membrane boundary shape. From the corresponding torsion problem [Love. A.E.H., 1944], it is noted that for a sector of a circle, with boundaries given by ($r = o$, $r = a$, $\theta = \pm\beta$)

$$u = \frac{1}{2} r^2 \frac{\cos 2\theta}{\cos 2\beta} + a^2 \sum_{n=0}^{\infty} \left[A_{2n+1} \left(-\frac{r}{a}\right)^{(2n+1)\pi/2\beta} \cos\left\{(2n+1)\frac{\pi\theta}{2\beta}\right\} \right] \qquad .....(8.24)$$

where

$$A_{2n+1} = (-1)^{n+1} \left[\frac{1}{(2n+1)\pi - 4\beta} - \frac{2}{(2n+1)\pi} + \frac{1}{(2n+1)\pi + 4\beta} \right] \qquad .....(8.25)$$

By symmetry the maximum value of (8.19) will be found along the line $\theta = o$. Computation of equation (8.24) along this line provides a profile of the membrane's deflected shape. This is plotted in figure 8.3, from $r/a = 0$ to $r/a = 1$, for a range of sector angles. Choosing the sector angle as $2\pi/3$ provides a representation of an aortic leaflet and is shown in figure 8.4.

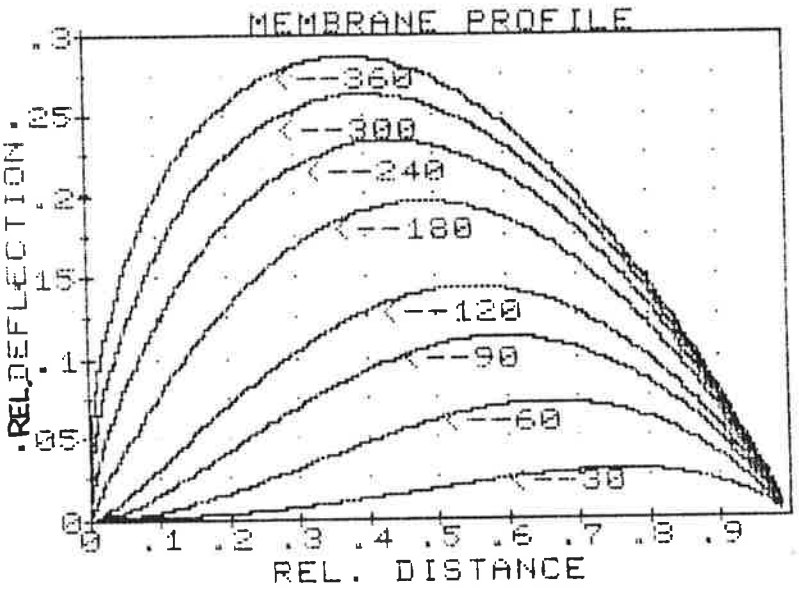

FIGURE 8.3 SECTOR MEMBRANE DEFLECTION PROFILES
ALONG θ=0 FROM r/a=0 TO r/a=1

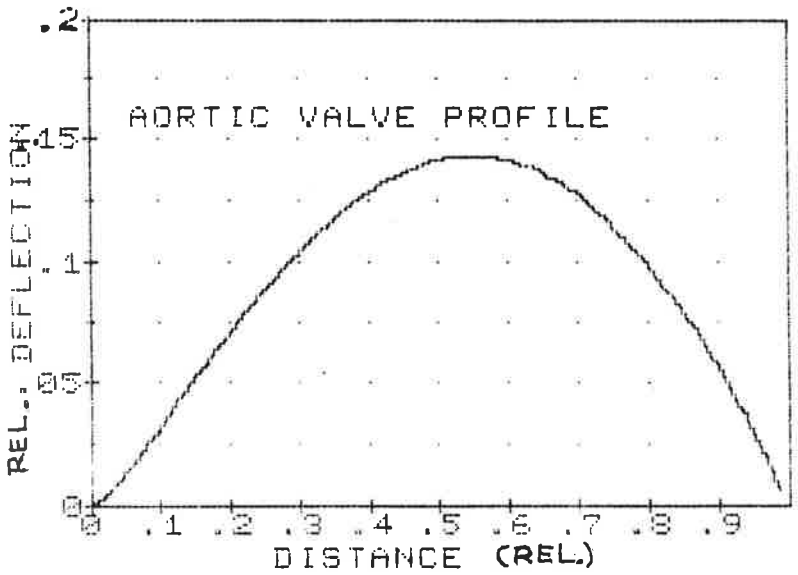

FIGURE 8.4 DEFLECTION PROFILE ALONG THE MID-LINE OF AN AORTIC LEAFLET MODEL, CONSIDERED AS A SECTOR MEMBRANE OF AN ANGLE $2\pi/3$

An iterative computer calculation yields the maximum value of u* (from equation 8.24) for the corresponding membrane. These are plotted in figure 8.5 for sector membranes. Corresponding fundamental frequencies are then calculated from equation (8.23) and are shown in figure 8.6. For the aortic leaflet model, the value of $u^* = 0.143a^2$ with the corresponding fundamental eigen values provided by equation (8.23).

8.3 Interaction of aortic valve vibrational and second heart heart sound spectral analyses:

The second heart sound spectra for several subjects were obtained as described in earlier chapters. The dominant frequency (maximum energy frequency) of the second heart sound spectrum for each subject is extracted along with the valve radius from 2-D echo-cardiograms. Constant $\sqrt{\rho/T}$ contours are computed from equation (8.23) with $u^* = 0.143a^2$ and drawn on the ω versus a coordinate space. This is shown in figure 8.7.

When the values of maximum energy frequency and the corresponding valve radius are depicted as coordinate points in figure 8.7, by means of the contour curves, a value of $\sqrt{\rho/T}$ can be designated to each of these points.

Thus the interaction of the valve vibrational and heart sound analyses furnishes the values of the tension in the vibrating valve membrane. For a patient, the increase of tension over a period of time may signify advent of valvular calcification.

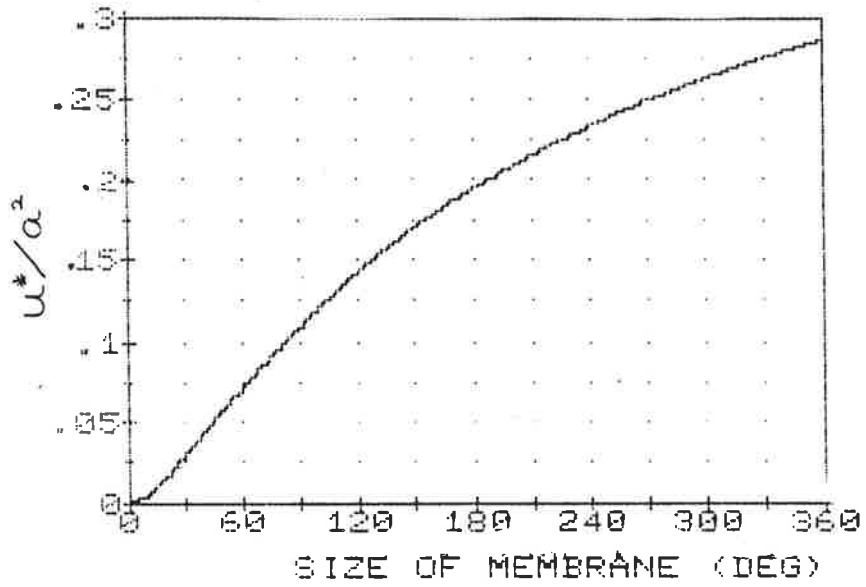

FIGURE 8.5 VALUES OF U^*/a^2 FOR SECTOR MEMBRANES

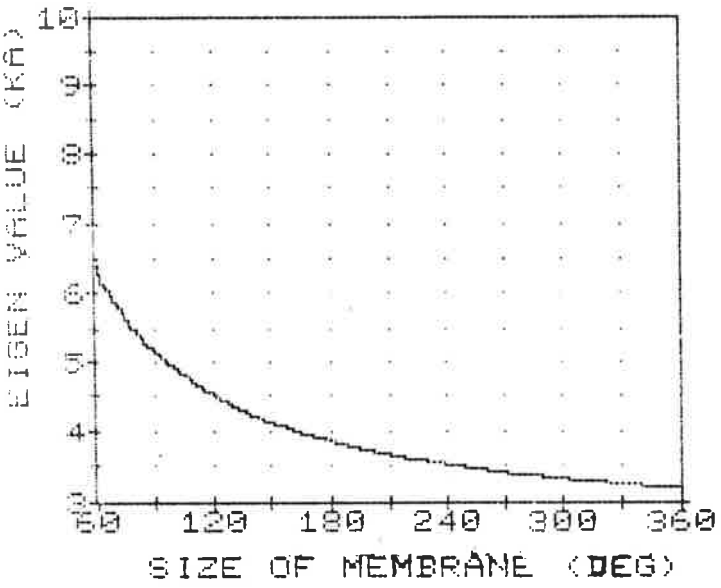

FIGURE 8.6 FUNDAMENTAL EIGEN VALUES OF SECTOR MEMBRANES

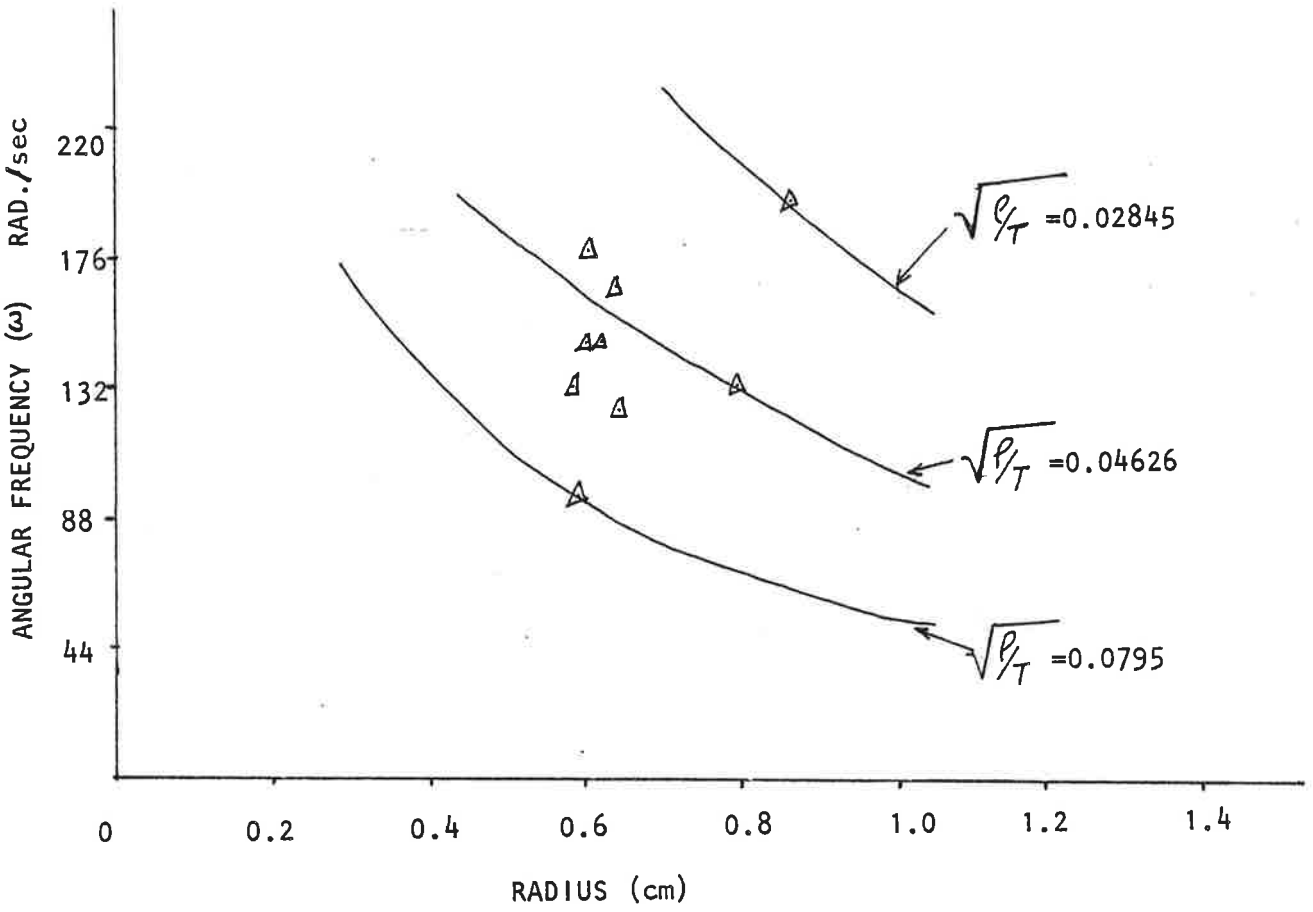

FIGURE 8.7 CLINICAL VALUES OF PREDOMINANT 2nd HEART SOUND FREQUENCY AND VALVE RADIUS SUPERIMPOSED ON MODEL DERIVED CONSTANT $\sqrt{\rho/T}$ CONTOURS PLOTTED ON "VIBRATIONAL FREQUENCY Vs VALVE MEMBRANE RADIUS" COORDINATE SPACE.

8.4 Non-invasive determination of pressure drop across aortic valve

8.4.1 Introduction:

Cardiac catheterization is an accepted method for the measurement of pressure drop across heart valves (e.g. aortic valve) during the period of blood flow through the valves, to ascertain the degree of valvular stenosis, (a disease which causes the heart valves to stiffen). This pressure drop along with the valve flow, is used to estimate the orifice area. This cardiac catheterization involves inserting a long Cannula into the patient's heart through one of the major arteries, for making various measurements such as pressure, flow etc. It is an important procedure enabling more accurate assessment of the clinical problem and clarifies the need for further surgical intervention. This method is not simple and could be painful to the patient.

A non-invasive method to determine the pressure drop across the aortic valve using information from two-dimensional echocardiography, has recently been developed [Ghista et al, 1983; Hearn et al, 1983]. The method has originated as a result of contributions from a team of several research workers. This work was carried out during the author's stay at the McMaster University Medical Centre where the author was a member of the research team which contributed to this work. In this method, it is demonstrated that through the use of echocardiography and simplifed fluid

mechanics, the pressure drop across the aortic valve can be determined to a reasonable accuracy.

8.4.2 Methodology

In the aortic outflow tract, the instantaneous pressure drop Δp across the aortic valve cannot be quantified merely in terms of the mean bloodflow velocity or flow rate in the aorta. The proposed method for determining the pressure gradient requires the use of Bernoulli's equation in conjuction with two dimensional echocardiography. Figure 8.8 shows the stop frame image of the 2-D echocardiograph taken along the parasternal long axis indicating the left ventricular outflow tract. Figure 8.9 shows the schematic characterization of the outflow tract indicating dimensions at various sections. The analytical formulations express the pressure drop across the aortic valve in terms of (i) the dimensions of the aortic ring (d_1), leaflet excursion (d_2) and of the aortic root about 1 cm distal to the valve leaflet tips (d_3), and (ii) the mean flow rate during the ejection phase. The above data can readily be obtained from the two-dimensional echocardiography. Figure 8.10 shows the apical 2-chamber view of the left ventricle. The endocardial boundary is outlined using the light pen arrangement system of the 2-D echocardiograph machine (varian 3400 2-D echo system). From this boundary, the instantaneous chamber volumes and the mean flow rate can be determined.

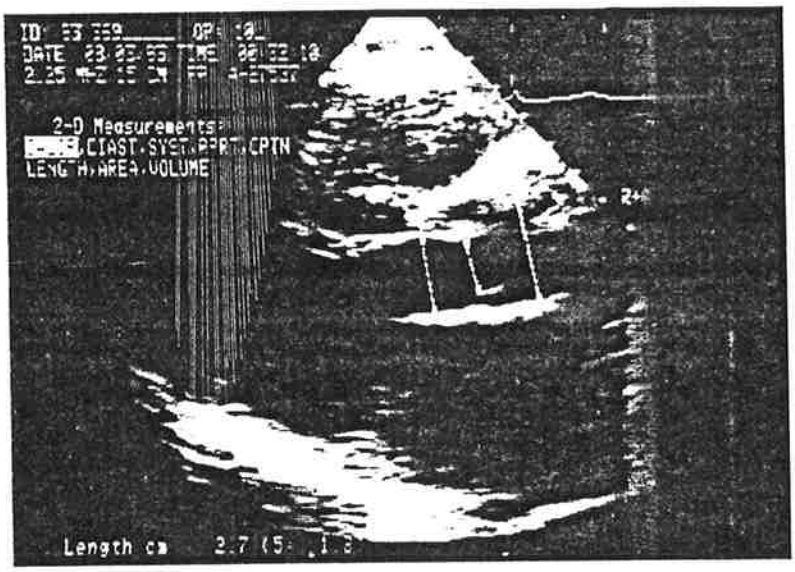

FIGURE 8.8 PARASTERNAL LONG AXIS VIEW OF THE LEFT VENTRICULAR OUTFLOW TRACT

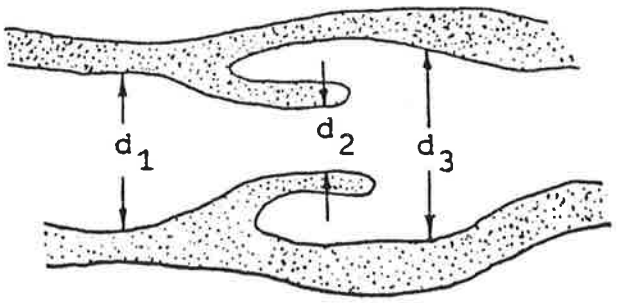

FIGURE 8.9 LEFT VENTRICULAR OUTFLOW TRACT DELINEATED FROM THE PARASTERNAL LONG AXIS VIEW OF LEFT VENTRICLE

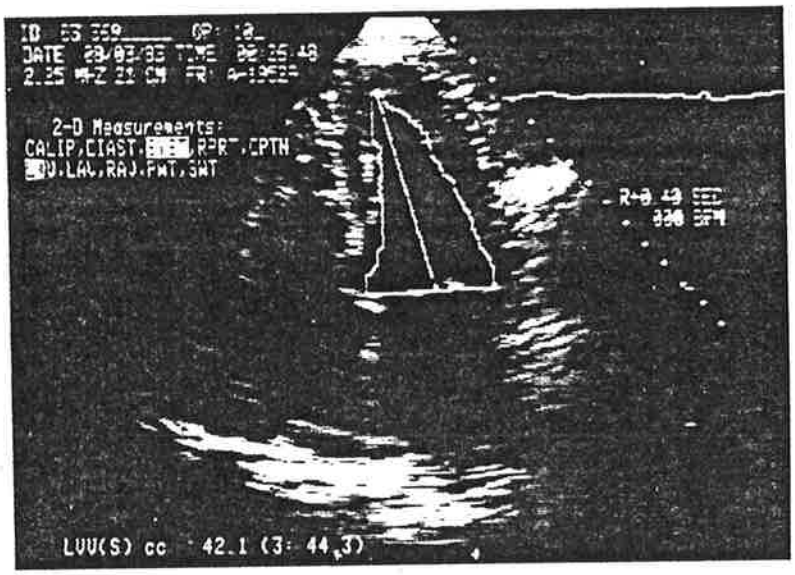

FIGURE 8.10 APICAL TWO CHAMBER VIEW (STOP FRAME IMAGE)
ENDOCARDIAL BOUNDRY OF THE LEFT VENTRICLE IS
OUTLINED USING A LIGHT PEN ATTACHED TO THE
VARIAN 3400 2-D ECHOCARDIOGRAPH MACHINE.

8.4.3 Analytical formulation of the pressure drop:

The Bernoulli equation is employed to determine the pressure gradient $(P_1 - P_3)$ across the aortic valve, at an instant during the ejection phase when the valve leaflets are fully opened. During this phase, the blood flow was assumed to be steady, and so the Bernoulli equation (applied between sections 1 and 3 of the parasternal long axis view) is written as

$$(P_1 - P_3) = \frac{Q^2}{2}\rho\left\{\left[\frac{1}{A_3^2} - \frac{1}{A_1^2}\right] + \frac{1}{A_2^2}\left[f\left(\frac{A_2}{A_1}\right)^2 + k\right]\right\} \qquad .....(8.26)$$

where

(i) P_1 and P_3 are the pressures at cross sections 1 and 3 of the left ventricular outflow tract and the aorta (1 cm distal to the valve leaflets)

(ii) Q, the volumetric flow rate of blood, is defined as the ratio of the change in volume to the change in time, between end-diastole and end-systole and expressed as:

$$Q = \frac{(EDV - ESV)}{t} \qquad .....(8.27)$$

where EDV and ESV are the end-diastolic and end-systolic volumes and t is the time interval between these instants.

(iii) A_1, A_2, A_3 are the cross sectional areas (assuming circular cross sections) of the left ventricular outflow tract, maximum aortic valve

opening and aortic root, corresponding to the cross sectional diameters d_1, d_2, and d_3 as indicated in figure 8.9.

(iv) ρ is the density of blood.

(v) $f(A_1/A_2)$ is the term that accounts for losses due to the contraction between the left ventricular outflow tract and the inlet of the aortic valve leaflets.

(vi) The term $k = [1 - (A_2/A_3)]^2$ accounts for losses due to the sudden expansion between the valve leaflets and the aortic root. The derivation of this energy loss coefficient can be done as follows:

Applying the momentum equation for incompressible steady flow through a sudden enlargement of flow tract between sections 2 and 3 (figure 8), we have

$$P_2 - P_3 = \rho V_3 (V_3 - V_2) \qquad .....(8.28)$$

where P_2, V_2 and P_3, V_3 represent the pressure and velocity at sections 2 and 3 respectively.

From continuity we have

$$A_2 V_2 = A_3 V_3 \qquad .....(8.29)$$

From (8.28) and (8.29)

$$P_2 - P_3 = \rho \frac{A_2}{A_3} V_2^2 \left(\frac{A_2}{A_3} - 1\right) \qquad .....(8.30)$$

now applying the modified Bernoulli equation between sections 2 and 3, with a term $kV_2^2/2$ accounting for the loss from the expansion; we obtain

$$\frac{P_2}{\rho} + \frac{V_2^2}{2} = \frac{P_3}{\rho} + \frac{V_3^2}{2} + K\frac{V_2^2}{2} \qquad .....(8.31)$$

wherein k = energy loss coefficient

substituting (8.30) in to (8.31) gives

$$\frac{KV_2^2}{2} = \frac{V_2^2}{2}\left[1 - \left(\frac{A_2}{A_3}\right)^2\right] + V_2^2\frac{A_2}{A_3}\left(\frac{A_2}{A_3} - 1\right) \qquad .....(8.32)$$

Hence

$$k = \left(1 - \frac{A_2}{A_3}\right)^2 \qquad .....(8.33)$$

The value for $f(A_2/A_1)$ can be obtained directly from the standard experimental data [John, J.E.A., and Haberman, W.L., 1980]. Figure 8.11 shows a plot of $f(A_2/A_1)$ against A_2/A_1. For any given ratio of A_2/A_1 the value of $f(A_2/A_1)$ can be read from the plot. This accounts for the pressure loss function due to sudden narrowing of the flow tract because of the aortic valve leaflets when opened (refer to figure 8.9).

8.4.4 Data acquisition

Eight patients were selected for this study. Prior to undergoing cardiac catheterization, all patients with aortic stenosis were studied echocardiographically. A Varian 3400 phased array ultrasonograph machine with a digital scan process was used. The measurements on the left ventricular outflow tract were made by freezing the (parasternal long axis view) frame corresponding to the instant when the aortic

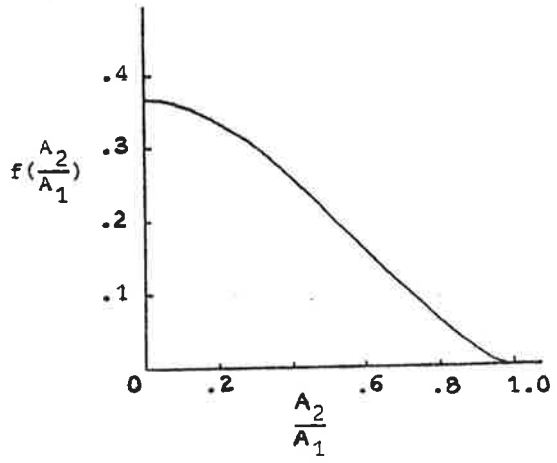

FIGURE 8.11 VARIATION OF THE ENERGY LOSS FUNCTION $f(A_2/A_1)$ WITH A_2/A_1, TO ACCOUNT FOR ENERGY LOSS DUE TO SUDDEN CONTRACTION (BETWEEN SECTIONS 1 AND 2 IN FIGURE 8.9)

valve is open; d_1, d_2 and d_3 are thus obtained. The end-diastolic and end-systolic left ventricular volumes were obtained from the apical two and four chamber views at end-diastole and end-systole using the single plane area-length method. The perimeter of the left ventricle was outlined using a light pen system of the Varian phased array ultrasonograph. The resulting area (A) was calculated and displayed on the video monitor A line L was measured to represent the maximum length between any two points on the endocardial outline (refer figure 8.9). The volume was then calculated according to the expression

$$V = \frac{8A^2}{3L} \qquad .....(8.34)$$

The time interval t between end-diastole and end-systole was measured as the difference in frame numbers between end-diastole and end-systole divided by the frame speed (number of frames/second) of the videotape recorder. The mean flow rate was obtained by using the above volumes and t in equation (8.27).

8.4.5 Discussion

The pressure drop across the aortic valve in eight patients are calculated. The mean flow rate was calculated using apical 2 chamber and 4 chamber views of the 2-D echocardiogram. Accordingly two values for the pressure drop were calculated for each patient. Table 8.1 shows the pressure drops calculated from the above measurements as well

as actual pressure drops obtained from catheterization procedures. The average pressure drops obtained from the two and four chamber views are also included in table 8.1. There is a good correlation between the non invasively computed average pressure drop and the actual pressure drop. The results thus demonstrate the efficacy of the non-invasive method in determining the pressure drop across the aortic valve.

TABLE 8.1

Patient	Actual (mm Hg)	2 Chamber (mm Hg)	4 Chamber (mm Hg)	Average (mm Hg)
TM(82-703)	57.0	64.0	56.0	60.0
LK(82-1571	35.0	27.9	32.6	30.0
WK(920)	20.0	22.5	16.3	19.4
SE(1731)	50.0	--	62.9	62.9
TF (-)	42.5	34.6	28.7	33.0
EK(1399)	31.0	37.6	20.6	29.0
AS(82-594)	61.0	69.5	--	69.5
JP (-)	64.0	--	62.7	62.7

CHAPTER IX

CONCLUSION

9.1 Conclusion:

The etiology of the heart sounds, based on vibrations of cardiac structures, has given impetus to investigations on (i) the spectral analysis of heart sounds and (ii) vibration analysis of heart valves (mitral and aortic) and left ventricular chamber, so as to attempt to noninvasively determine the valvular and myocardial properties and their pathologies, by correlating the heart sound signal analysis and the corresponding structural (valve or chamber) vibration analyses.

The frequency analysis techniques described in this thesis provide effective and efficient methods for processing heart sounds and thereby increasing the diagnostic value of phonocardiograms. FFT analysis using moving windows, provides temporal variations in heart sound spectra. This technique enhances the means of studying the spatial and temporal relationships of the cardiac structural resonances.

The LPC technique, as applied to heart sounds analysis in this thesis, provides a better spectral estimation of heart sounds. The selective linear predictive coding procedure, described in chapter six, enables heart sound spectral estimation (over a well defined frequency range) with higher frequency resolution. The efficacy of this technique in

enhancing the frequency peaks in the heart sound spectrum is demonstrated.

The second heart sound spectral energy correlations with the 2-dimensional echocardiographically derived aortic valve dimensions (in children) have demonstrated high correlation in the frequency range 120-140 HZ. This implies that a shift of the spectral peak in this band width should be noted, in order to track valvular degeneration. Likewise, for tracing myocardial degeneration, one should determine the spectral band width which yields best correlations with chamber dimensions.

The proportionate energy of the second heart sound in this (120-140 HZ) band width is however very small (<10%). Considering the very recent observations made by Luisada et. al., [1983] on the contribution of the cardiac valves to the production of heart sounds, this correlation validates the observation made by Luisada concering cardiac vibrations being the result of accelerations and decelerations caused in the entire cardiohemic system with the cardiac valves contributing minimally to the production of heart sounds.

The aortic valve vibrational model together with the maximum energy frequency peak in the second heart sound spectrum, as indicated in chapter eight, provides a quantitative method for the determination of the aortic valve pathology or dysfunction. This technique would also enable to track the alteration in the valve membrane elasticity over

a period of time, in the case of progressive degeneration of the valve. Also, the noninvasive method of determining the pressure drop across the aortic valve described in chapter eight provides a clinically implementable procedure for the investigation of the extent of the aortic stenosis.

9.2 Recommendations

The thesis has provided detailed analyses techniques for heart sounds in general, and a noninvasive method of determining valvular pathology based on aortic valve vibrational model and spectra of second heart sounds. Methods for accurate heart sound frequency determination based on linear predictive coding have been delineated. This powerful technique could be used to model the heart sound signals in desired frequency ranges and thus develop parametric models to represent the genesis of heart sounds.

A possible spectral modelling procedure based on SLPC technique, for future work, is proposed in figure 9.1. The model parameters would then help characterise the valvular health-pathology status. Ranges of the values of the model parameters, for the first and second heart sounds, could be first established for normal subjects. Then any deviations in the parametric values from their normal ranges would indicate abnormalities.

As the LPC is a sensitive technique for frequency peak determination, it could be employed to sensitively track the shifts in the frequency peaks of the heart sound spectra due

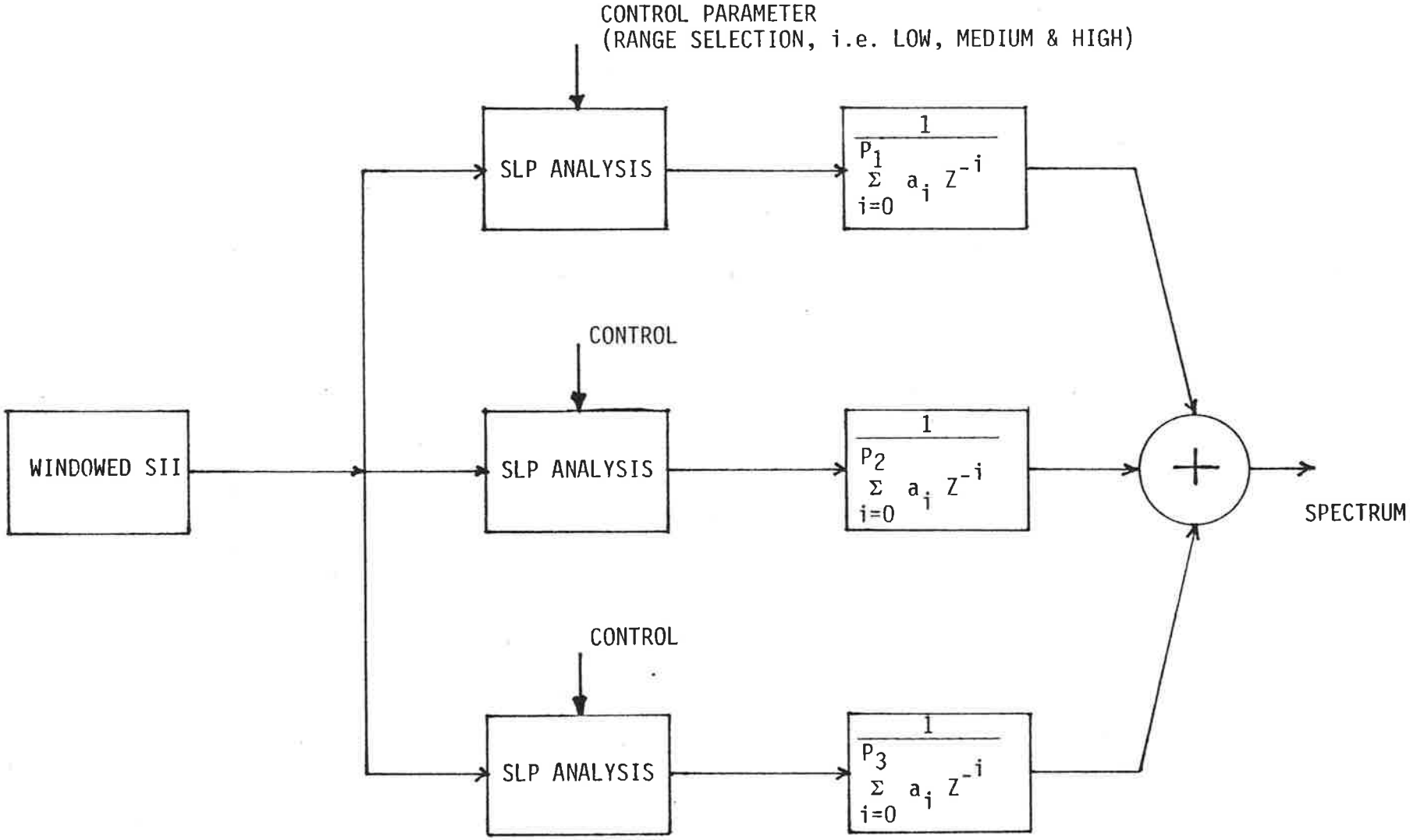

FIGURE 9.1 PROPOSED HEART SOUND SPECTRAL MODELLING PROCEDURE BASED ON SLPC TECHNIQUE.

to deterioration of implanted bioprosthetic mitral and aortic valves.

The complete understanding of the genesis of precordial heart sounds requires the use of such sensitive frequency analysis techniques in identifying the sources of the various frequency resonances seen in the heart sound spectra. Extensive studies are required to establish relationships between the frequency peaks and the pathologies of the corresponding structures producing them. The author has already commenced research work in this direction.

APPENDIX A

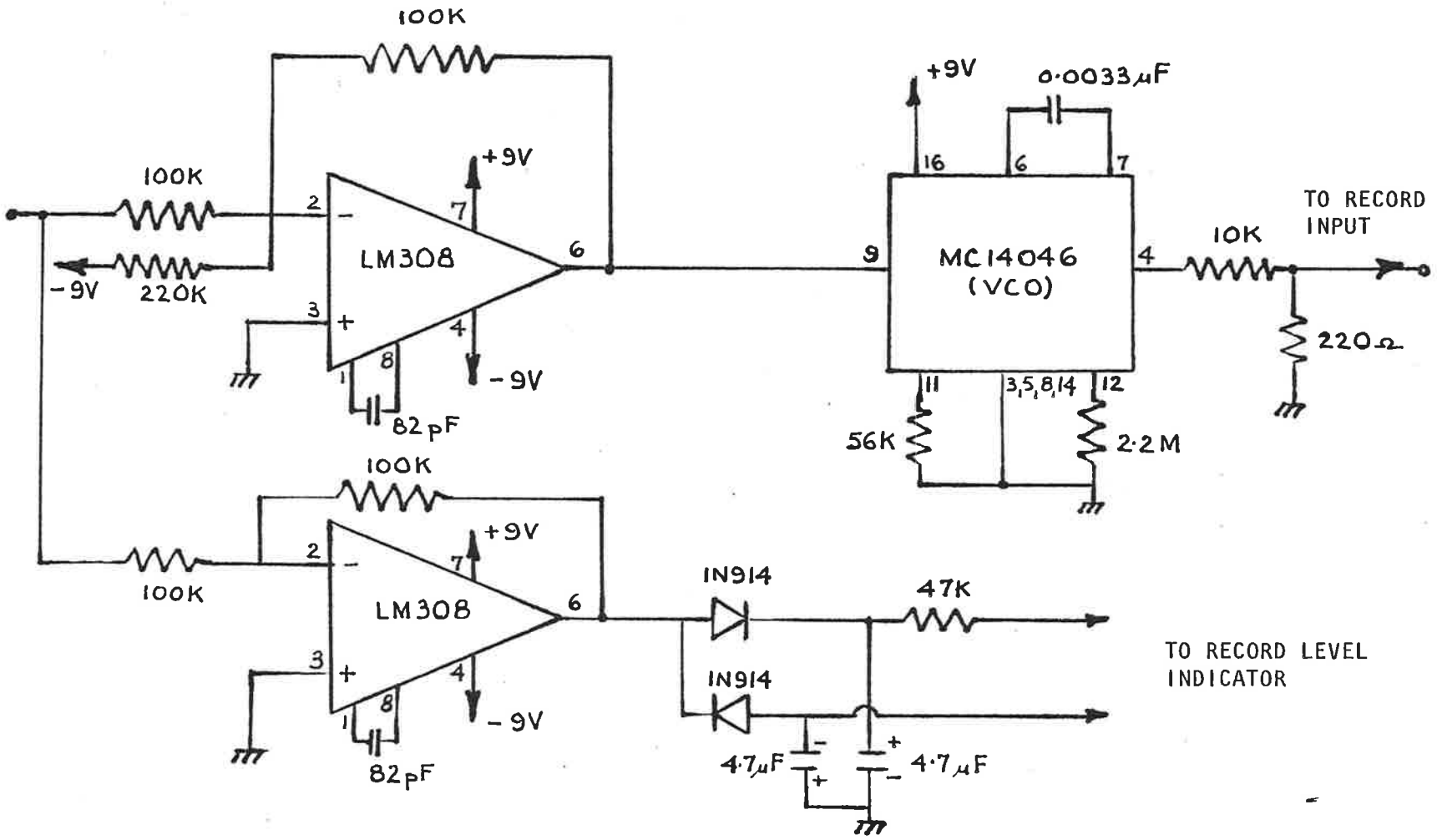

FIGURE A.1 MODULATOR

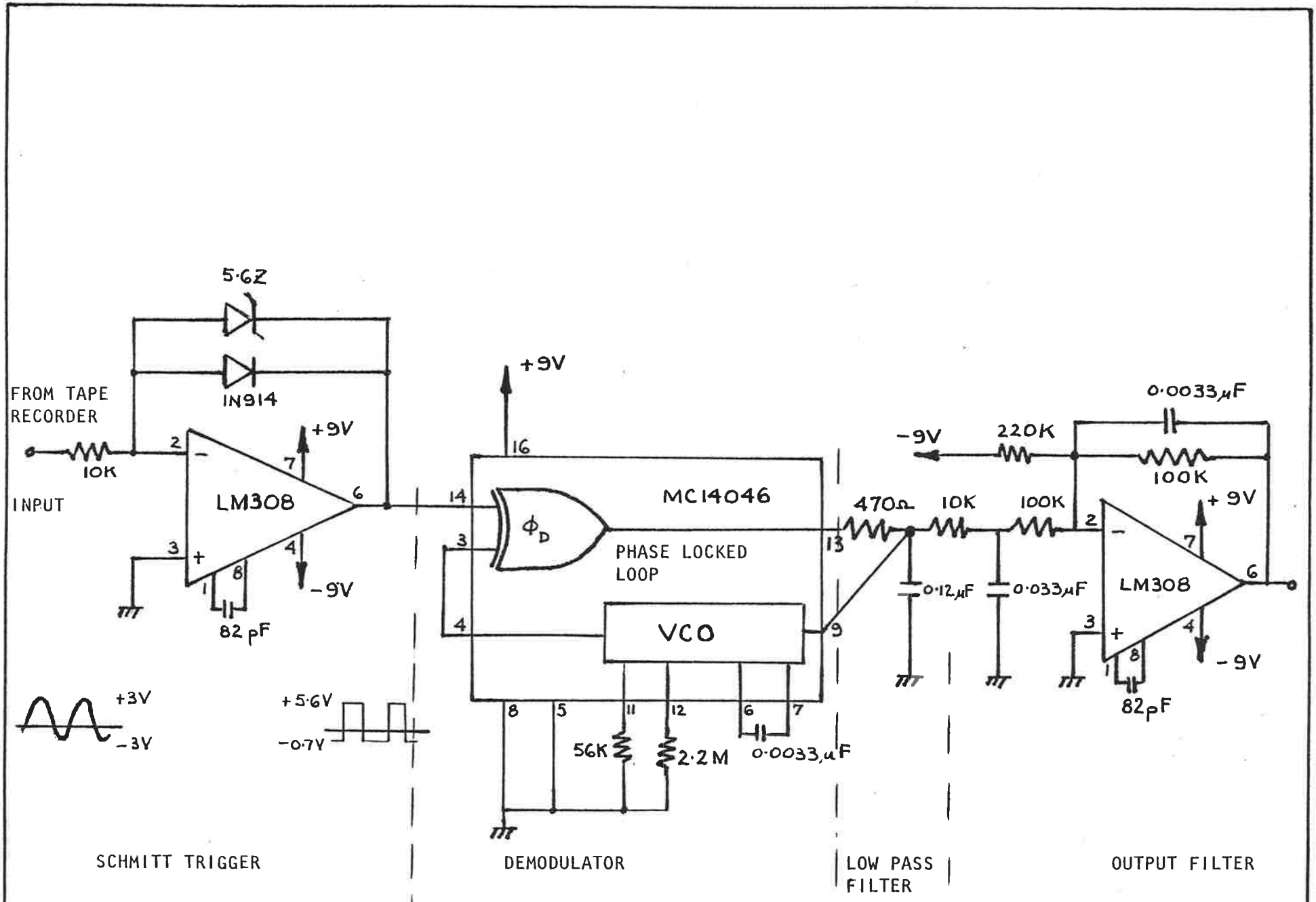

FIGURE A.2 DEMODULATOR

APPENDIX B

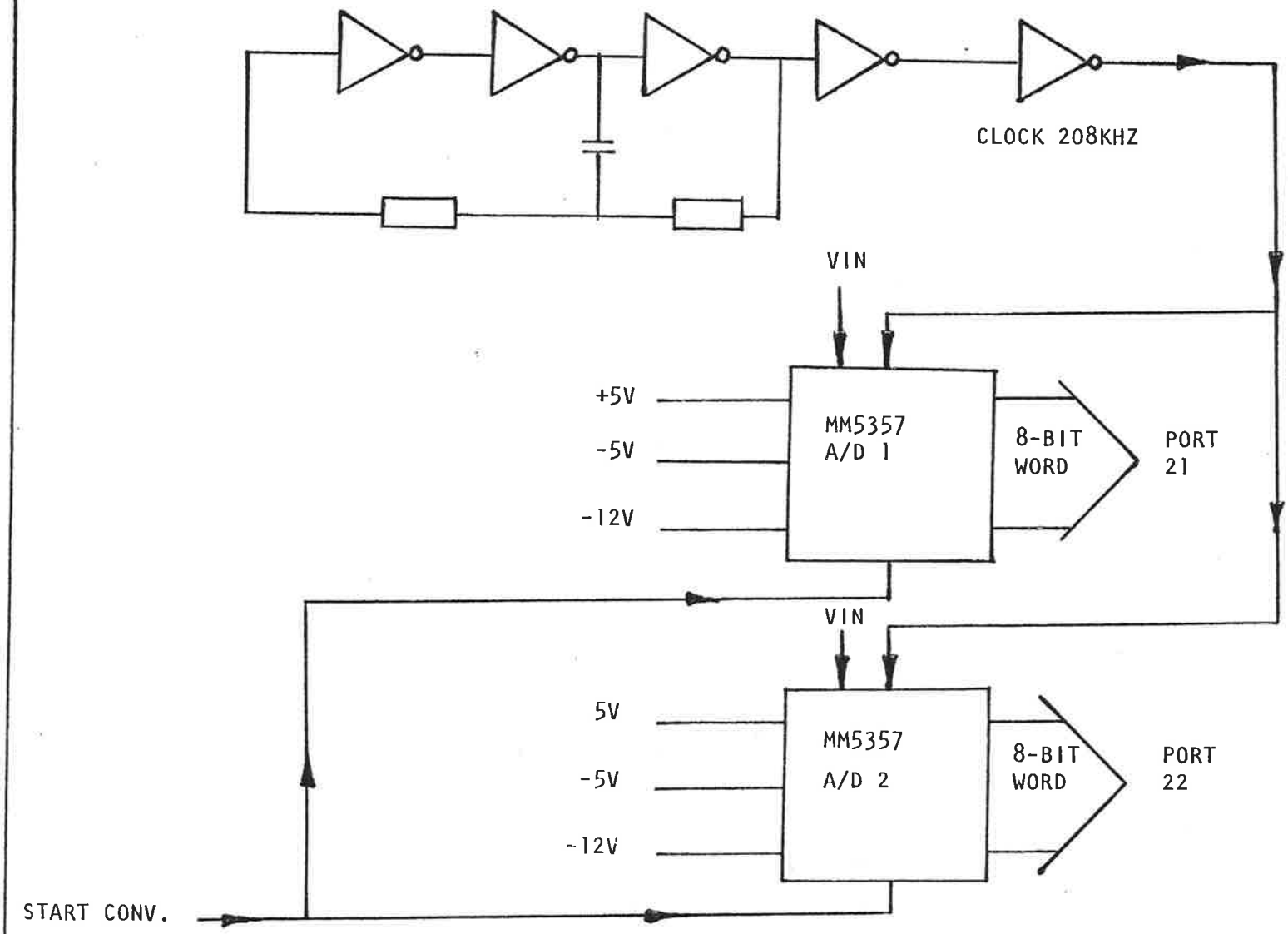

FIGURE B.1 2 CHANNEL A/D AND CLOCK ARRANGEMENT

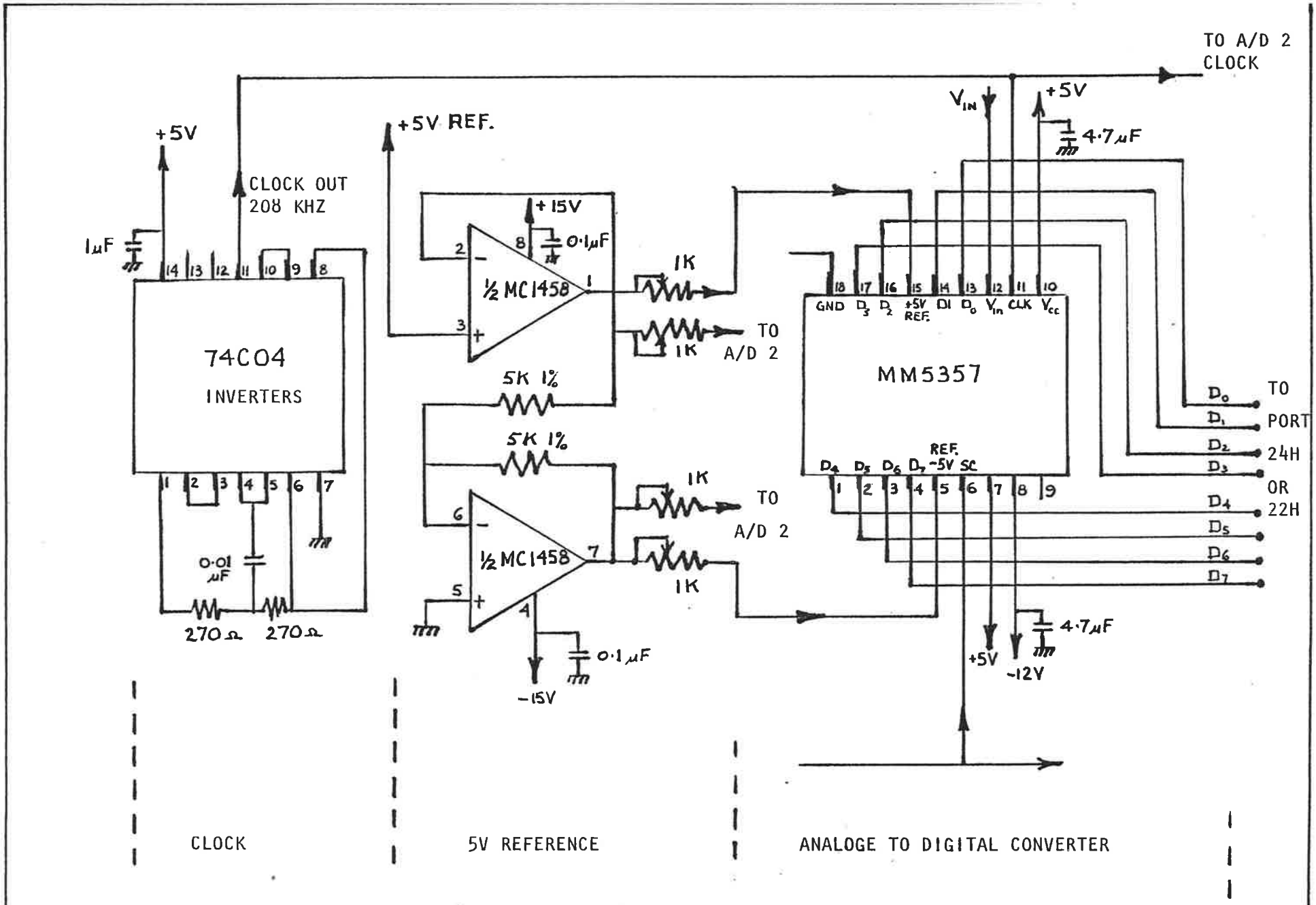

FIGURE B.2 A/D CHANNEL WITH CLOCK AND REFERENCE

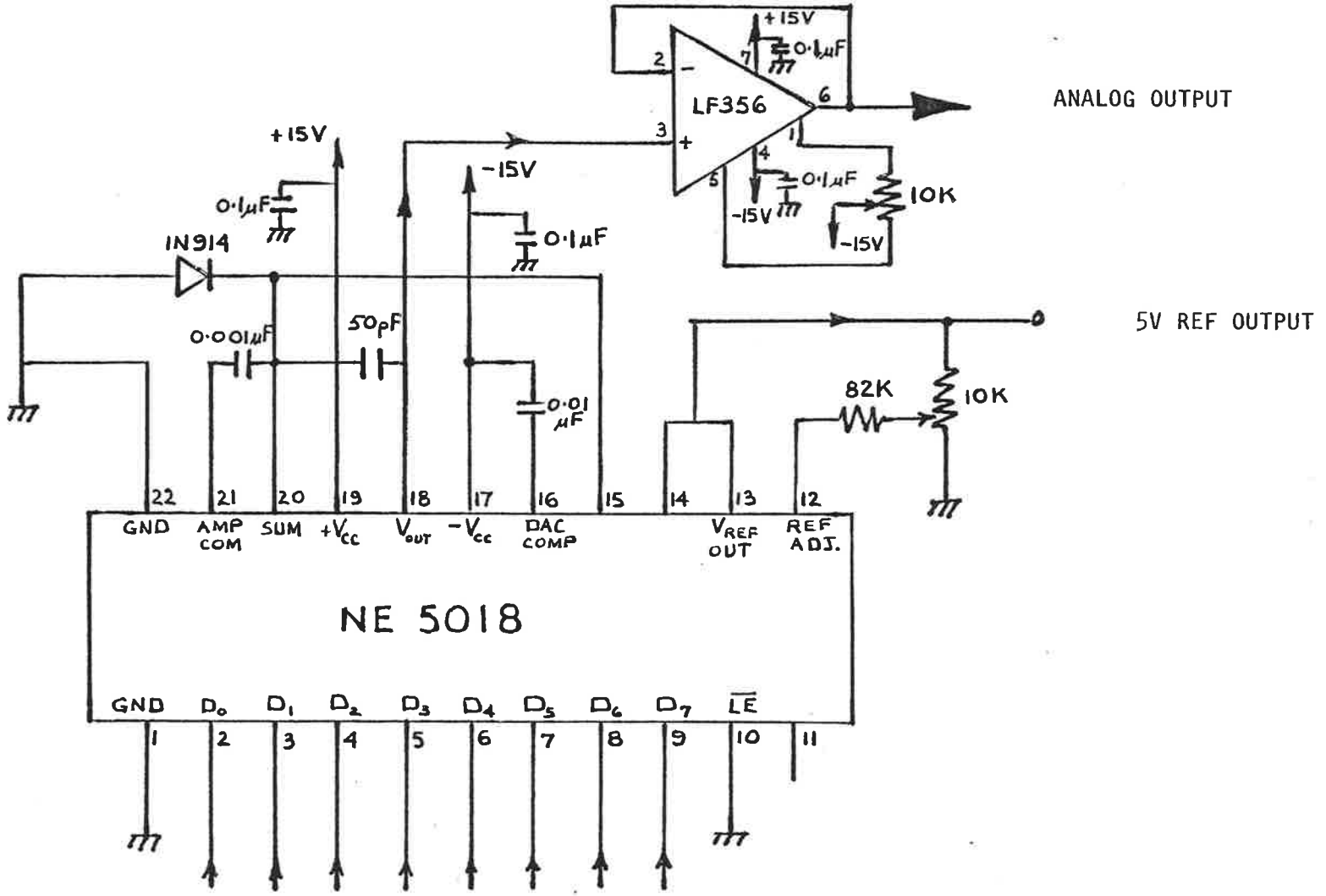

FIGURE B.3 D/A CHANNEL

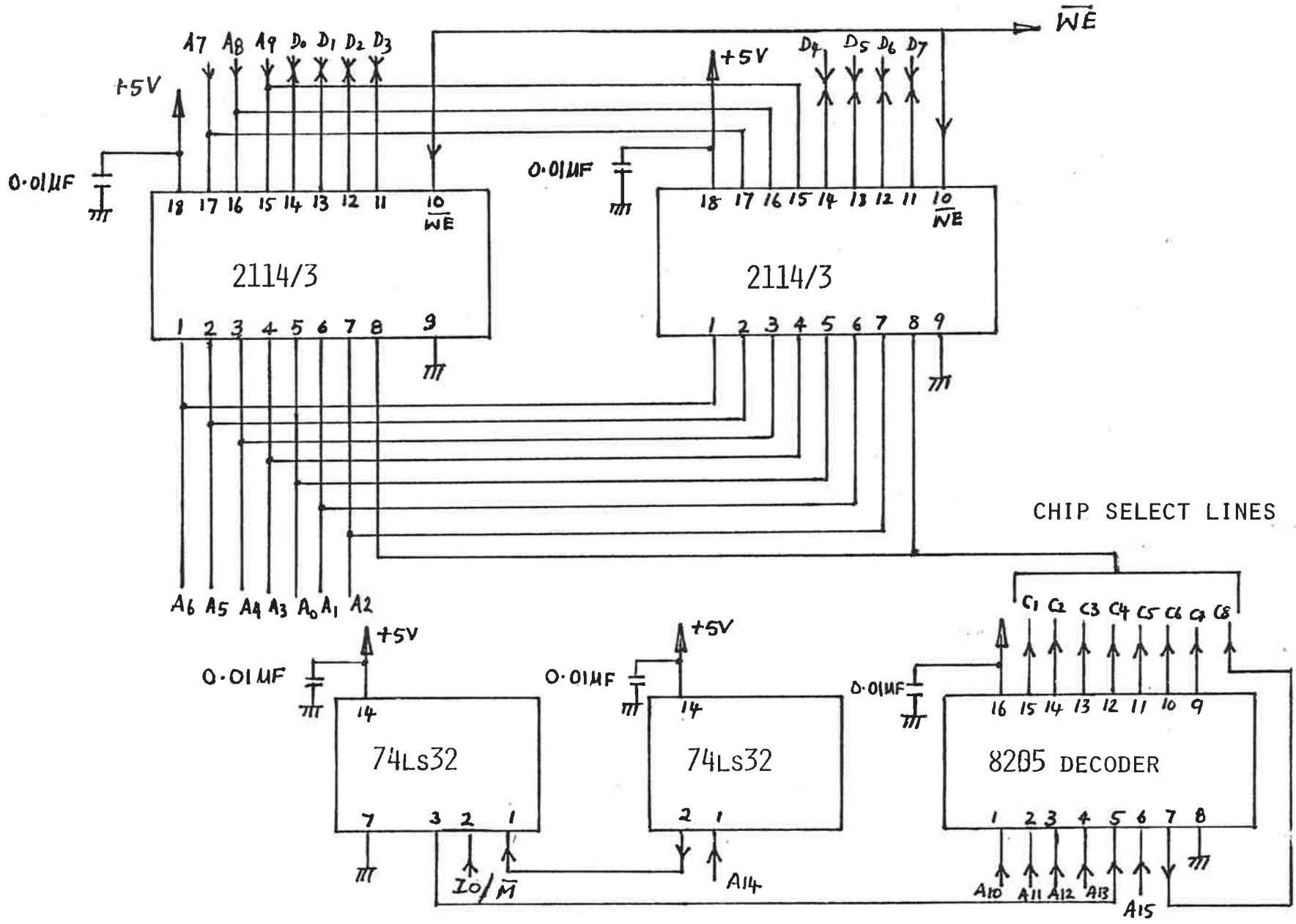

FIGURE B.4 MEMORY PAIR SETUP/ ADDRESS DECODING

APPENDIX C

AUTOCORRELATION METHOD FOR SOLVING LINEAR PREDICTION COEFFICIENTS

Consider the range of summation as $-\infty < n < \infty$ in equation [4.6].

The signal is defined only for a known number of samples

i.e.

$$S_n = \begin{cases} S_n W_n & 0 \leq n \leq N-1 \\ 0 & \text{otherwise} \end{cases} \qquad \text{.....[A.c.1]}$$

where 'W_n' is some window function

N is the length of the analysis data segment.

Equation [4.6] becomes

$$\sum_{n=k}^{N-1} S_{n-k} S_n = \sum_{i=1}^{P} a_i \sum_{n=0}^{N-1} S_{n-i} S_{n-k}$$

$$\text{for } 1 \leq k \leq P \qquad \text{....[A.c.2]}$$

Now,

$$\sum_{n=k}^{N-1-|k|} S_n S_{n+|k|} = R(k) \qquad \text{....[A.c.3]}$$

is the auto correlation function of 'S_n'

Also, R(k) is an even function of k.

i.e.

$$R(k) = R(-k) \qquad \text{....[A.c.4]}$$

Therefore the resulting equation from [A.c.2] is;

$$R_k = \sum_{i=1}^{P} a_i R_{k-i} \quad \text{for } 1 \leq k \leq P \qquad \text{...[A.c.5]}$$

Without loss of generality, the autocorrelation coefficients

can be normalised, as

$$r_k = R_k / R_o \qquad \text{....[A.c.6]}$$

Thus, equation [A.c.5] becomes

$$r_k = \sum_{i=1}^{P} a_i \, r_{k-i} \qquad \text{....[A.c.7]}$$

Therefore, for a given predictor order P, P simultaneous equations can be obtained from equation [A.c.7]. For the sake of argument, consider the predictor order to be 4. Hence we can write the following set of equations, for p = 4 as

$$\begin{aligned}
a_1 r_0 + a_2 r_1 + a_3 r_2 + a_4 r_{+3} &= r_1 \\
a_1 r_1 + a_2 r_0 + a_3 r_1 + a_4 r_2 &= r_2 \\
a_1 r_2 + a_2 r_1 + a_3 r_0 + a_4 r_1 &= r_3 \\
a_1 r_3 + a_2 r_2 + a_3 r_1 + a_4 r_0 &= r_4
\end{aligned} \qquad \text{....[A.c.8]}$$

Equation [A.c.8] can be written in the matrix from as

$$\begin{bmatrix} r_0 & r_1 & r_2 & r_3 \\ r_1 & r_0 & r_1 & r_2 \\ r_2 & r_1 & r_0 & r_1 \\ r_3 & r_2 & r_1 & r_0 \end{bmatrix} \begin{bmatrix} a_1 \\ a_2 \\ a_3 \\ a_4 \end{bmatrix} = \begin{bmatrix} r_1 \\ r_2 \\ r_3 \\ r_4 \end{bmatrix} \qquad \text{....[A.c.9]}$$

The equation [A.c.9] is known as the autocorrelation matrix with the same diagonal elements. Therefore this equation is

also known a Toeplitz matrix. The symmetric Toeplitz matrix allows an efficient recursive computation using Robinson's method to solve the equations for the parameters a_i [Robinson, 1967]. The most efficient method known for solving this particular set of equations is Durbin's recursive procedure [Durbin, 1959].

The minimum total squared error 'E_0' can be obtained by using equation [4.6] in equation [4.3] and rearranging

$$E_0 = \sum_{n}^{N-1} S_n^2 + \sum_{i=1}^{P} a_i \sum_{n}^{N-1} S_n S_{n-i} \qquad \ldots[A.c.10]$$

Equation (A.c.10) can be rewritten as

$$E_0 = R(0) + \sum_{i=1}^{P} a_i R(i) \qquad \ldots[A.c.11]$$

Therefore from the predictor coefficients and the autocorrelation coefficients, the total minimum squared error E_0 can be calculated. This is also regarded as the system gain factor.

i.e. from equation [4.10]

$$S(Z) = \frac{E(Z)}{1 - \sum_{i=1}^{P} a_i z^{-i}}$$

$$S(Z) = \frac{A}{1 - \sum_{i=1}^{P} a_i z^{-i}} \qquad \ldots..[A.c.12]$$

A can be regarded as E_0 (gain term).

COVARIANCE METHOD OF SOLVING FOR PREDICTOR CONSTANTS

The range of summation is $0 \leq n \leq N-1$. The signal 'S_n' does not require special definition outside the range $-P \leq n \leq N-1$.

Rewriting equation [4.6] with the above range,

$$\sum_{n=0}^{N-1} S_{n-k} S_n = \sum_{i=1}^{P} a_i \sum_{n=0}^{N-1} S_{n-i} S_{n-k}$$

$$\text{for} \quad 1 \leq k \leq P \quad \text{.....[A.c.13]}$$

$$\text{let} \qquad \sum_{n=o}^{N-1} S_{n-i} S_{n-k} = \phi_{ik} \quad \text{.....[A.c.14]}$$

where ϕ_{ik} is the covariance of the signal 'S_n' over the given interval.

Equation [A.c.13] now reduces to

$$\phi_{0k} = \sum_{i=1}^{P} a_i \phi_{ik} \qquad 1 \leq k \leq P \qquad \text{.....[A.c.15]}$$

expanding equation [A.c.15] in matrix form

$$\begin{bmatrix} \phi_{11} & \phi_{12} & \cdots & \phi_{1P} \\ \phi_{21} & \phi_{22} & \cdots & \phi_{2P} \\ \phi_{31} & \phi_{32} & \cdots & \phi_{3P} \\ \vdots & \vdots & & \vdots \\ \phi_{P1} & \phi_{P2} & & \phi_{PP} \end{bmatrix} \begin{bmatrix} a_1 \\ a_2 \\ a_3 \\ \vdots \\ a_P \end{bmatrix} \qquad \begin{bmatrix} \phi_{10} \\ \phi_{20} \\ \phi_{30} \\ \vdots \\ \phi_{P0} \end{bmatrix} \quad \text{...[A.c.16]}$$

The above symmetric matrix of (p x p) order is called covariance matrix. The diagnol elements are not equal in

this case. Hence [A.c.15] is not a Toeplitz matrix. The covariance normal equations can be solved by a method called the square root method [Makhoul and Wolf, 1972].

APPENDIX D

LIST OF AUTHOR'S PUBLICATIONS RELATING TO THIS THESIS

"Towards quantitative determination of valvular calcification and pressure drops across malfunctioning heart valves:" Proceedings of the 1983 Frontiers of Engineering & Computing in Health Care, IEEE Publication, Columbus, Ohio, U.S.A. Sep. 1983.

"A study of orifice shape effects in the determination of mitral valve area by two-dimensional echo cardiography:" ACTA Cardiologica vol. XXXVIII, 1983, 3, pp. 199-208.

"Spectral analysis of second heart sound in normal children by selective linear prediction coding:" Journal of Medical and Biological Engineering & Computing, England (22, 229-239, 1984).

"Spectral energy of the first heart sound in relation to mitral valve size parameter:" The Journal of Australasian Physical and Engineering Sciences in Medicine. Vol. 6, No. 2, pp. 76-81, 1983.

"Application of digital processing of heart sounds to heart valve modelling:" Proceedings of IFAC Symposium on Theory and Application of Digital control held in New Delhi, vol. 1, Session 7, pp. 1-3, January, 1982.

"Linear prediction in heart sound analysis:" Presented at "BECON '81," the 1981 National Biomedical Engineering Conference held in Sydney, Australia, Oct. 1981.

"Microprocessor based on-line biomedical signal data acquisition system:" Presented at "BECON '81," the National Biomedical Engineering Conference held in Sydney, Australia, Oct. 1981.

"A study of temporal variation in heart sound frequency spectra using Fast Fourier Transform:" The Journal of Australasian Physical and Engineering Sciences in Medicine. Vol. 4, No. 2, pp. 47-50 May, 1981.

"An instrumentation system and analysis procedure for phonocardiographic studies:" Australian Journal of Biomedical Engineering. Vol. 2, No. 1, pp. 16-20. March 1981.

"Atrio ventricular valve response to systolic pressure loading:" Proceedings of Second International Conference on Mechanics in Medicine and Biology, pp. 134-135. Osaka, Japan. June 1980.

"Spectral analysis of second heart (SII) using linear prediction coding:" Proceedings of Second International Conference on Mechanics in Medicine and Biology, pp. 102-103. Osaka, Japan. June 1980.

"A mathematical model for the non-invasive study of human mitral valve tissue:" Proceedings of the Second International Conference on Mathematical Modelling. St. Louis, U.S.A. July 1979.

Nandagopal, D., Mazumdar, J., Karolyi, G., and Hearn, T., (1981) An instrumentation system and analysis procedure for phonocardiographic studies.
Australian Journal of Biomedical Engineering, v. 2 (1), pp. 16-20.

Nandagopal, D., and Mazumdar, J., (1981) A study of temporal variation in heart sound frequency spectra using fast fourier transform.
Australasian Physical and Engineering Sciences in Medicine, v. 4 (2), pp. 47-50.

Nandagopal, D., Bogner, R.E., and Mazumdar, J., (1980) Spectral analysis of second heart (SII) using linear prediction coding.
Proceedings of the second International Conference on Mechanics in Medicine and Biology, Osaka, Japan, pp. 102-103.

Nandagopal, D., Mazumdar, J., Bogner, R.E., and Karolyi, G., (1982) Application of digital processing of heart sounds to heart valve modelling.
Theory and Application of Digital Control – Proceedings of the IFAC Symposium, New Delhi, v. 1, session 7, pp. 1-3.

Hearn, T.C., Gopal, D.N., Ghista, D.N., Robinson, J., Tihal, H., Mazumbar, J., and Bogner, R., (1983) Towards quantitative determination of valvular calcification and pressure drops across malfunctioning heart valves.
Proceedings of the 1983 Frontiers of Engineering and Computing in Health Care, Columbus, Ohio, pp. 127-131.

Hearn, T.C.,Mazumbar, J., Goldblatt, E., Nandagopal, D., and Fazzalari, N.L., (1983) Spectral energy of the first heart sound in relation to mitral valve size parameter. *Australasian Physical and Engineering Sciences in Medicine, v. 6 (2), pp. 76-81.*

Nandagopal, D., Mazumbar, J., Bogner, R.E., and Goldblatt, E., (1984) Spectral analysis of second heart sound in normal children by selective linear prediction coding.
Medical and Biological Engineering and Computing, v. 22 (3), pp. 229-239.

BIBLIOGRAPHY

ADOLPH, R.J., STEPHENS, J.F., and TANAKA, K. "The clinical value of frequency analysis of the first heart sound in myocardial infarction." Circulation (1970), XLI, 1003-1014.

ALEXANDER, S.T. and ZEIDLER, J.R. "Detection of narrowband signals in noise using adaptive Linear Prediction Filters." Proceedings of 1977 IEEE Control and Decision Conference, New Orleans, L.A., USA, (1977) 7-9.

ANASTASSIADES, P.C., QUINONES, M.A., GAASCH, W.H., ADYANTHAYA, A.V., WAGGONER, A.D., and ALEXANDER, J.K. "Aortic valve closure: echo-cardiographic, phono-cardiographic, and hemodynamic assessment." American Heart Journal, (1976) 91, 228-232.

ATAL, B.S. "Determination of the vocal tract shape directly from the speech wave." Journal of the Acoustic Society of America, (1970b) 47, 65(A).

ATAL, B.S. and HANAUER, S.L. "Speech analysis and synthesis by linear prediction of speech wave." Journal of the Acoustic Society of America, (1971) 50, 637-655.

BLICK, E.F., SABBAH, H.N., and STEIN, P.D. "One dimensional model of diastolic semilunar valve vibrations productive of heart sounds." Journal of Biomechanics (1978) 12, 223-227.

BOX, G.E., and JENKINS, G.M. "Time series analysis forecasting and control." (1970) San Francisco, California: Holden-Day Inc.

CAMPBELL, G., and ROBERTS, R. "Spectral estimation of cardio vascular sounds." Biomedical Science Instrumentation (1978) 14:27-31, 17-18.

COOLEY, J.W. and TUKEY, J.W. "An algorithm for machine calculation of complex Fourier series." Mathematics of Computing (1965) Volume 19, 297-301.

DURBIN, J. "Efficient estimation of parameters in moving average models." Biometrika (1959) Volume 46 parts 1 and 2. 306-316.

FENWICK, P.B.C., MICHIE, P., DOLLIMORE, J., and FENTON, G.W. "Mathematical simulation of the electroencephalogram using an autoregressive series." Biomedical Computing (1971) Volume 2, 281-307.

GRESCH, W. "Spectral analysis of EEG's by autoregressive decomposition of time series." Mathematical BioScience (1970) Volume 7, 205-222.

GHISTA, D.N., and RAO, A.P. "Structural mechanics of the mitral valve: Stresses sustained by the valve; non-traumatic determination of the stiffness of the in-vivo valve." Journal of Biomechanics (1972) 5, 295-367.

GHISTA, D.N., and RAO, A.P. "Mitral valve mechanics stress/strain characteristics of excised leaflets, analysis of its functional mechanics and its medical application." Medical and Biological Engineering (1973) Volume 11, 691-702.

GHISTA, D.N., ROBINSON, J.G., FALLEN, E., TIHAL, H., STEIN, P., SUBBARAJ, K., HEARN, T., GOPAL, D.N., HARVEY, R., and STRITE, R. "Clinical cardiac mechanics--Simplistic formulations of segmental properties and compensatory mechanisms." Proceedings of the Pittsburg conference on Modelling & Simulation May 1983 Pittsburg, USA.

HARRIS, F.J. "On the use of windows for harmonic analysis with the discrete Fourier transform." Proceedings of the IEEE, (1978) Volume 66, No. 1, 51-83.

HASKEW, J.R., KELLY, J.M., KELLY, R.M., and McKINNEY, H.T. "Results of a study of linear prediction vocoder." IEEE Transactions on Communication, (1973) Volume 21, 1008-1014.

HEARN, T.C., MAZUMDAR, J., HUBBARD, R., and EUSTER, G. "Temporal and heart size effects in first heart sound spectra." Medical and Biological Engineering & Computing, (1979) Volume 17, 563-568.

HEARN, T.C. "Mathematical studies on Atrio-Ventricular valve vibration." Ph.D. thesis, Department of Applied Mathematics, University of Adelaide (1980).

HEARN, T.C., MAZUMDAR, J., and MAHER, L.J. "First heart sound spectra in relation to auterior mitral - leaflet closing velocity." Medical and Biological Engineering & Computing, (1982) Volume 20, 466-472.

HEARN, T.C., MAZUMDAR, J., GOLDBLATT, E., NANDAGOPAL, D., and FAZZALARI, N.L. "Spectral energy of the first heart sound in relation to mitral valve size parameter." Australasian Physical & Engineering Sciences in Medicine, (1983) Volume 6, No. 2, 76-81.

HEARN, T.C., GOPAL, D.N., GHISTA, D.N., ROBINSON, J., TIHAL, H., MAZUMDAR, J., and BOGNER, R.E. "Towards quantitative determination of valvular calcification and pressure drops across malfunctioning heart valves." Proceedings of IEEE Frontiers of Engineering and Computing in Health Care. (1983) 127-131.

ISNER, J.M., HORTON, J., and RONAN, Jr. J.A. "Systolic click from a Swan-Ganz catheter: phono-echocardiographic depiction of the underlying mechanism." The American Journal of Cardiology, (1979) Volume 43, 1046-1048.

ITAKURA, F.I. and SAITO, S. "A Statistical method for estimation of speech spectral density and formant frequencies." Electronics and Communications in Japan, (1970) 53A, 36-43.

IWATA, A., ISHII, N., SUZUMURA, N. and IKEGAYA, K. "Algorithm for detecting the first and the second heart sounds by spectral tracking." Medical and Biological Engineering & Computing (1980) Vol. 18, 19-26.

JAMES, M.L., SMITH, G.M., and WOLFORD, J.C. "Applied numerical methods for digital computation with Fortran and CSMP." IEP - A Dun Donnally publisher (1977) New York, second edition, 141-155.

JOHN, J.E.A., and HABERMAN, W.L. "Introduction to fluid mechanics." 2nd edition Prentice Hall, Inc., (1980) New Jersey.

JONES, R., MAZUMDAR, J., and CHIANG, FU-PEN. "Further studies in the application of the method of constant deplection lines to plate bending problems." Int. J. Engng. Sci. (1975) 13, 423-443.

KORBEL, B.W. "An initial digital processing system for heart sound analysis." Project report department of Electrical Engineering (1980) University of Adelaide.

KOTLER, M.N., SEGAL, B.L., and PARRY, W.R. "Echocardiographic and phonocardiographic correlation of heart sounds and murmurs." Cardio Vascular Clinics (1978). Volume 9(2), 39-57.

LANIADO, S., YELLIN, E.L., MILLER, H. and FRATER, R.W.M. "Temporal relation of the first heart sound to closure of the mitral valve." Circulation, (1973), 47, 1006-1014.

LEWIS, B.S., LEWIS, N., and GOTSMAN, M.S. "Effect of respiration on echocardiographic ventricular dimensions and relationship to the second heart sound." European Journal of Cardiology, (1979) 10/2, 89-99.

LIM, K.O., LIEW, Y.C., and OH, C.H. "Analysis of mital and aortic valve vibrations and their role in the production of the first and second heart sounds." Physics in Medicine and Biology (1980) Volume 25, No. 4, 727-733.

LOVE, A.E.H. "A treatise on the mathematical theory of elasticity." Dover publications (1944) New York, USA.

LUISADA, A.A., LIN, C.K., ARAVANIS, C., TESTELLI, M., and MORRIS, J. "On the mechanism of production of heart sounds." American Heart Journal (1958), 55: 383-399.

LUISADA, A.A., MacCANON, D.M., KUMAR, S., and FEIGEN, L.P. "Changing views on the mechanism of the first and second heart sounds." American Heart Journal (1974) 88: 503-514.

LUISADA, A.A. and PORTALUPPI, F. "The main heart sounds as vibrations of the cardiohemic system: old controversy and new facts." American Journal of Cardiology, (1983) Vol. 52, 1133-1136.

MAKHOUL, J. and WOLF, J.J. "Linear prediction and the spectral analysis of speech." BBN Report No. 2304, Cambridge, Massachusetts: Bolt, Beranek and Newman, Inc., (1972).

MAKHOUL, J. "Spectral analysis of speech by linear prediction." IEEE Transactions on Audio and Electroacoustics, (1973), 21, 140-148.

MAKHOUL, J. "Linear Prediction: a tutorial review." Proceedings of the IEEE., (1975), 63, 561-580.

MARKEL, J.D., and GRAY, A.H. "Linear prediction of speech." Springer-Verlag Publishing Co., (1976) 161-163.

MAZUMDAR, J., "Transverse vibration of membranes of arbitrary shape by the method of constant-deflection contours." Journal of Sound and Vibration (1973), 27, 47-57.

MAZUMDAR, J., HEARN, T., and GHISTA, D.N. "Determination of in vivo constitutive properties and normal-pathogenic states of mitral valve leaflets and left ventricular myocardium" in Applied Physiological Mechanics. Harwood, Academic Publishing Co., New York (1980) (edited by D.N. Ghista).

MAZUMDAR, J. and WOODARD-KNIGHT, DEOBRAH. "A Mathematical Study of Semilunar Valve Vibration." Journal of Biomechanics (in Press) (1984).

McKUSICK, V.A. "CardioVascular Sound in Health and Disease." Williams & Wilkins Baltimore (1956) USA.

MILLS, P.G., CHAMUSCO, R.F., MOOS, S. and CRAIGE, E. "Echophonocardiographic studies of the contribution of the atrioventricular valves to the first heart sound." Circulation (1976), Volume 54, 944-951.

NANDAGOPAL, D., BOGNER, R.E., and MAZUMDAR, J. "Spectral analysis of second heart sound (SII) using linear prediction coding." Proceedings of 2nd International Conference on Mechanics in Medicine and Biology (1980). Osaka, Japan. 102-103.

OZAWA, Y., SMITH, D., and CRAIGE, E., "Origin of the third heart sound-studies in human subjects." Circulation, (1983), No. 2, 399-404.

PRAKASH, R., MOORTHY, K. and ARONOW, W.S. "First heart sound: a phonocardiographic correlation with mitral, tricuspid and aortic valvular events." Catheterisation and Cardiovascular diagnosis, (1976), 8, 381-387.

RABINER, L.R., and SCHAFER, R.W. "Digital processing of speech signals." Englewood Cliffs, New Jersey: Prentice Hall Inc. (1978).

RANGARAJ, M.R., and MOORTHY, I.S.N. "Quantitative analysis of the phonocardiogram for detection of murmurs." Journal of Biomedical Engineering, (1979), 1, 247-252.

RENNER, W.F., and RENNER, A.B. "The quality of resonance of the first heart sound after myocardial infarction: clinical significance." Circulation, (1979), 59, 1144-1148.

ROBINSON, E.A. "Predictive decomposition of time series with application to seismic exploration." Geophysics, (1967), 32, 418-484.

RONAN, Jr., J.A. "Cardiac sound and ultrasound: Echocardiographic and phonocardiographic correlations - Part I and II." Current Problems in Cardiology (1981) Volume VI, No. 5/6.

RUKAVINA, D. "A Study of the effects of infarction on heart sound spectra." Ph. D. Thesis, Department of Electrical Engineering, University of Wisconsin (1970).

RUSHMER, R.F. "Cardiovascular Dynamics (Third edition)." W.B. Saunders Co., Philadelphia, (1970).

SABBAH, H.N., and STEIN, P.D. "Investigation of the theory and mechanism of the origin of the second heart sound." Circulation Research, (1976), 39, 874-882.

SABBAH, H.N., KHAJA, F., ANBE, D.T., FOLGER, G.M., and STEIN, P.D. "Determinants of the amplitude of the aortic component of the second heart sound in aortic stenosis." American Journal of Cardiology (1976), 41, 830-835.

SARKADY, A.A., CLARK, R.R., and WILLIAMS, R. "Computer analysis of techniques for phonocardiogram diagnosis." Journal of Computers and Biomedical Research, (1976), 9, 349-363.

SNEDECOR, G.W., and COCHRAN, W.G. "Statistical methods." Iowa State University Press, (1967) Ames, Iowa, USA.

STEIN, P.D., and SABBAH, H.N. "Origin of the second heart sound: clinical relevance of new observations." The American Journal of Cardiology. (1978), Volume 41, 108-110.

STEIN, P.D., SABBAH, H.N., LAKIER, J.B. and GOLDSTEIN, S. "Frequency spectrum of the aortic component of the second heart sound in patients with normal valves, aortic stenosis and aortic porcine xenografts." The American Journal of Cardiology, (1980), Volume 46, 48-52.

VAN VOLLENHOVEN, E., VAN ROTTERDAM, A., DERENBOS, T. and SCHLESINGER, F.G. "Frequency analysis of heart murmurs." Medical and Biological Engineering & Computing (1969), 7, 227-230.

VAN VOLLENHOVEN, E., SUZUMURA, H., GHISTA, D.N., MAZUMDAR, J., and HEARN, T. "Phonocardiography: analysis of instrumentation and vibration of heart structures to determine their constitutive prperties." In Ghista, D.N. (Ed.) Advances in Cardio Vascular Physics (1979). Karger Switzerland, 2, 68-118.

WAKITA, H. "Direct estimation of vocal tract shape by inverse filtering of acoustic speech waveforms." IEEE transactions on Audio and Electroacoustics. (1973), AU-21, 417-427.

YOGANATHAN, A.P., GUPTA, R., UDWADIA, F.E., MILLER, J.W., CORCORAN, W.H., SARMA, R., JOHNSON, J.L., and BING, R.J. "Use of the fast Fourier transform for frequency analysis of the first heart sound in normal man." Medical and Biological Engineering & Computing, (1976) 14, 69-73.

YOGANATHAN, A.P., GUPTA, R., UDWADIA, F.E., CORCORAN, W.H., SARMA, R., and BING, R.J. "Use of the fast Fourier transform in the frequency analysis of the second heart sound in normal man." Medical and Biological Engineering & Computing, (1976) 14, 455-459.